# A Palladium Nanocatalyst Enabling Green Heteroaryl Suzuki Cross-Coupling and Anticancer Activity with Photophysical and TD-DFT Insights of Biaryl Products

Maruboina Hemanth Kumar,[a] Shivabasayya V Salimath,[a] Priyadarshini A N,[b] Sudhanva M. S.,[b] Asad Syed,*[c] Ali H. Bahkali,[c] Meenakshi Verma,[d] Bhari Mallanna Nagaraja,[a] and Siddappa A. Patil*[a]

[a]*Centre for Nano and Material Sciences, Jain (Deemed-to-be University), Jain Global Campus, Kanakapura, Bangalore, Karnataka, 562112, India. E-mail: p.siddappa@jainuniversity.ac.in*
[b]*Adichunchanagiri Institute for Molecular Medicine, Adichunchanagiri Institute of Medical Sciences, Adichunchanagiri University, BG Nagara-571448, Karnataka, India.*
[c]*Department of Botany and Microbiology, College of Science, King Saud University, P.O. 2455, Riyadh, 11451, Saudi Arabia. E-mail: assyed@ksu.edu.sa*
[d]*University Centre for Research & Development, Department of Chemistry, Chandigarh University, Gharuan, Mohali, India.*

## ***Table of contents***

## 1. General considerations

Fourier transform infrared (FT-IR) spectra were exquisitely captured using a PerkinElmer spectrometer (L160000A, PerkinElmer, USA). The sophisticated gas chromatography-mass spectrometry (GC-MS) analysis was performed using the Shimadzu GC-MS-TQ8030 system (Tokyo, Japan). Surface morphology and elemental distribution were meticulously examined using field-emission scanning electron microscopy (FE-SEM) (JEOL JSM-7100F, JEOL, Singapore) combined with energy-dispersive X-ray spectroscopy (EDX). High-resolution transmission electron microscopy (HR-TEM) images were obtained using a JEOL/JEM 2100 microscope. X-ray photoelectron spectroscopy (XPS) was analyzed by using PHI 5000 Versa Probe II, ULVAC-PHI Inc., USA. The total Pd content loaded on the nanocatalyst was precisely quantified by inductively coupled plasma-optical emission spectroscopy (ICP-OES) (Optima 5300 DV, PerkinElmer, USA). Powder X-ray diffraction (*p*-XRD) measurements were conducted using an Ultima IV X-ray diffractometer (Rigaku, Japan). Thermogravimetric (TG) analysis was performed with a TGA Q500 V20.10 Build 36 analyzer at a heating rate of 10 °C $min^{-1}$ in an $N_2$ atmosphere. Proton, carbon-13, and fluorine-19 nuclear magnetic resonance ($^{1}H$, $^{13}C$, and $^{19}F$ NMR) spectra were recorded at 400 MHz, 100 MHz, and 376 MHz in deuterated chloroform and dimethyl sulphoxide ($CDCl_3$ δ = 7.26 ppm, 77.5 ppm; DMSO 2.50 ppm, 39.52 ppm). $^{1}H$ coupling constants (J) are reported in Hertz (Hz), with multiplicities specified as follows: s (singlet), d (doublet), dd (doublet of doublets), t (triplet), q (quartet), and m (multiplet).

## 2. Experimental section

### 2.1 Materials

All solvents were utilized without any prior purification. *Acacia pachyceras Mimosaceae* (APM) plant leaves were gathered from local farmers in the Yadavanahalli area of Bangalore, Karnataka, India. Sodium-montmorillonite (Na-MMT), Palladium acetate ($Pd(OAc)_2$), 3,5-dibromo pyridine, 3-bromoquinoline, 4,7-dichloroquinoline, and phenylboronic acids, along with various bases, were obtained from esteemed suppliers such as Sigma-Aldrich and Avra Chemical Company and employed directly without additional purification. All primary and secondary antibodies were procured from Cell Signaling Technologies (Danvers, MA, USA). Unless specified otherwise, all reactions were conducted in accurately oven-dried glassware, utilizing magnetic stirring and heating via a silicone oil bath under aerobic conditions. The progress of reactions was monitored using thin-layer chromatography (TLC) on 0.25 mm Merck TLC silica gel plates, with ultraviolet (UV) light serving as the visualizing agent. For the purification of reaction products, column chromatography was executed using silica gel (60-120 mesh, Merck) with hexane and ethyl acetate as eluents. The process of concentrating the solutions involved the removal of volatile solvents using a rotary evaporator attached to a dry

diaphragm pump (10-15 mm Hg), followed by further reduction to a constant weight using an oil pump (300 mTorr), a technique referred to as concentration in *vacuo*.

**2.2 Methods**

**Preparation of APM leaves extract**

APM leaves were collected from the Bangalore locality, washed with tap water followed by distilled water, and shade-dried. The dried leaves were ground into a fine powder, and 2.0 g of powder was mixed in a 100 ml ethanol-distilled water mixture (EtOH: $H_2O$) (1:1, v/v) and stirred at 80 °C for 2 h. The mixture was then filtered to obtain a clean extract, which was stored in the refrigerator for further use.

**Synthesis of Palladium nanoparticles supported by APM leaves extract on Na-MMT (APM-PdNPs@Na-MMT)**

In a 50 ml solution of APM leaves extract, Na-MMT was added and subjected to ultrasonication for 10 min to ensure uniform dispersion. Subsequently, $Pd(OAc)_2$ was added, followed by an additional 10 min of ultrasonication. The resulting suspension was stirred at 80 °C for 24 h, followed by solvent evaporation on a hot plate at the desired temperature. The obtained residue was ground, washed successively with distilled water and ethanol by centrifugation, and dried at 50 °C overnight to afford a black APM-PdNPs@Na-MMT nanocatalyst.

**General procedure for the synthesis of 3,5-diphenylpyridines**

A 25 mL round-bottom flask containing APM-PdNPs@Na-MMT nanocatalyst (0.46 mol% Pd), 3,5-dibromo pyridine (**1a**) (0.42 mmol, 1.0 equiv.), phenylboronic acid (**2a**) (1.26 mmol, 3.0 equiv.), $K_2CO_3$ (3.5 equiv.), and EtOH: $H_2O$ (5.0 mL) was allowed to react at 80 °C for the required time. TLC was used to track the reaction's development. The APM-PdNPs@Na-MMT nanocatalyst was separated by centrifugation once the reaction was finished and the mixture had cooled to room temperature. The organic layer was separated using ethyl acetate (3 × 10 mL) in a separatory funnel, and the reaction mixture was dried over anhydrous $Na_2SO_4$ after being quenched with water. The dried organic layer was vacuum-concentrated, and the products were isolated by column chromatography using *n*-hexane and ethyl acetate as eluents to afford the corresponding products in good to excellent yields. All of the separated products had their $^1H$ and $^{13}C$ NMR spectra recorded.

**General procedure for the synthesis of 3-phenylquinolines**

APM-PdNPs@Na-MMT nanocatalyst (0.46 mol% Pd), 3-bromoquinoline (**4**) (0.48 mmol, 1.0 equiv.), **2a** (0.72 mmol, 1.5 equiv.), $K_2CO_3$ (2.0 equiv.), and PEG-200 (3.0 mL) were added to a 25 mL round-bottom flask and allowed to react at 100 °C for the necessary amount of time. The progress of the reaction was monitored using TLC. After the reaction was complete and the mixture had cooled to room temperature, the APM-PdNPs@Na-MMT nanocatalyst was separated by centrifugation. The reaction mixture was quenched with water and then dried over anhydrous $Na_2SO_4$ after the organic layer was separated using ethyl acetate (3 × 10 mL)

in a separatory funnel. After the dried organic layer was vacuum-concentrated, the respective products were obtained in good to excellent yields using column chromatography utilizing n-hexane and ethyl acetate as eluents. The $^{1}H$ and $^{13}C$ NMR spectra of every isolated product were recorded.

**General procedure for the synthesis of 7-chloro-4-phenylquinolines**

A 25 mL round-bottom flask was filled with APM-PdNPs@Na-MMT nanocatalyst (0.46 mol% Pd), 4,7-dichloroquinole (**6**) (0.50 mmol, 1.0 equiv.), **2a** (0.75 mmol, 1.5 equiv.), $K_2CO_3$ (2.0 equiv.), and PEG-200 (3.0 mL). The mixture was then allowed to react at 100 °C for the required period of time. Using TLC, the reaction's development was tracked. The APM-PdNPs@Na-MMT nanocatalyst was separated by centrifugation after the reaction was completed, and the mixture was cooled to room temperature. After the organic layer was separated using ethyl acetate (3 × 10 mL) in a separatory funnel, the reaction mixture was dried over anhydrous $Na_2SO_4$ and quenched with water. The corresponding compounds were produced in good to exceptional yields employing column chromatography with n-hexane and ethyl acetate as eluents after the dried organic layer was vacuum-concentrated. Each isolated product's $^{1}H$ and $^{13}C$ NMR spectra were noted.

**Procedure for recovery of the APM-PdNPs@Na-MMT nanocatalyst**

The catalyst's durability and recyclability are crucial elements in organic transformations, particularly in real-world industrial applications. To overcome this challenge, the APM-PdNPs@Na-MMT nanocatalyst was separated by centrifugation after the reaction was complete, washed with water (2 × 20 mL) and methanol (2 × 20 mL), and then gently dried at 50 °C overnight. For the next round of reactions, the dried recycled R-APM-PdNPs@Na-MMT nanocatalyst was used as such.

**Theoretical calculations of synthesized molecules: DFT**

Density functional theory (DFT) is a widely used theoretical technique for investigating a variety of chemical and physical properties. It can be used to assess the optical and electronic properties of atoms and molecules, ascertain the kinetic and thermodynamic stability of compounds, carry out structural optimizations, clarify reaction mechanisms, and examine molecular interactions. The Gaussian 16W software program was used for all theoretical computations in this investigation. DFT and time-dependent DFT (TD-DFT) methods were used to perform geometry optimizations and electronic structure computations at the B3LYP/6-311G(d,p) level of theory. To account for the solvent effect, both the DFT and TD-DFT studies were associated with the conductor-like polarizable continuum model (CPCM) in a dimethyl sulfoxide (DMSO) medium. GaussView 6.1 was used to display and evaluate the generated molecular structures and characteristics, as displayed in Fig. S7, S9, S11, S14, S16, and S19. The electronic parameters, energies of frontier molecular orbitals ($E_{HOMO}$ and $E_{LUMO}$), energy band gap (ΔE), which explains the eventual charge transfer interaction within the molecule, electronegativity (χ), chemical potential (μ), global hardness (η), global softness (S) and global electrophilicity index (ω) were calculated by means of equations SE1-E6.

$$\Delta E = ELUMO - EHOMO \text{ ----------(SE1)}$$

$$\mu = \frac{IP + EA}{2} \text{ ----------}$$

$$\eta = -\frac{ELUMO - EHOMO}{2} \text{ ----------(SE3)}$$

$$S = \frac{1}{\eta} \text{ ----------(SE4)}$$

$$\omega = \frac{\mu 2}{2\eta} \text{ ----------(SE5)}$$

$$\chi = - \mu \text{ ----------(SE6)}$$

**UV-Vis and Fluorescence studies**

We recorded absorption and emission spectra using a UV-Visible spectrophotometer (UV-1900i, Shimadzu, Japan) and steady-state fluorescence spectra using a highly sensitive Horiba FluoroMax Plus instrument (USA), exciting the samples at their respective absorption maxima. As a standard reference, we used quinine sulfate (ref = 0.54 in 0.5 M $H_2SO_4$) to calculate the fluorescence quantum yield of the compounds. To reduce reabsorption effects, the absorbance values at the excitation wavelength were maintained below 0.1, and adjustments were made for variations in solvent refractive indices. The quantum yield was calculated using the equation below: to the new molecules' emission spectra to determine the luminescence quantum yields (ϕf) in 10% DMSO (aq).

$$\varphi = \varphi R \times \frac{Is}{IR} \times \frac{ODR}{ODS} \times \frac{\eta S}{\eta R} \text{ ----------(E7)}$$

Notations involved herein are as ϕ = quantum yield, I = peak area, OD = absorbance at $\lambda_{max}$ of sample(s) and reference(R), η = refractive index of solvent (s) and reference (R). The subscript R refers to quinine sulfate. Also, the molar extinction coefficient (ε) and Stokes' Shift were calculated. The molar extinction coefficient (ε) was calculated using Beer–Lambert's law, A = εcl. All the compounds exhibited good molar extinction coefficients (ε). The Stoke's Shift (the difference in wavelength (or energy) between the absorption maximum and the emission maximum of a molecule) was calculated using the following equation:

$$\Delta \bar{\upsilon} = \bar{\upsilon}_{abs} - \bar{\upsilon}_{em} \text{ ----------(E8)}$$

**Cell lines and culture conditions**

Human Colorectal cancer; HCT116 cell lines were procured from NCCS, Pune, India, authenticated by STR analysis, and the cells were tested for mycoplasma contamination. Cells were cultured in F12K media with 2 mM L-glutamine (Thermo Fisher Scientific, Inc.; Waltham, MA, USA) containing 10% FBS (Gibco; Grand Island, NY, USA). Cells were cultured in a humidified Incubator with 5% $CO_2$ at 37 °C.

**MTT and Trypan Blue Dye Exclusion Assay**

MTT and Trypan Blue dye exclusion assays were performed as follows. Briefly, cells treated with different concentrations of Nanocomposites (10, 25 & 50 µg/mL), incubated, and

subjected to MTT and Trypan Blue dye assays; DMSO was used as a negative control. The plates were subjected to spectrophotometric absorbance at 570 nm using a Tecan Microplate Reader (Tecan Instruments, Switzerland). The Trypan Blue-treated cells were counted using the Thermo Fisher Countess III FL for calculating the percentage of live and dead cells. The data were analyzed using Microsoft Excel.

**Apoptotic analysis by Hoechst/ PI and Acridine orange/ PI dual Staining**

The H/PI and AO/PI double staining assay was conducted following the protocol. Briefly, HCT116 cells were seeded at a density of 1 x $10^5$ cells per well in 6-well plates and allowed to attach overnight. Subsequently, they were treated with increasing concentrations of nanocomposites and incubated for 48 h before undergoing H/PI and AO/PI double staining.

**Migration assay / Wound Healing Assay**

The migration assay was conducted following the protocol described. Briefly, cells were seeded at a density of 2 × $10^5$ cells per well in a 12-well plate and allowed to attach overnight. The cells were allowed to grow until they reached complete confluency. Subsequently, a scar was created using a sterile tip, and the cells were treated with increasing concentrations of nano composites. After 24 h of incubation, the cells were imaged to assess the extent of scar/wound recovery.

## 3. Results and discussion

### 3.1. Qualitative analysis of phytochemicals

**Table S1** Qualitative analysis of phytochemicals present in the APM leaves extract

| Sl. No | Secondary metabolite | Test | Result |
|---|---|---|---|
| 1 | Flavonoids | Concentrated $H_2SO_4$ Test | Positive, as the solution turned orange-red |
| 2 | Alkaloids | Wagner's Test | Positive result, as evidenced by the formation of precipitate |
| 3 | Phenols | Ferric Chloride Test | Positive as the solution turned to bluish-black |
| 4 | Saponins | Foam Test | Persistent foam (lasting ≥10 minutes) indicates the presence of saponins |
| 5 | Triterpenoids | Liebermann-Burchard Test | Positive, as the solution turned red/orange |
| 6 | Tannins | 10% NaOH Test | Positive, as the formation of an emulsion |
| 7 | Steroids | Salkowski Test | Positive, as the formation of a yellow-brown layer at the interface |

### 3.2. EDX analysis

**Table S2** Elemental composition of Na-MMT and APM-PdNPs@Na-MMT

| Sample | O (%) | Na (%) | Mg (%) | Al (%) | Si (%) | Pd (%) |
|---|---|---|---|---|---|---|
| Na-MMT | 60 | 2 | 2 | 11 | 25 | - |
| APM-PdNPs@Na-MMT | 70 | 0.7 | 2.3 | 8.5 | 17 | 1.5 |

### 3.3. Comparison of Catalytic Parameters of Pd Sources in Optimization

**Table S3** Comparison of catalytic parameters of different Pd sources evaluated in the optimization study

| Sl. No | Catalyst (mol%) | Yield (%) | TON | TOF ($h^{-1}$) |
|---|---|---|---|---|
| 1 | $Pd(OAc)_2$ | 93 | 202 | 40.4 |
| 2 | PdNPs | 91 | 198 | 39.6 |
| 3 | Pd/C | 92 | 200 | 40.0 |
| **4** | **APM-PdNPs@Na-MMT** | **98** | **213** | **42.6** |

### 3.4. Plausible reaction mechanism

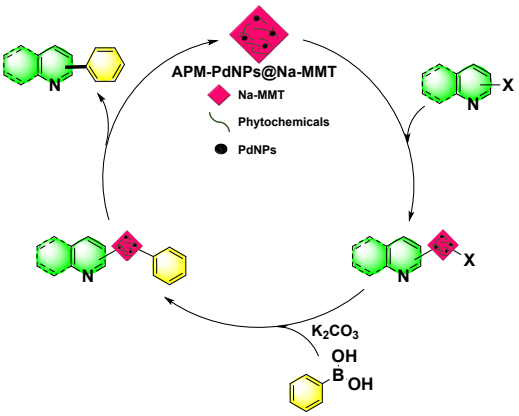


**Scheme S1** Plausible reaction mechanism.

### 3.5. Characterization of recycled APM-PdNPs@Na-MMT nanocatalyst

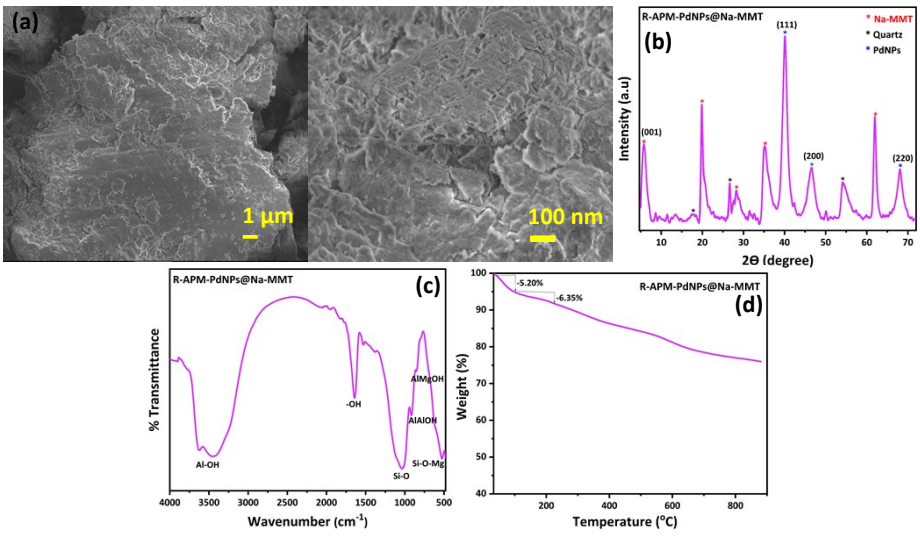


**Fig. S1** FE-SEM, *p*-XRD, FTIR, and TG analysis of recycled R-APM-PdNPs@Na-MMT nanocatalyst.

### 3.6. Hot filtration test for APM-PdNPs@Na-MMT nanocatalyst

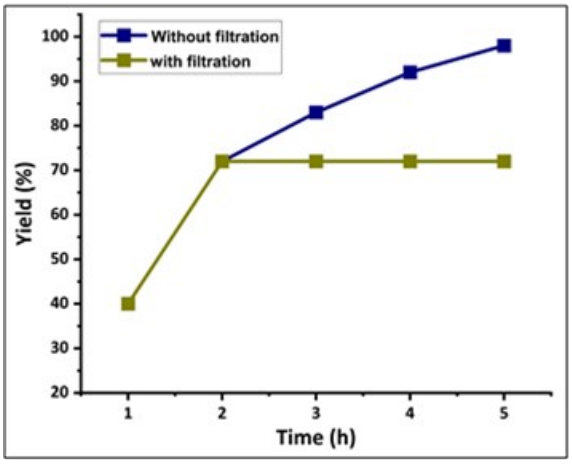


**Figure S2.** Hot filtration test for APM-PdNPs@Na-MMT nanocatalyst.

### 3.7. Catalytic Efficiency Comparison of Literature Pd Catalysts

**Table S4** Comparison of the catalytic efficiency of APM-PdNPs@Na-MMT with literature-reported Pd catalysts for Suzuki-Miyaura coupling

| Sl. No | Catalyst (mol%) | Substrate | Temperature (°C) | Yield (%) | TON | TOF | Ref. |
|---|---|---|---|---|---|---|---|
| 1 | Palladium-bis(NHC) complex (0.25) | N-heteroaryl chloride | 80 | 12 | 100 | 8.3 | [1] |
| 2 | PdNPs@oakgum (0.3) | Aryl chloride | 80 | 70 | 233 | 12.9 | [2] |
| 3 | Bis(oxamato)palladate(II) complex (5) | Aryl bromide | 120 | 65 | 14 | 6.5 | [3] |
| 4 | $SiO_2$-pA-Cyan-Cys-Pd (0.5) | Aryl bromide | 100 | 88 | 176 | 32 | [4] |
| | | Aryl chloride | 100 | 52 | 104 | 17.3 | |
| 5 | Pd-ATBA-MNPs (0.82) | Aryl bromide | 80 | 90 | 110 | 94 | [5] |
| | | Aryl chloride | 100 | 68 | 83 | 36.8 | |
| 6 | $Pd(OAc)_2$/L1-3 (2) | N-heteroaryl chloride | 100 | 83 | 41.5 | 71 | [6] |
| 7 | POPD (2.5) | N-heteroaryl chloride | 100 | 84 | 33.6 | 1.6 | [7] |
| | | N-heteroaryl bromide | 100 | 69 | 27.6 | 1.3 | |
| 8 | PdNPs (3) | N-heteroaryl bromide | 80 | 90 | 30 | 3.3 | [8] |
| | | Aryl chloride | 80 | 70 | 23.3 | 1.1 | |
| **9** | **APM-PdNPs@Na-MMT (0.46)** | **N-heteroaryl bromide** | **80** | **98** | **213.1** | **42.6** | **This work** |

| | | | | | |
|---|---|---|---|---|---|
| | **N-heteroaryl bromide** | **100** | **>99** | **245.9** | **163.7** |
| | **N-heteroaryl chloride** | **100** | **97** | **251** | **62.75** |

### 3.8. TD-DFT analysis

The frontier molecular orbitals (FMOs), *i.e.,* the highest occupied molecular orbital (HOMO) and the lowest unoccupied molecular orbital (LUMO), were analysed in the DFT calculations. The HOMO represents a molecule's ability to donate electrons, with a higher $E_{HOMO}$ value indicating stronger electron-donating capacity. Conversely, the LUMO corresponds to a molecule's ability to accept electrons, and a lower $E_{LUMO}$ value suggests a greater electron-accepting ability. The computed DFT parameters for all optimized structures of all molecules in Figure S3, S5, S7, S10, S12, S15, and S17 were calculated by means of equations SE1-SE6 and listed in Table S3. Among the studied compounds, four derivatives, **3i**, **3g**, **3k**, and **5e**, exhibited the lowest energy gap values. The energy gap of all derivatives was determined by equation SE1 and is displayed in Table S3. The frontier molecular orbitals of all derivatives are illustrated in Figures S4, S6, S8, S9, S13, S16, and S18. Generally, larger $E_{HOMO}$-$E_{LUMO}$ gaps correspond to lower molecular stability and higher reactivity, whereas smaller gaps indicate more stable and less reactive compounds.

The molecular electrostatic potential (MEP) is a valuable tool for predicting the reactive sites of electrophilic and nucleophilic species within a molecule. MEP surface analysis for all synthesized compounds was performed using DFT calculations at the B3LYP/6-311G'(d, p) level of theory. The resulting MEP maps display colour variations corresponding to different electrostatic potential regions: green indicates regions of zero potential (neutral), blue represents the most positive potential (electrophilic sites), and red corresponds to the most negative potential (nucleophilic sites). Oxygen and nitrogen atoms, due to their lone pairs of electrons, generally act as nucleophilic centres, whereas hydrogen atoms commonly serve as electrophilic centres. Consequently, nucleophilic interactions are favoured in areas of high negative electrostatic potential, while electrophilic species preferentially interact with regions of lower potential. The electrostatic potential surfaces of these compounds are displayed in Figure S2, S4, S6, S9, S11, S14, and S16. The most negative and most positive electrostatic potential values of selected molecule **7b** with a band gap of 6.8 eV are highlighted in Table S3.

Time-dependent DFT (TD-DFT) calculations yielded the corresponding wavelengths, excitation energies, oscillator strengths, and major orbital contributions for all synthesized derivatives. Theoretical UV-Vis absorption spectra of all derivatives are displayed in Figure S8, S13, and S18, and Table S4. For the synthesized derivatives under investigation, the computed absorption energies varied from **4.8** to **6.0** eV. Theoretical simulations indicate that of all compounds, **3i** displays electronic transitions mostly involving the HOMO → LUMO and LUMO → HOMO orbitals, with an estimated absorption wavelength of 252 nm and an excitation energy of **5.94** eV. Similarly, all the synthesized compounds exhibit an absorbance maximum

in the range of 200-500 nm in theoretical experiments, as displayed in Figures S9, S14, and S18. Comparably, the observed spectrum from experimental absorbance illustrates an absorption maximum range of 240-336 nm, whereas the theoretical results for compound **3a** show a dominating HOMO → LUMO transition with a predicted wavelength of 265 nm and an excitation energy of **5.0** eV. The projected energy gap of **5.20** eV for the molecules closely matches the experimentally observed UV-Vis absorption band at 260 nm, demonstrating the strong agreement between theoretical and experimental results Table S4.

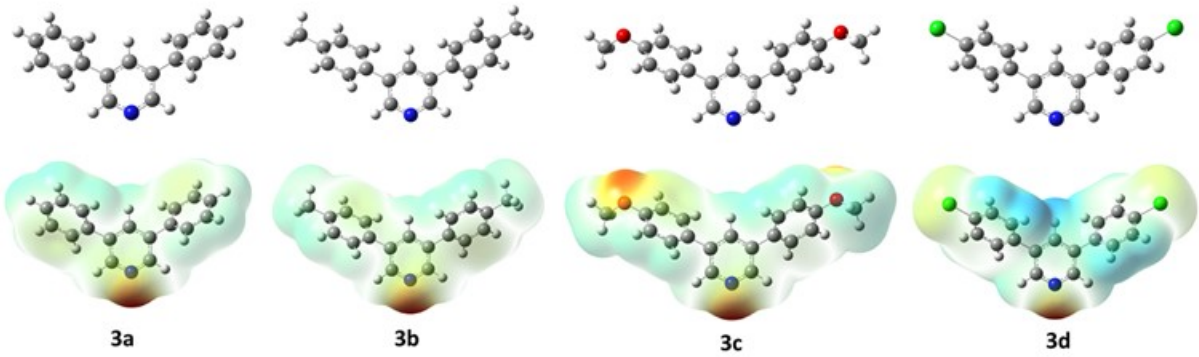


**Fig. S3** Optimized molecular structures and electrostatic potential mapped (ESP) on the surface of compounds (**3a**-**3d**) using DFT/B3LYP- 6311-G (d,p) basis set.

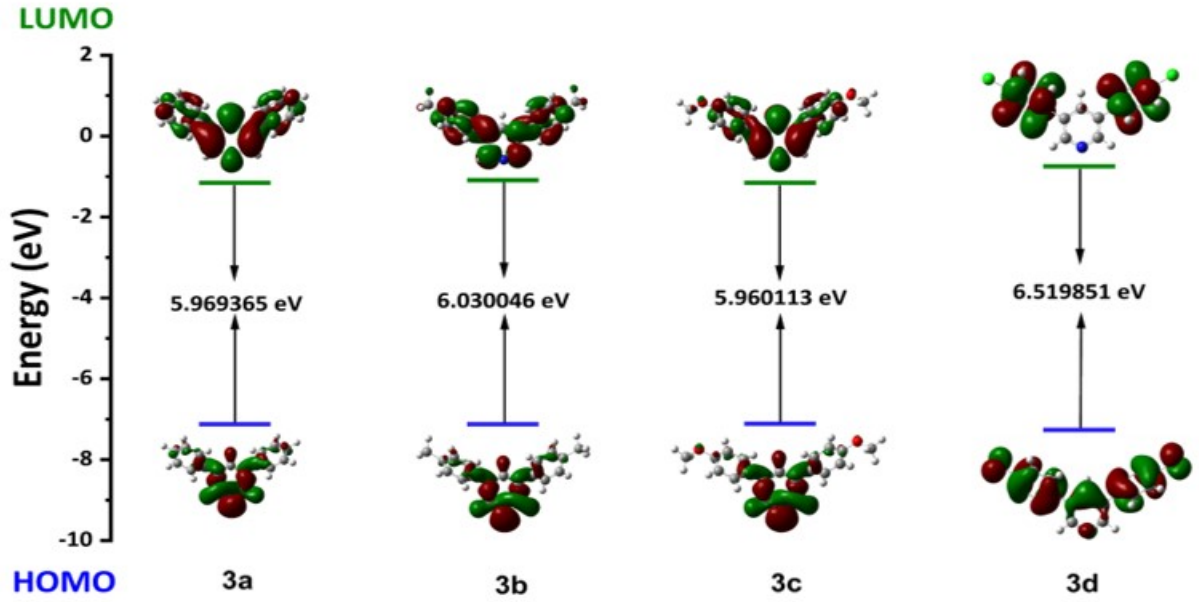


**Fig. S4** FMOs of (**3a**-**3d**).

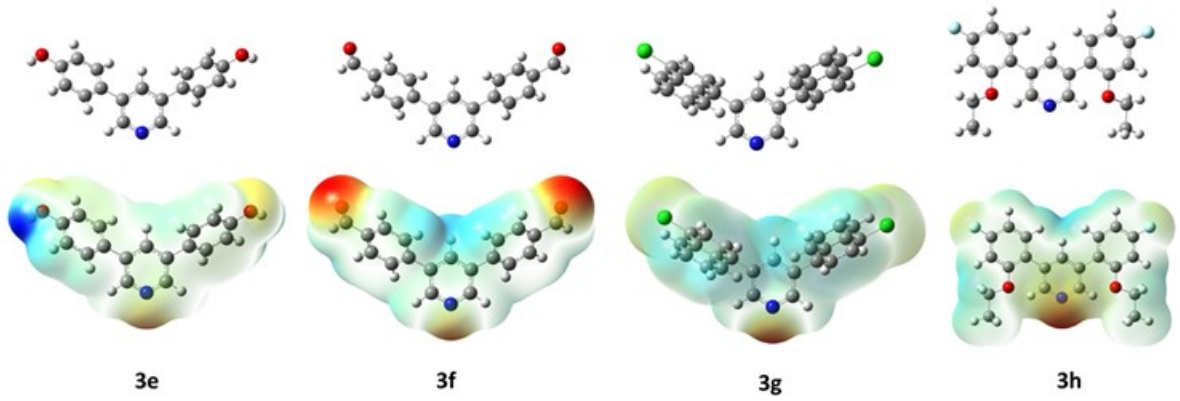


**Fig. S5** Optimized molecular structures and electrostatic potential mapped (ESP) on the surface of compounds (**3e-3f**) using DFT/B3LYP- 6311-G (d,p) basis set.

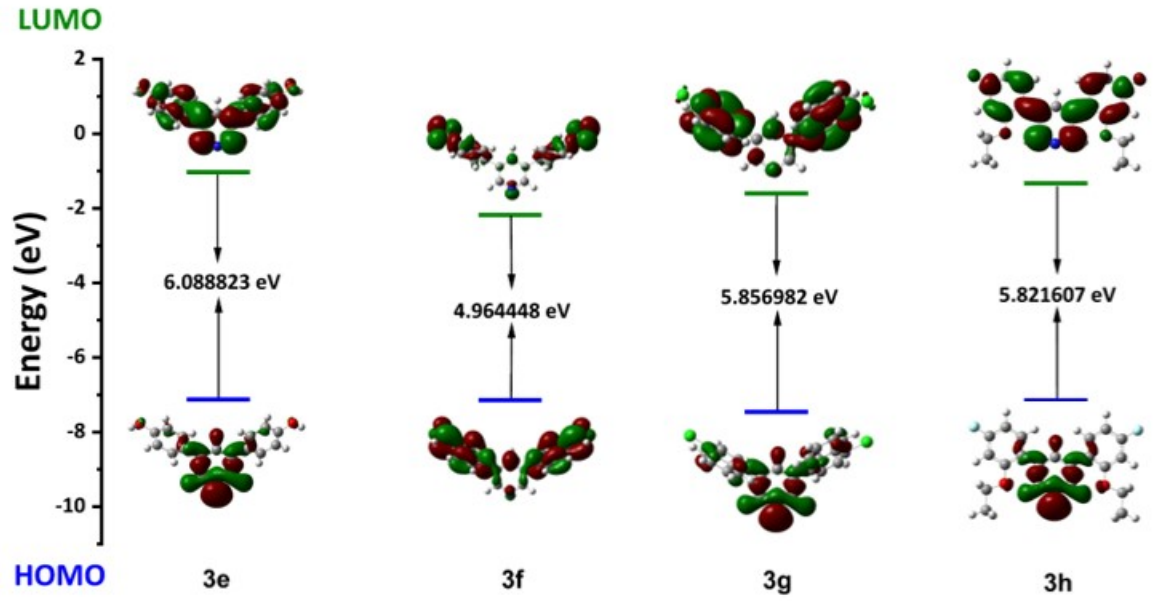


**Fig. S6** FMOs of (**3e-3h**).

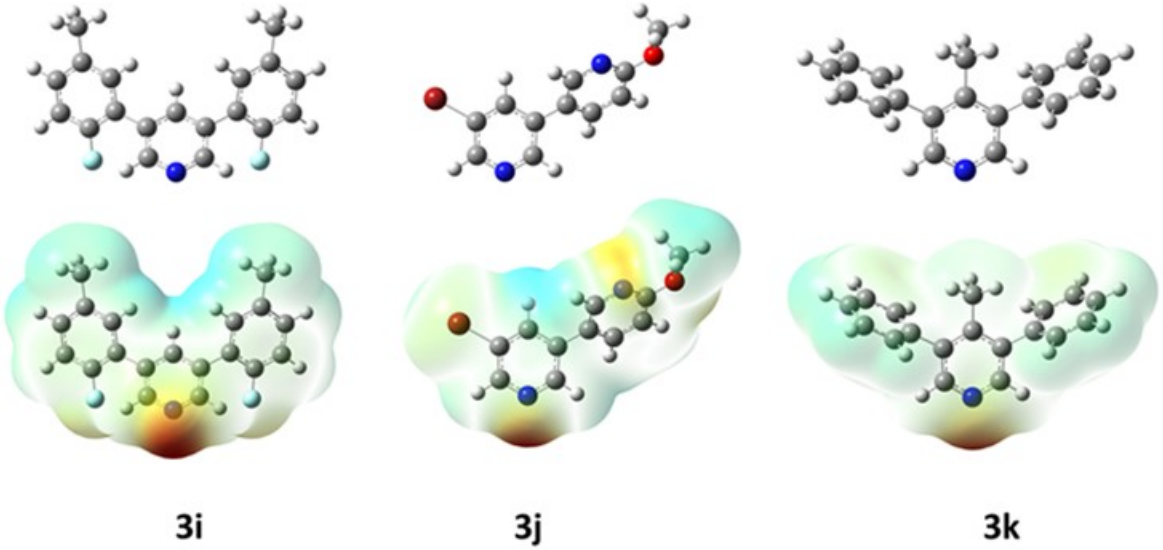


**Fig. S7** Optimized molecular structures and electrostatic potential mapped (ESP) on the surface of compounds (**3i-3l**) using DFT/B3LYP- 6311-G (d,p) basis set.

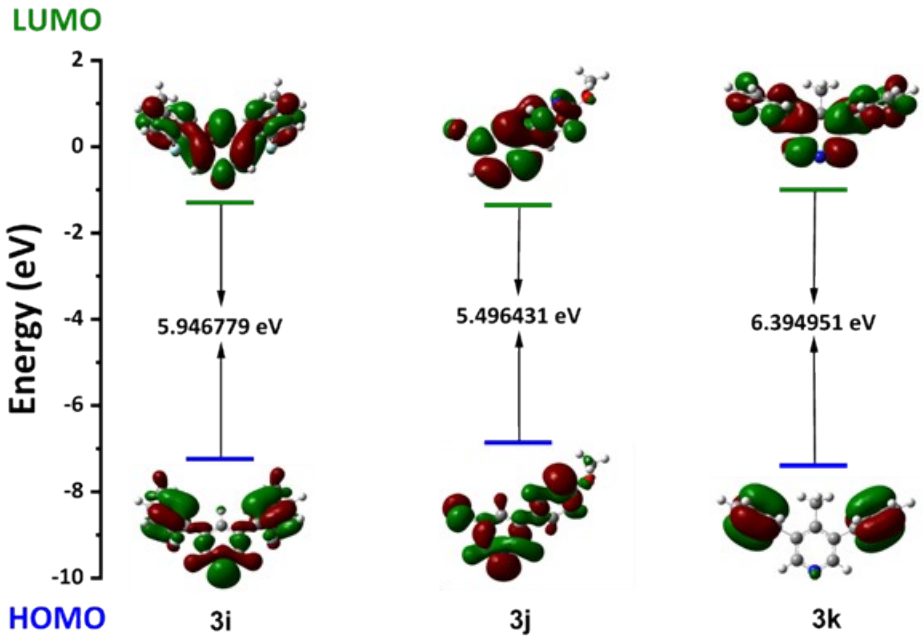


**Fig. S8** FMOs of (**3i-3l**).

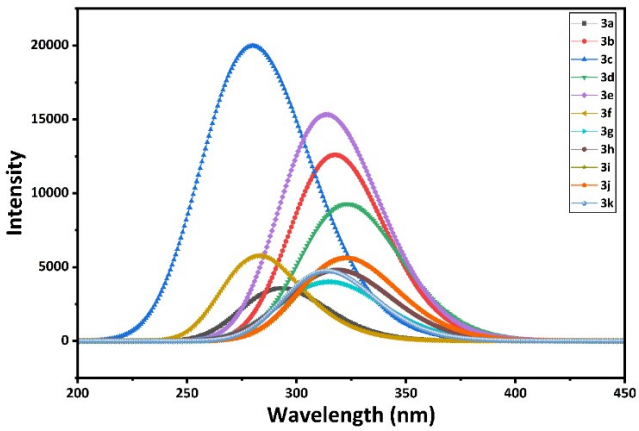


**Fig. S9** TD-DFT UV-Vis spectra of (**3a-3l**) molecules in the DMSO medium.

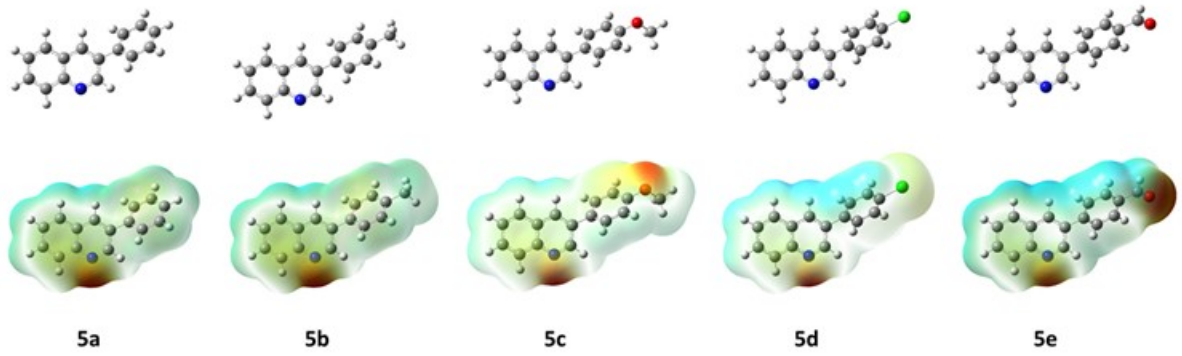


**Fig. S10** Optimized molecular structures and electrostatic potential mapped (ESP) on the surface of compounds (**5a-5e**) using DFT/B3LYP- 6311-G (d,p) basis set.

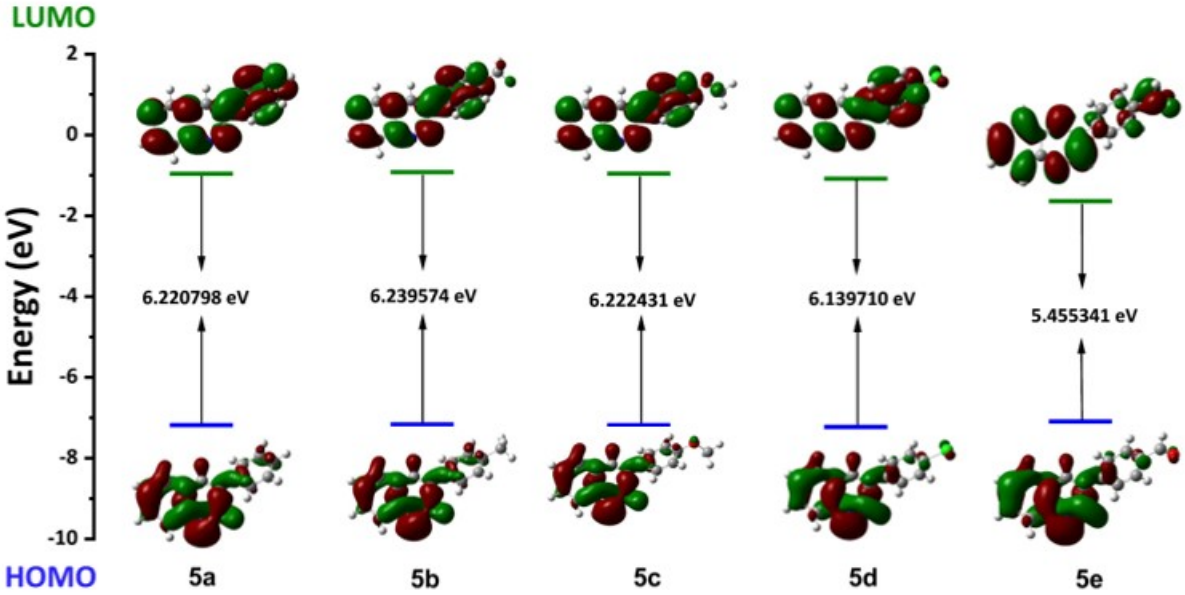


**Fig. S11** FMOs of (**5a-5e**).

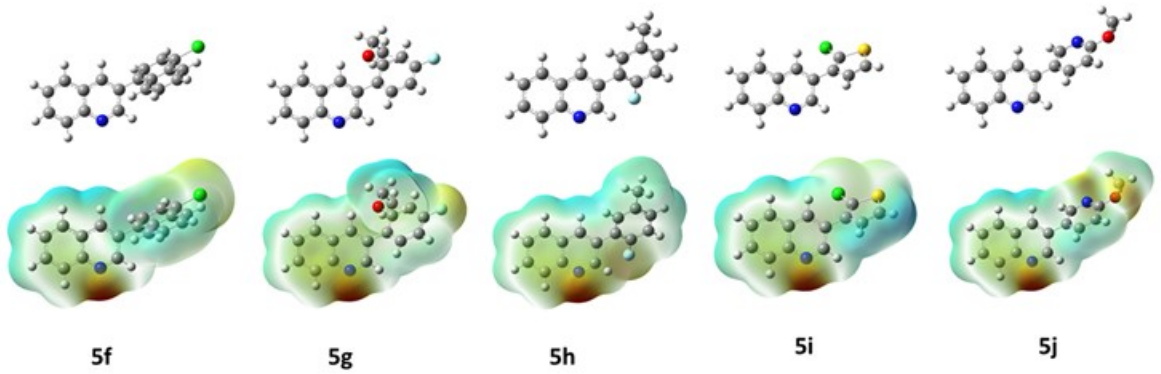


**Fig. S12** Optimized molecular structures and electrostatic potential mapped (ESP) on the surface of compounds (**5f-5j**) using DFT/B3LYP- 6311-G (d,p) basis set.

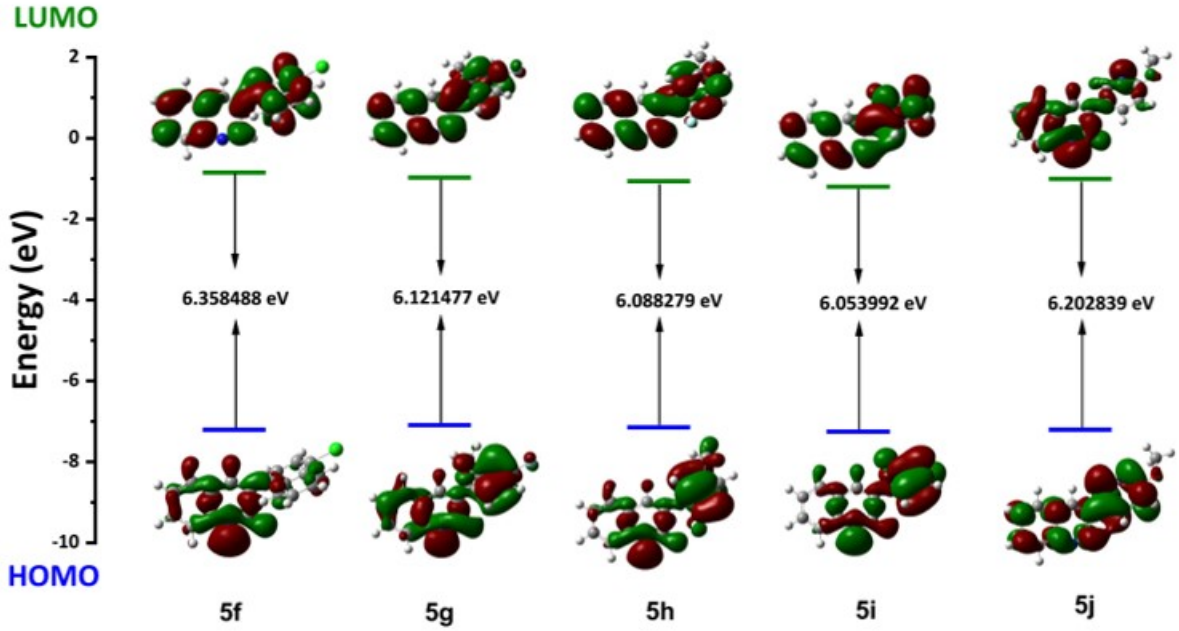


**Fig. S13** FMOs of (**5f-5j**).

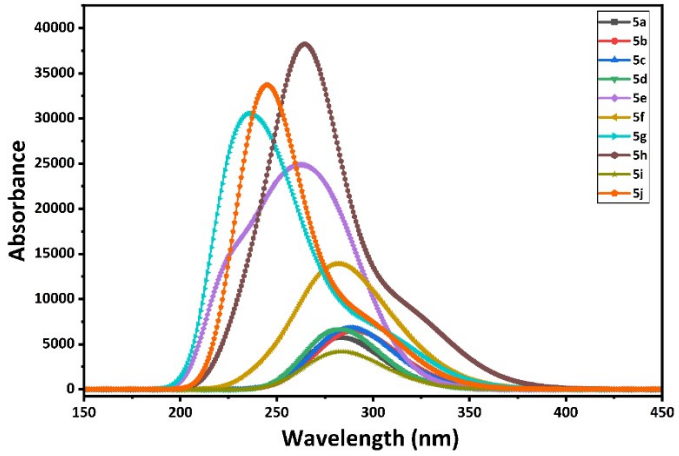


**Fig. S14** TD-DFT UV-Vis spectra of (**5a-5k**) molecules in the DMSO medium.

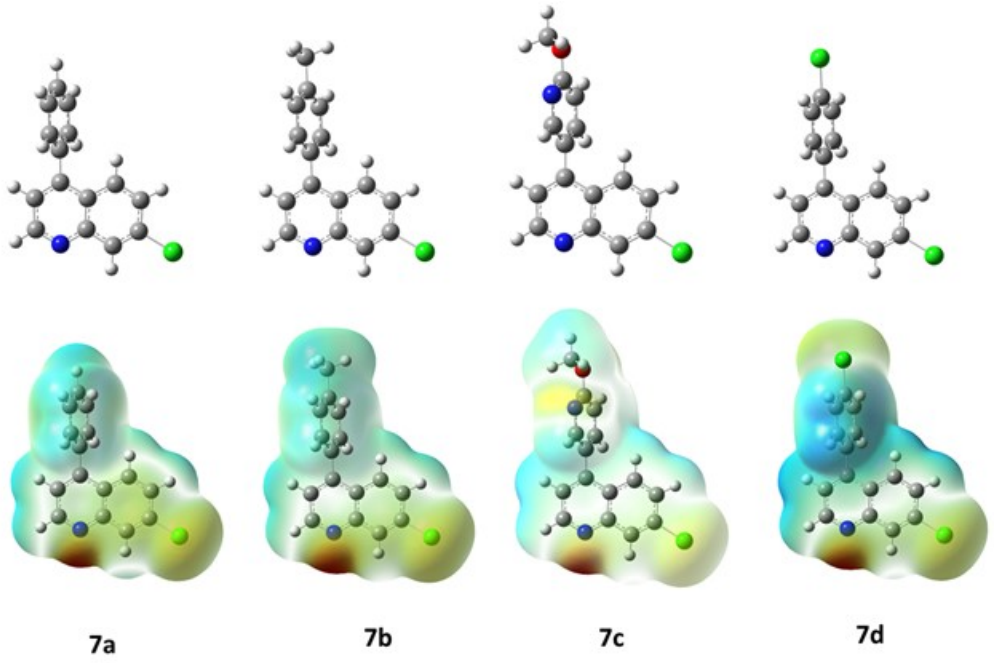


**Fig. S15** Optimized molecular structures and electrostatic potential mapped (ESP) on the surface of compounds (7a-7d) using DFT/B3LYP- 6311-G (d,p) basis set.

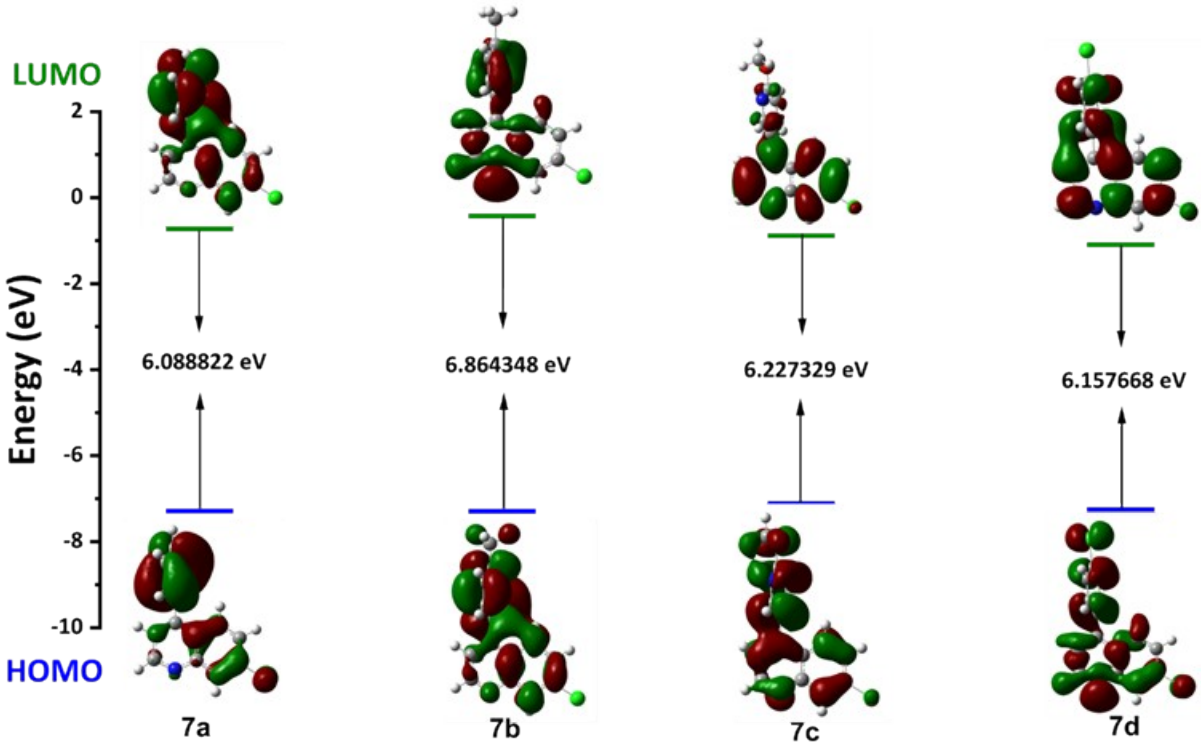


**Fig. S16** FMOs of (**7a-7d**).

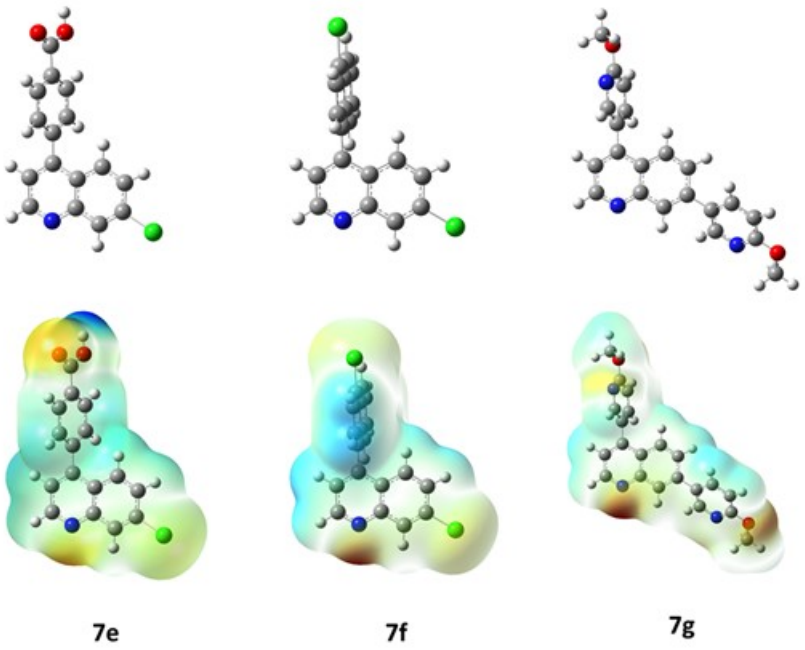


**Fig. S17** Optimized molecular structures and electrostatic potential mapped (ESP) on the surface of compounds (**7e-7f**) using DFT/B3LYP- 6311-G (d,p) basis set**.**

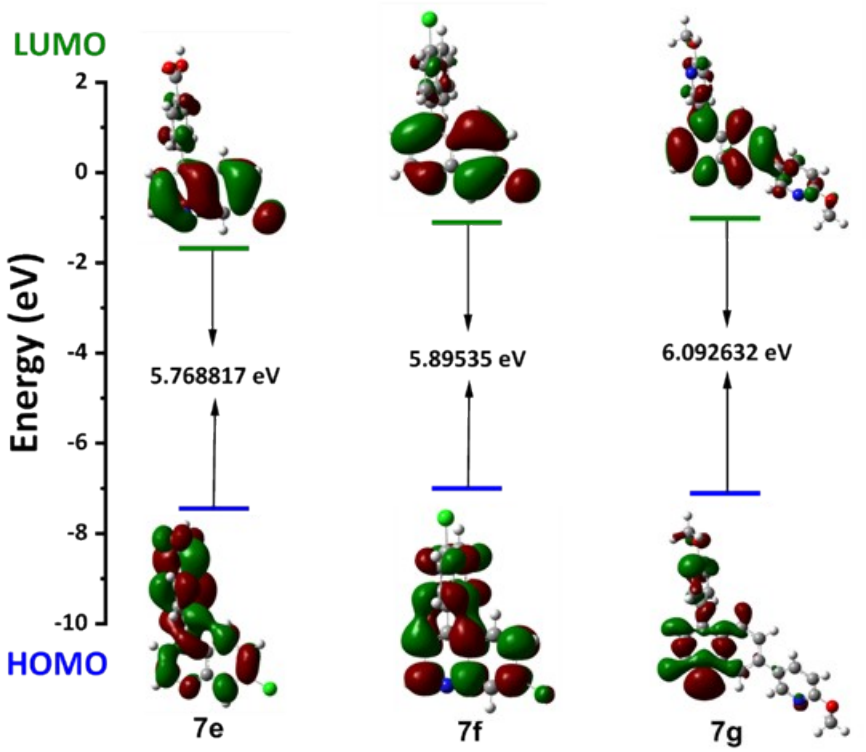


**Fig. S18** FMOs of (**7e-7f**).

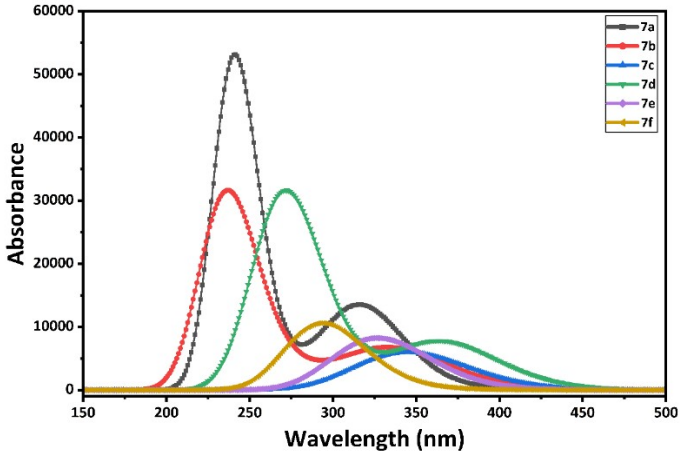


**Fig. S19** TD-DFT UV-Vis spectra of (**7a-7g**) molecules in the DMSO medium.

**Table S5** Calculated molecular electronic parameters of synthesized molecules.

| Compounds | Energy (Kcal/mol) | DM[a] | HOMO[b] (ev) | LUMO[c] (ev) | (ΔE)[d] (ev) | χ[e] (ev) | μ[f] (ev) | η[g] (ev) | S[h] (ev) | ω[i] (ev) |
|---|---|---|---|---|---|---|---|---|---|---|
| **3a** | -445661.52 | 2.6 | -7.12449 | -1.15512 | 5.969365 | 4.139805 | -4.13981 | 2.407125 | 0.415433 | 20.62664 |
| **3b** | -495004.89 | 2.9 | -7.12204 | -1.09199 | 6.030046 | 4.107015 | -4.10702 | 2.46903 | 0.405017 | 20.82327 |
| **3c** | -589377.40 | 1.7 | -7.11197 | -1.15186 | 5.960113 | 4.131915 | -4.13192 | 2.404125 | 0.415952 | 20.52248 |
| **3d** | -1022475.45 | 0.1 | -7.26354 | -0.74369 | 6.519851 | 4.003615 | -4.00362 | 2.88808 | 0.346251 | 23.14642 |
| **3e** | -540067.530 | 1.5 | -7.1136 | -1.02478 | 6.088823 | 4.06919 | -4.06919 | 2.53202 | 0.394942 | 20.96298 |
| **3f** | -587899.26 | 3.9 | -7.14435 | -2.17991 | 4.964448 | 4.66213 | -4.66213 | 1.392265 | 0.718254 | 15.13076 |
| **3g** | -1215293.21 | 0.7 | -7.45592 | -1.59894 | 5.856982 | 4.52743 | -4.52743 | 2.12902 | 0.4697 | 21.81992 |
| **3h** | -763256.56 | 0.1 | -7.15279 | -1.33118 | 5.821607 | 4.241985 | -4.24199 | 2.245215 | 0.445392 | 20.20069 |
| **3i** | -619560.19 | 6.7 | -7.2415 | -1.29472 | 5.946779 | 4.26811 | -4.26811 | 2.32603 | 0.429917 | 21.18637 |
| **3j** | -1997487.39 | 2.4 | -6.80911 | -1.31268 | 5.496431 | 4.060895 | -4.0609 | 2.091875 | 0.47804 | 17.24842 |
| **3k** | -470325.37 | 3.1 | -7.16639 | -0.77144 | 6.394951 | 3.968915 | -3.96892 | 2.811755 | 0.35565 | 22.14578 |
| **5a** | -397095.49 | 2.3 | -7.17837 | -0.95757 | 6.220798 | 4.06797 | -4.06797 | 2.631615 | 0.379995 | 21.77448 |
| **5b** | -421767.97 | 2.5 | -7.15796 | -0.91838 | 6.239574 | 4.03817 | -4.03817 | 2.6606 | 0.375855 | 21.69296 |
| **5c** | -468953.90 | 2.6 | -7.17782 | -0.95539 | 6.222431 | 4.066605 | -4.06661 | 2.63352 | 0.37972 | 21.77562 |
| **5d** | -685502.16 | 2.6 | -7.22109 | -1.08138 | 6.139710 | 4.151235 | -4.15124 | 2.529165 | 0.395387 | 21.79224 |
| **5e** | -468214.65 | 3.3 | -7.09701 | -1.64166 | 5.455341 | 4.369335 | -4.36934 | 1.906845 | 0.524426 | 18.20187 |
| **5f** | -781912.30 | 2.1 | -7.20939 | -0.8509 | 6.358488 | 4.030145 | -4.03015 | 2.753795 | 0.363135 | 22.36366 |
| **5g** | -555907.34 | 3.3 | -7.09701 | -0.97553 | 6.121477 | 4.03627 | -4.03627 | 2.572975 | 0.388655 | 20.95878 |
| **5h** | -484044.45 | 4.5 | -7.15143 | -1.06315 | 6.088279 | 4.10729 | -4.10729 | 2.512565 | 0.398 | 21.19327 |
| **5i** | -886765.89 | 0.5 | -7.25565 | -1.20166 | 6.053992 | 4.228655 | -4.22866 | 2.426165 | 0.412173 | 21.69176 |
| **5j** | -479020.50 | 2.3 | -7.20939 | -1.00655 | 6.202839 | 4.10797 | -4.10797 | 2.598145 | 0.38489 | 21.92239 |
| **7a** | -685516.28 | 5.9 | -7.28448 | -0.72817 | 6.088822 | 4.006325 | -4.00633 | 2.91407 | 0.343163 | 23.38634 |
| **7b** | **-710170.94** | **5.3** | **-7.28993** | **-0.42559** | **6.864348** | **3.85776** | **-3.85776** | **3.219375** | **0.310619** | **23.95587** |
| **7c** | -742763.60 | 2.3 | -7.11061 | -0.88328 | 6.227329 | 3.996945 | -3.99695 | 2.672025 | 0.374248 | 21.34356 |
| **7d** | -973905.89 | 2.5 | -7.25211 | -1.09444 | 6.157668 | 4.173275 | -4.17328 | 2.531615 | 0.395005 | 22.04559 |
| **7e** | -803825.81 | 3.4 | -7.44776 | -1.67894 | 5.768817 | 4.56335 | -4.56335 | 2.04494 | 0.489012 | 21.29208 |
| **7f** | -1070319.10 | 3.2 | -7.00095 | -1.1056 | 5.89535 | 4.053275 | -4.05328 | 2.394875 | 0.417558 | 19.67275 |
| **7g** | -656607.79 | 2.5 | -7.11007 | -1.01743 | 6.092632 | 4.06375 | -4.06375 | 2.537605 | 0.394072 | 20.95309 |

**Table S6** Comparison of experimental and theoretical excitation spectral details. *H-HOMO, L-LUMO

| Code | Experimental | Theoretical Prediction | | | |
|---|---|---|---|---|---|
| | Abs (nm) | Abs. max (nm) | Oscillator strength (ŧ) | Transition | Orbital Contribution |
| **3a** | 260 | 265 | 0.4095 | $S_0 \rightarrow S_4$ | H → L 49.9%, H+1 → L+1 45.4%, H-1 → L+1 4.7%. |
| **3b** | 255 | 268 | 0.4946 | $S_0 \rightarrow S_7$ | H → L 55%, H–2 → L 12%, H-2 → L 2.3%, H → L+1 8%. |
| **3c** | 252 | 271 | 0.5088 | $S_0 \rightarrow S_5$ | H-1 → L 61.7%, H-2 → L 30.7%, H-3 → L 0.0%, H-4 → L 5.2%, H → L+1 2.4%. |
| **3d** | 300 | 268 | 0.5490 | $S_0 \rightarrow S_3$ | H → L 72.2%, H-1 → L 14.7%, H-2 → L 5.3%, H → L+1 7.8%. |
| **3e** | 386 | 275 | 0.6481 | $S_0 \rightarrow S_5$ | H-2 → L+1 53.4%, H → L+1 25.0%, H-1 → L 18.6%, H-6 → L 3.0%. |
| **3f** | 294 | 247 | 0.4812 | $S_0 \rightarrow S_6$ | H-1 → L 89.9%, H-4 → L+1 3.9%, H-2 → L+1 3.2%, H-6 → L+1 3.0%. |
| **3g** | 272 | 228 | 0.5006 | $S_0 \rightarrow S_8$ | L+1 51.1%, H → L+1 25.7%, H-1 → L 20.0%, H-6 → L 3.3%. |
| **3h** | 320 | 266 | 0.6972 | $S_0 \rightarrow S_6$ | H-2 → L+1 53.5%, H-1 → L 28.9%, H → L+1 15.3%, H-8 → L 2.2%. |
| **3i** | 302 | 258 | 0.3974 | $S_0 \rightarrow S_5$ | H-1 → L 28%, H-2 → L 10%, H → L 2%, H-3 → L 3%. |
| **3j** | 275 | 256 | 0.5844 | $S_0 \rightarrow S_6$ | H-2 → L 33%, H-3 → L+1 6%, H-2 → L+1 2%, H-3 → L+4 4%. |
| **3k** | 258 | 246 | 0.6504 | $S_0 \rightarrow S_4$ | H → L 23%, H-2 → L 9%, H-1 → L 2%, H-1 → L+2 4%, H → L+1 2%. |
| **5a** | 255 | 281 | 0.4245 | $S_0 \rightarrow S_4$ | H-1 → L 22%, H-2 → L 8%, H → L 3%, H-4 → L 2%. |
| **5b** | 258 | 290 | 0.5411 | $S_0 \rightarrow S_5$ | H → L 33%, H-2 → L 11%, H-1 → L 1%, H-1 → L+1 2%, H → L+1 1%. |
| **5c** | 253 | 292 | 0.4868 | $S_0 \rightarrow S_6$ | H-1 → L 22%, H → L+1 13%, H-2 → L 8%, H → L 3%, H-4 → L 2%. |
| **5d** | 251 | 288 | 0.4103 | $S_0 \rightarrow S_3$ | H–3 → L 2%, H–1 → L 13%, H–2 → L 11%, H → L 21%. |
| **5e** | 269 | 265 | 0.6558 | $S_0 \rightarrow S_2$ | H → L 29%, H–2 → L 15%, H–1 → L 2%, H → L+1 1%, H–1 → L+1 2%. |
| **5f** | 272 | 282 | 0.3764 | $S_0 \rightarrow S_{12}$ | H → L+1 17%, H → L 11%, H-3 → L 5%, H-2 → L 2%, H-1 → L 2%, H-2 → L+1 9%, H-3 → L+1 2%. |
| **5g** | 300 | 230 | 0.6480 | $S_0 \rightarrow S_{10}$ | H-2 → L 27%, H → L 8%, H → L+1 5%, H-2 → L+1 6%, H-1 → L 2%. |
| **5h** | 259 | 268 | 0.3703 | $S_0 \rightarrow S_8$ | H →L 32%, H-2 → L 9%, H → L+1 4%, H → L+2 1%. |
| **5i** | 256 | 278 | 0.4583 | $S_0 \rightarrow S_5$ | H-1 → L 23%, H → L+1 9%, H-2 → L 8%, H → L+2 3%, H → L 2%, H-3 → L 2%. |
| **5j** | 255 | 248 | 0.5863 | $S_0 \rightarrow S_{10}$ | H-3 → L 43%, H-3 → L+1 4%, H-3 → L+2 1%, H-3 → L+5 1%. |
| **7a** | 262 | 245 | 0.5916 | $S_0 \rightarrow S_9$ | H → L+1 20%, H-2 → L 19%, H-4 → L 7%, H-3 → L 2%. |
| **7b** | 338 | 243 | 0.4666 | $S_0 \rightarrow S_{10}$ | H-3 → L 2%, H-2 → L 22%, H-1 → L 8%, H → L 17%. |
| **7c** | 248 | 338 | 0.4240 | $S_0 \rightarrow S_4$ | H → L 44%, H-1 → L 1%, H → L+2 1%. |
| **7d** | 250 | 286 | 0.5473 | $S_0 \rightarrow S_7$ | H → L 39%, H-3 → L 4%, H → L+1 2%, H-1 → L 1%, H-3 → L+1 1%. |
| **7e** | 258 | 278 | 0.5157 | $S_0 \rightarrow S_3$ | H → L 48%, H-2 → L 1%. |
| **7f** | 251 | 298 | 0.6959 | $S_0 \rightarrow S_4$ | H-3 → L 25%, H-1 → L 19%, H-2 → L 1%, H → L 1%. |
| **7g** | 295 | 218 | 0.5049 | $S_0 \rightarrow S_3$ | H → L 27%, H-2 → L 18%, H-1 → L 2%, H-3 → L 1%. |

### 3.9. Photophysical studies

The UV-Vis absorption spectra for all synthesized molecules (**3a-3k**, **5a-5j**, and **7a-7g**) were determined in DMSO at a concentration of $2 \times 10^{-5}$ M at room temperature. Overall, the absorption bands of these compounds ranged from 200-500 nm. The experimental spectra displayed distinct absorption features, with compound **3e** exhibiting a high absorbance of 386 nm and compound **7c** displaying a lower absorbance of 248 nm. The experimental and theoretical UV-Vis spectra were obtained from TD-DFT calculations and were compared. The experimentally measured wavelengths and the theoretical wavelengths were highlighted in

Figures S9, S14, S18, and Table S4. All synthesized compounds **3a-k**, **5a-j**, and **7a-g** exhibited UV-Vis absorption values that closely matched the theoretical absorption band values, as represented in Table S4. The calculated theoretical and experimental absorption wavelengths, oscillator strengths, and energy values.

Furthermore, all compounds were subjected to fluorescence studies, and most exhibited favorable fluorescence emission within the range of 300-600 nm, as displayed in Figures S22, S23, and S24, and in Table S5. The introduction of various aryl and heteroaryl groups at the 3,5-diphenylpyridine, 3-phenylquinoline, and 7-chloro-4-phenylquinoline moieties resulted in notable differences in the intensity of absorption and emission spectra, despite exhibiting similar absorption and fluorescence maxima, as illustrated in Figures S9, S14, S18, S22, S23, and S24. The molecules **5d**, **7d**, and **7f**, chloro-substituted compounds, displayed the lowest blue-shifted emission maxima at 251, 251, and 250 nm. In contrast, compounds **3b** and **7b**, which incorporated methyl and hydroxy groups, displayed red-shifted emission maxima at 386 and 338 nm, respectively. This red shift was attributed to the electronic effects of the substituents.

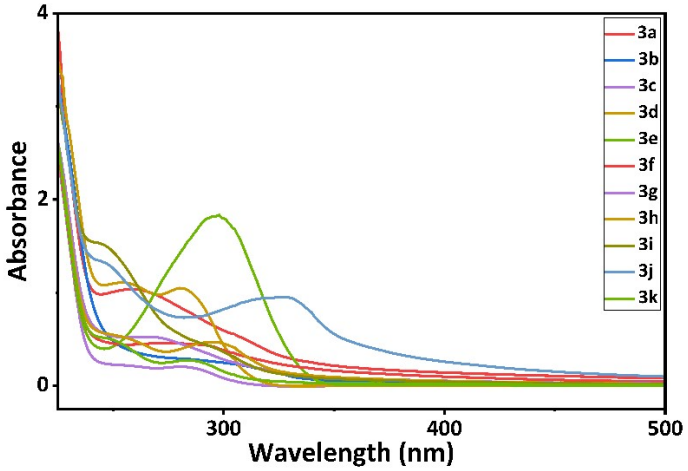


**Fig. S20** UV-Vis spectra of (**3a-3l**) molecules in the DMSO medium.

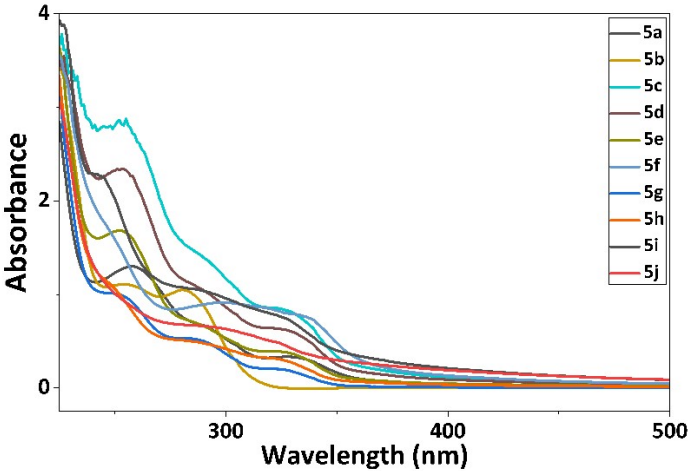


**Fig. S21** UV-Vis spectra of (**5a-5j**) molecules in the DMSO medium.

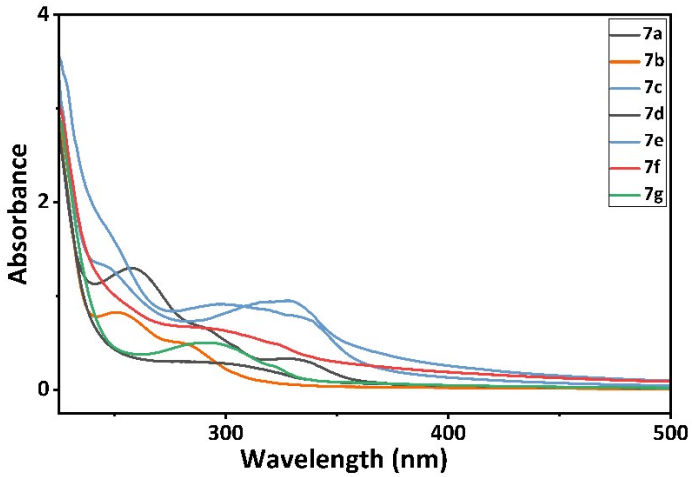


**Fig. S22** UV-Vis spectra of (**7a-7g**) molecules in the DMSO medium.

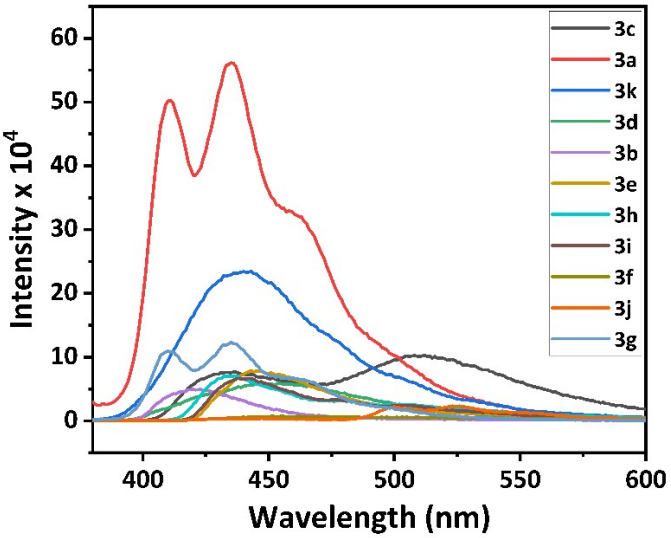


**Fig. S23** Fluorescence spectra of (**3a-3l**) molecules in the DMSO medium.

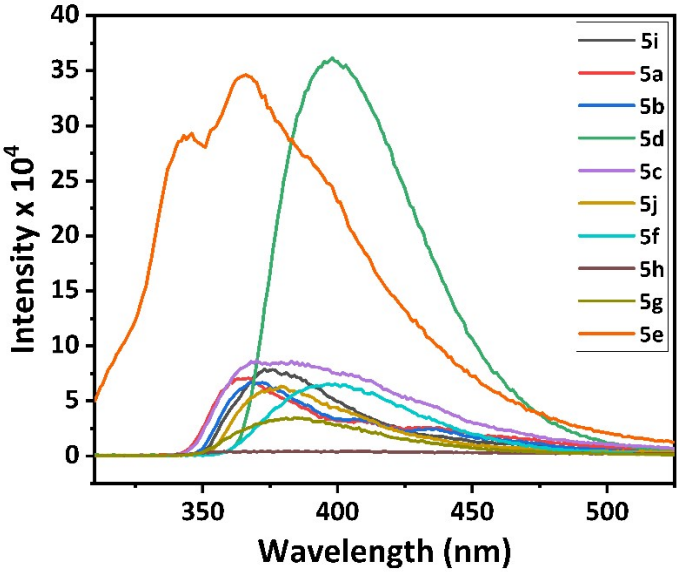


**Fig. S24** Fluorescence spectra of (**5a-5j**) molecules in the DMSO medium.

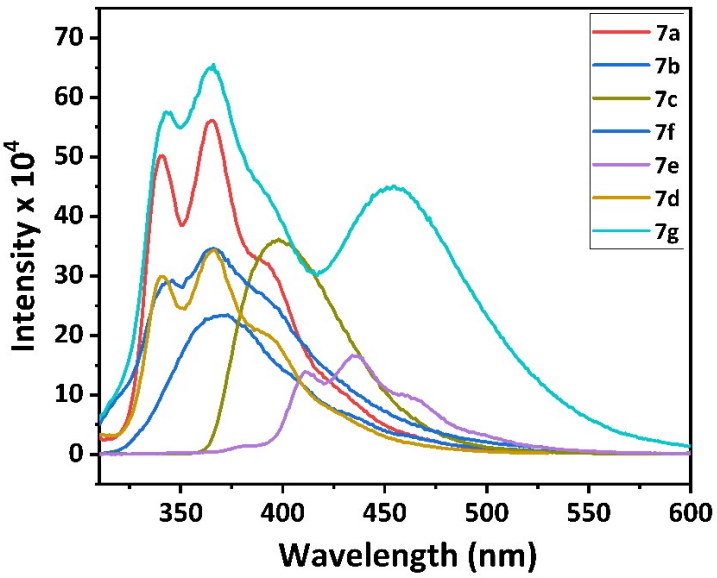


**Fig. S25** Fluorescence spectra of (**7a-7g**) molecules in the DMSO medium.

**Table S7** Photophysical characterization of all molecules: [a] Absorption maxima; [b] Wavelength of Emission spectra; [c] Stokes shift; [d] Optical density; [e] Extinction coefficient; and [f] Quantum yield.

| Molecules | $\lambda_{max}$ [a] (nm) | Energy ev | $\lambda_f$ [b] (nm) | Stoke's shift [c] | OD [d] | $\varepsilon$ [e] ($M^{-1}cm^{-1}$) | ($\phi_f$) [f] |
|---|---|---|---|---|---|---|---|
| **3a** | 260 | 4.76 | 371 | 111 | 1.7 | 85000 | 0.022354421 |
| **3b** | 255 | 4.86 | 398 | 143 | 1.6 | 80000 | 0.022140285 |
| **3c** | 252 | 4.92 | 378 | 126 | 1.7 | 85000 | 0.02194045 |
| **3d** | 300 | 4.13 | 386 | 86 | 2.8 | 140000 | 0.013044905 |
| **3e** | 386 | 3.21 | 365 | 21 | 1.5 | 75000 | 0.025751476 |
| **3f** | 294 | 4.21 | 410 | 116 | 2.7 | 135000 | 0.012736164 |
| **3g** | 272 | 4.55 | 397 | 125 | 2.3 | 115000 | 0.015440733 |
| **3h** | 320 | 3.87 | 385 | 65 | 2.2 | 110000 | 0.01664573 |
| **3i** | 302 | 4.10 | 380 | 78 | 1.9 | 95000 | 0.019527608 |
| **3j** | 275 | 4.50 | 387 | 112 | 2.2 | 110000 | 0.016559706 |
| **3k** | 258 | 4.80 | 436 | 178 | 2.4 | 120000 | 0.013473751 |
| **5a** | 255 | 4.86 | 435 | 180 | 2.3 | 115000 | 0.014091887 |
| **5b** | 258 | 4.80 | 435 | 177 | 3.3 | 165000 | 0.009821618 |
| **5c** | 253 | 4.90 | 371 | 118 | 2.3 | 115000 | 0.016522833 |
| **5d** | 251 | 4.94 | 434 | 183 | 2.4 | 120000 | 0.013535842 |
| **5e** | 269 | 4.60 | 371 | 102 | 2.0 | 100000 | 0.019001258 |
| **5f** | 272 | 4.55 | 439 | 167 | 1.9 | 95000 | 0.016903169 |
| **5g** | 300 | 4.13 | 351 | 51 | 2.3 | 115000 | 0.017464305 |

| | | | | | | | |
|---|---|---|---|---|---|---|---|
| **5h** | 259 | 4.78 | 431 | 172 | 3.2 | 160000 | 0.010222544 |
| **5i** | 256 | 4.84 | 436 | 180 | 2.4 | 120000 | 0.013473751 |
| **5j** | 255 | 4.86 | 356 | 101 | 2.3 | 115000 | 0.01721902 |
| **7a** | 262 | 4.73 | 362 | 100 | 1.9 | 95000 | 0.020498595 |
| **7b** | 338 | 3.66 | 338 | 18 | 1.5 | 75000 | 0.026402497 |
| **7c** | 248 | 5.02 | 428 | 180 | 0.8 | 40000 | 0.041176791 |
| **7d** | 250 | 4.96 | 436 | 186 | 2.3 | 115000 | 0.014059567 |
| **7e** | 258 | 4.80 | 434 | 176 | 1.8 | 90000 | 0.01804779 |
| **7f** | 251 | 4.94 | 434 | 183 | 1.3 | 65000 | 0.024989247 |
| **7g** | 295 | 4.20 | 435 | 140 | 1.3 | 65000 | 0.024931801 |

## 3.10 Cancer studies

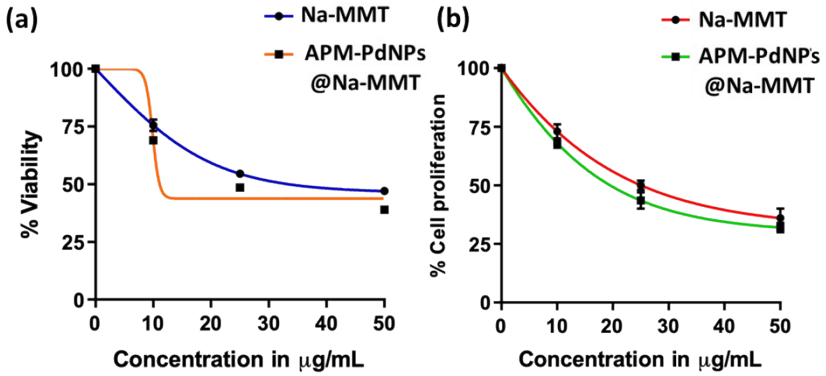


**Fig. S26** Effect of Na-MMT and APM-PdNPs@Na-MMT against Normal Kidney (Hek) cells (a) MTT analysis of Na-MMT and APM-PdNPs@Na-MMT against Normal Kidney (Hek) cells, and (b) Trypan blue dye exclusion analysis of Na-MMT and APM-PdNPs@Na-MMT against Normal Kidney (Hek) cells.

## 3.11 Literature comparison of anticancer activity of Pd-based nanomaterials

**Table S8** Comparison of anticancer activity of biogenic and clay Pd-based nanomaterials

| Entry | Catalyst / Nanomaterial | Synthesis source | Cancer cell line | Key anticancer results | Ref. |
|---|---|---|---|---|---|
| 1 | Biogenic PdNPs (CGPdNPs) | Couroupita guianensis fruit extract | A549 lung cancer cells | Exhibited strong cytotoxic activity toward lung cancer cells in the MTT assay while maintaining good hemocompatibility | [9] |
| 2 | Green-synthesized PdNPs | Urtica plant extract | MDA-MB-231 (breast), HT-29 (colon), MIA-PaCa-2 (pancreatic) | $IC_{50}$ values of 31.17, 20.38, and 29.33 μg $mL^{-1}$, respectively; minimal toxicity toward healthy L929 fibroblast cells | [10] |
| 3 | Biogenic PdNPs | Agaricus bisporus mushroom extract | PK13 cell line | Maximum 79% growth inhibition with $IC_{50}$ ≈ 26.1 μg $mL^{-1}$, demonstrating strong cytotoxic potential | [11] |

| | | | | | |
|---|---|---|---|---|---|
| 4 | Neem gum-coated PdNPs (NG@Pd NPs) | Orthosiphon stamineus leaf extract + neem gum coating | A549 lung cancer cells | Showed dose-dependent antiproliferative activity, with ~50% inhibition at ~45.6 µg $mL^{-1}$ and ROS-mediated apoptosis | [12] |
| 5 | PdNPs biosynthesized using propolis | Saudi propolis extract | MCF-7 breast cancer cells | Demonstrated significant anticancer activity with $IC_{50}$ ≈ 104.79 µg $mL^{-1}$ | [13] |
| 6 | Kaolin@CS-Pectin/Pd nanocomposite | Chitosan-pectin modified kaolin support | NCI-H661, NCI-H1563, NCI-H1299 lung cancer cells | Exhibited cytotoxic effects with $IC_{50}$ values 66-85 µg $mL^{-1}$, indicating potential anticancer activity | [14] |
| **7** | **APM-PdNPs@Na-MMT** | **Acacia pachyceras leaf extract** | **HCT116 colon cancer cells** | **Selective cytotoxicity toward HCT116 cells while showing minimal toxicity toward normal HEK cells** | **This work** |

## 4. Spectroscopic data of newly obtained Products

### 4.1. 3,5-diphenylpyridines [15]

### 3,5-diphenylpyridine (3a)

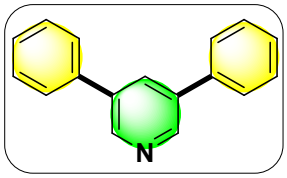


Purified by column chromatography (10% ethyl acetate in hexane), Pale pink solid. $^1$H NMR (400 MHz, $CDCl_3$, δ) 8.81 (d, *J* = 2.0 Hz, 2H, Ar H), 8.04 (d, *J* = 2.2 Hz, 1H, Ar H), 7.65-7.62 (m, 4H, Ar H), 7.49 (t, *J* = 7.6 Hz, 4H, Ar H), 7.44-7.40 (m, 2H, Ar H). $^{13}$C NMR (100 MHz, $CDCl_3$, δ) 147, 137.8, 136.7, 133, 129.2, 128.3, 127.3.

### 3,5-di-p-tolylpyridine (3b)

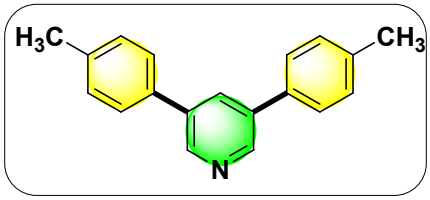


Purified by column chromatography (8% ethyl acetate in hexane), Pale pink crystalline solid. $^1$H NMR (400 MHz, $CDCl_3$, δ) 8.78 (d, *J* = 2.4 Hz, 2H, Ar H), 8.00 (t, *J* = 2.0 Hz, 1H, Ar H), 7.53 (d, *J* = 8.4 Hz, 4H, Ar H), 7.30 (d, *J* = 8.0 Hz, 4H, Ar H), 2.41 (s, 6H; $CH_3$). $^{13}$C NMR (100 MHz, $CDCl_3$, δ) 146.6, 138.2, 136.5, 135, 132.5, 129.9, 127.1, 21.2 ($CH_3$).

### 3,5-bis(4-methoxyphenyl) pyridine (3c)

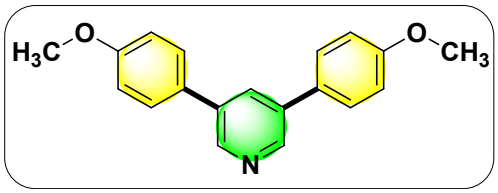


Purified by column chromatography (13 % ethyl acetate in hexane), Pale yellow solid. $^1$H NMR (400 MHz, $CDCl_3$, δ) 8.71 (d, *J* = 2.0 Hz, 2H, Ar H), 7.95 (t, *J* = 2.2 Hz, 1H, Ar H), 7.57-7.54 (m, 4H, Ar H), 7.03-6.99 (m, 4H, Ar H), 3.85 (s, 6H; $CH_3$). $^{13}$C NMR (100 MHz, $CDCl_3$, δ) 159.9, 145.9, 136.3, 132.1, 130.2, 128.4, 114.6, 55.4 ($CH_3$).

### 3,5-bis(4-chlorophenyl) pyridine (3d)

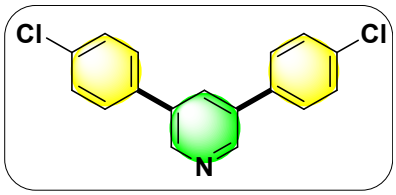


Purified by column chromatography (8% ethyl acetate in hexane), White solid. $^1$H NMR (400 MHz, $CDCl_3$, δ) 8.84 (s, 2H, Ar H), 7.97 (t, *J* = 13.0 Hz, 2H, Ar H), 7.55-7.34 (m, 8H, Ar H). $^{13}$C NMR (100 MHz, $CDCl_3$, δ) 145.7, 136.3, 135.5, 135.1, 135, 133.5, 129.6, 128.5, 128.

**4,4'-(pyridine-3,5-diyl) diphenol (3e)**

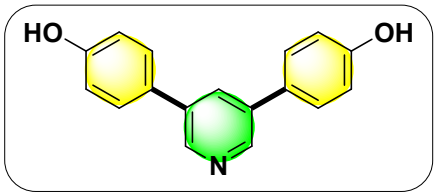


Purified by column chromatography (23% ethyl acetate in hexane), White solid. $^{1}$H NMR (400 MHz, $CDCl_3$, δ) 7.29-7.25 (m, 3H, Ar H), 7.13-7.01 (m, 6H, Ar H), 6.83-6.80 (m, 2H, Ar H), 6.41-6.35 (m, 2H, Ar H). $^{13}$C NMR (100 MHz, $CDCl_3$, δ) 156.9, 155.9, 142.5, 130.5, 130, 119.7, 114.5, 114.1, 108, 103.

**4,4'-(pyridine-3,5-diyl) di benzaldehyde (3f)**

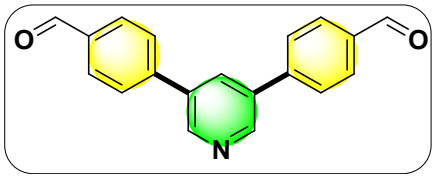


Purified by column chromatography (17% ethyl acetate in hexane), Pale pink solid. $^{1}$H NMR (400 MHz, $CDCl_3$, δ) 10.06 (s, 2H; CHO), 8.73 (d, *J* = 32.4 Hz, 2H, Ar H), 8.05 (t, *J* = 2.0 Hz, 2H, Ar H), 7.99-7.96 (m, 4H, Ar H), 7.78-7.70 (m, 4H, Ar H). $^{13}$C NMR (100 MHz, $CDCl_3$, δ) 191.6 (CHO), 150.5, 146.4, 145.6, 142.1, 137.2, 136.3, 136, 130.5, 130.4, 128.1, 127.9.

**3,5-bis(4-chloronaphthalen-1-yl)pyridine (3 g)**

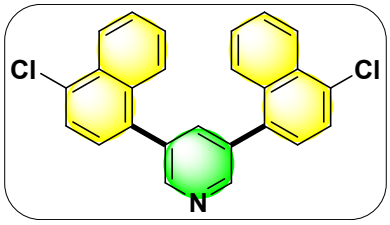


Purified by column chromatography (5% ethyl acetate in hexane), White solid. $^{1}$H NMR (400 MHz, $CDCl_3$, δ) 8.81 (d, *J* = 2.0 Hz, 2H, Ar H), 8.40-8.37 (m, 2H, Ar H), 7.94-7.89 (m, 3H, Ar H), 7.68-7.63 (m, 4H, Ar H), 7.58-7.53 (m, 2H, Ar H), 7.42 (d, *J* = 7.6 Hz, 2H, Ar H). $^{13}$C NMR (100 MHz, $CDCl_3$, δ) 149.5, 138.7, 135.4, 135.2, 132.7, 132.6, 131.1, 127.5, 127.4, 125.8, 125.1.

**3,5-bis(2-ethoxy-4-fluorophenyl) pyridine (3h)**

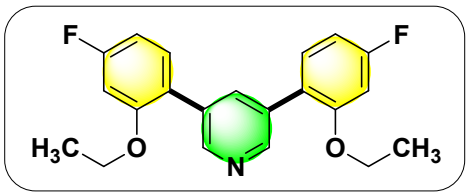


Purified by column chromatography (11% ethyl acetate in hexane), Pale yellow solid. $^{1}$H NMR (400 MHz, $CDCl_3$, δ) 8.68 (d, *J* = 2.4 Hz, 2H, Ar H), 7.90 (t, *J* = 2.0 Hz, 2H, Ar H), 7.31-7.27 (m, 2H, Ar H), 6.76-6.69 (m, 4H, Ar H), 4.04 (q, *J* = 21.2 Hz, 4H; $CH_2$), 1.37 (t, *J* = 7.0 Hz, 6H; $CH_3$). $^{13}$C NMR (100 MHz, $CDCl_3$, δ) 164.8, 162.3, 157.2, 157.1, 148.4, 137.4, 132.9, 132.6, 131.5, 131.4, 123.3, 123.2, 107.5, 107.3, 100.6, 100.4, 64.4 ($CH_2$), 14.6 ($CH_3$). $^{19}$F NMR (376 MHz, $CDCl_3$, δ) -110.91-(-110.98) (m, 1F).

**3,5-bis(2-fluoro-5-methylphenyl) pyridine (3i)**

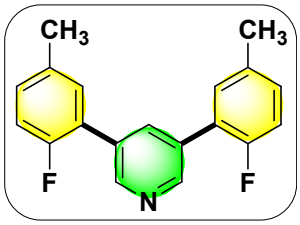


Purified by column chromatography (8% ethyl acetate in hexane), Orange solid. $^{1}$H NMR (400 MHz, $CDCl_3$, δ) 8.76 (s, 2H, Ar H), 8.02 (s, 1H, Ar H), 7.28-7.25 (m, 2H, Ar H), 7.18-7.15 (m, 2H, Ar H), 7.07 (dd, *J* = 10.4, 8.4 Hz, 2H, Ar H), 2.38 (s, 6H; $CH_3$). $^{13}$C NMR (100 MHz, $CDCl_3$, δ) 159.4, 156.9, 148.4, 136.6, 134.2, 131.0, 130.9, 130.6, 130.5, 125, 124.9, 116.1, 115.9, 20.7 ($CH_3$). $^{19}$F NMR (376 MHz, $CDCl_3$, δ) -112.98-(-123.04) (m, 1F).

**5-bromo-6'-methoxy-3,3'-bipyridine (3j)**

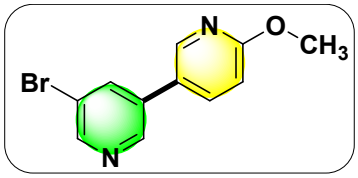


Purified by column chromatography (45% ethyl acetate in hexane), White solid. $^{1}$H NMR (400 MHz, $CDCl_3$, δ) 8.78 (d, *J* = 2.0 Hz, 1H, Ar H), 8.63 (d, *J* = 2.0 Hz, 1H, Ar H), 8.35 (dd, *J* = 2.6, 0.6 Hz, 1H, Ar H), 7.94 (t, *J* = 2.0 Hz, 1H, Ar H), 7.73 (dd, *J* = 8.6, 2.6 Hz, 1H, Ar H), 3.97 (s, 3H; $CH_3$). $^{13}$C NMR (100 MHz, $CDCl_3$, δ) 164.5, 149.5, 145.9, 145.3, 137.3, 136.4, 135.3, 125.3, 121.1, 111.5, 53.8 ($CH_3$).

**4-methyl-3,5-diphenylpyridine (3k)**

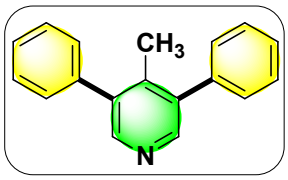


Purified by column chromatography (13% ethyl acetate in hexane), Pale orange solid. $^{1}$H NMR (400 MHz, $CDCl_3$, δ) 8.42 (s, 2H, Ar H), 7.48-7.34 (m, 10H, Ar H), 2.16 (s, 3H; $CH_3$). $^{13}$C NMR (100 MHz, $CDCl_3$) δ 148.7, 142.4, 138.2, 129.5, 128.5, 127.7, 18 ($CH_3$).

**4.2. 3-phenylquinolines** [16-18]

**3-phenylquinoline (5a)**

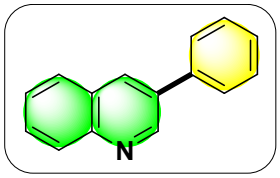


Purified by column chromatography (11% ethyl acetate in hexane), Orange solid. $^{1}$H NMR (400 MHz, $CDCl_3$, δ) 9.17 (d, *J* = 1.6 Hz, 1H, Ar H), 8.23 (d, *J* = 2.0 Hz, 1H, Ar H), 8.14 (d, *J* = 8.4 Hz, 1H, Ar H), 7.82 (t, *J* = 8.4 Hz, 1H, Ar H), 7.71-7.65 (m, 3H, Ar H), 7.55-7.46 (m, 3H, Ar H), 7.42-7.38 (m, 1H, Ar H). $^{13}$C NMR (100 MHz, $CDCl_3$, δ) 149.9, 147.3, 137.9, 133.9, 133.3, 129.5, 129.2, 128.2, 128.1, 127.5, 127.1.

**3-(p-tolyl) quinoline (5b)**

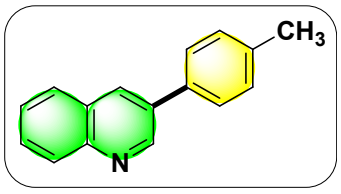


Purified by column chromatography (12% ethyl acetate in hexane), Orange solid. $^{1}$H NMR (400 MHz, $CDCl_3$, δ) 9.16 (d, *J* = 2.4 Hz, 1H, Ar H), 8.21 (d, *J* = 3.6 Hz, 1H, Ar H), 8.13 (d, *J* = 8.8 Hz, 1H, Ar H), 7.81 (d, *J* = 9.2 Hz, 1H, Ar H), 7.69-7.65 (m, 1H, Ar H), 7.58-7.50 (m, 3H, Ar H), 7.28 (d, *J* = 8.8 Hz, 2H, Ar H), 2.39 (s, 3H; $CH_3$). $^{13}$C NMR (100 MHz, $CDCl_3$, δ) 149.9, 147.1, 138.1, 134.9, 133.8, 132.9, 129.9, 129.3, 129.1, 128.1, 128, 127.2, 127, 21.2 ($CH_3$).

**3-(4-methoxyphenyl) quinoline (5c)**

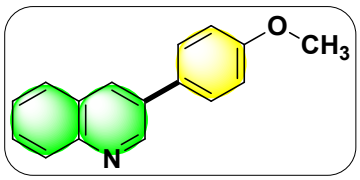


Purified by column chromatography (12% ethyl acetate in hexane), Orange solid. $^{1}$H NMR (400 MHz, $CDCl_3$, δ) 9.12 (d, *J* = 2.4 Hz, 1H, Ar H), 8.12 (dd, *J* = 13.6, 6.4 Hz, 2H, Ar H), 7.74 (dd, *J* = 8.2, 1.8 Hz, 1H, Ar H), 7.64-7.45 (m, 1H, Ar H), 6.97-6.93 (m, 2H, Ar H), 3.77 (s, 3H; $CH_3$). $^{13}$C NMR (100 MHz, $CDCl_3$, δ) 159.9, 149.3, 146.4, 138.1, 133.5, 132.7, 129.9, 129.3, 128.5, 128.4, 128.2, 127.9, 127.1, 114.7, 55.3 ($CH_3$).

**3-(4-chlorophenyl) quinoline (5d)**

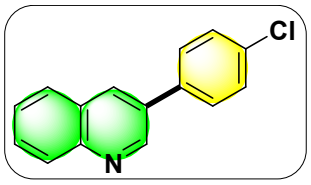


Purified by column chromatography (18% ethyl acetate in hexane), Yellow solid. $^{1}$H NMR (400 MHz, $CDCl_3$, δ) 9.08 (d, *J* = 2.0 Hz, 1H, Ar H), 8.17 (d, *J* = 2.0 Hz, 1H, Ar H), 8.11 (d, *J* = 8.4 Hz, 1H, Ar H), 7.79 (dd, *J* = 8.2, 1.4 Hz, 1H, Ar H), 7.70-7.66 (m, 1H, Ar H), 7.57-7.50 (m, 3H, Ar H), 7.44-7.40 (m, 2H, Ar H). $^{13}$C NMR (100 MHz, $CDCl_3$, δ) 149.5, 147.5, 136.3, 134.4, 133.1, 132.6, 129.6, 129.3, 128.6, 128, 127.2.

**4-(quinolin-3-yl) benzaldehyde (5e)**

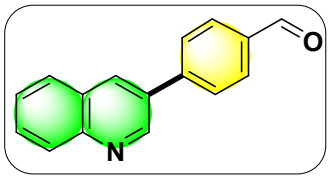


Purified by column chromatography (22% ethyl acetate in hexane), Yellow solid. $^{1}$H NMR (400 MHz, $CDCl_3$, δ) 10.08 (s, 1H; CHO), 9.19 (d, *J* = 2.4 Hz, 1H, Ar H), 8.37 (d, *J* = 2.4 Hz, 1H, Ar H), 8.16 (d, *J* = 8.8 Hz, 1H, Ar H), 8.03-8.00 (m, 2H, Ar H), 7.91-7.85 (m, 3H, Ar H), 7.77-7.73 (m, 1H, Ar H), 7.62-7.58 (m, 1H, Ar H). $^{13}$C NMR (100 MHz, $CDCl_3$, δ) 191.7 (CHO), 174.2, 163.4, 149.2, 147.5, 143.7, 135.8, 134.3, 132.5, 130.6, 130.3, 129, 128.3, 128, 127.9, 127.5, 116.2.

**3-(4-chloronaphthalen-1-yl) quinoline (5f)**

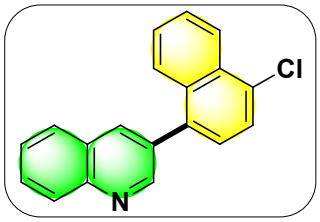


Purified by column chromatography (11% ethyl acetate in hexane), Orange solid. $^{1}$H NMR (400 MHz, $CDCl_3$, δ) 9.02 (d, *J* = 2.4 Hz, 1H; Ar H), 8.37 (d, *J* = 9.2 Hz, 1H, Ar H), 8.22-8.18 (m, 2H, Ar H), 7.85-7.73 (m, 3H, Ar H), 7.64-7.45 (m, 4H, Ar H), 7.37 (d, *J* = 8.0 Hz, 1H, Ar H). $^{13}$C NMR (100 MHz, $CDCl_3$, δ) 151.7, 151.4, 147.4, 137.2, 136.5, 135.7, 133, 132.8, 132.5, 131.1, 129.9, 129.4, 128, 127.6, 127.4, 127.3, 126, 125.8, 125.1.

**3-(2-ethoxy-4-fluorophenyl) quinoline (5g)**

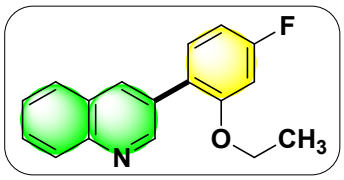


Purified by column chromatography (12% ethyl acetate in hexane), Pale orange solid. $^{1}$H NMR (400 MHz, $CDCl_3$, δ) 9.08 (d, *J* = 2.0 Hz, 1H, Ar H), 8.18 (d, *J* = 2.0 Hz, 1H, Ar H), 8.11 (d, *J* = 8.4 Hz, 1H, Ar H), 7.80 (d, *J* = 8.0 Hz, 1H, Ar H), 7.70-7.66 (m, 1H, Ar H), 7.53-7.49 (m, 1H, Ar H), 7.35-7.31 (m, 1H, Ar H), 6.78-6.70 (m, 2H, Ar H), 4.02 (q, *J* = 7.2 Hz, 2H; $CH_2$), 1.33 (t, *J* = 6.8 Hz, 3H; $CH_3$). $^{13}$C NMR (100 MHz, $CDCl_3$, δ) 164.9, 162.4, 157.3, 157.2, 151.9, 146.7, 135.5, 131.8, 131.7, 131.2, 129.3, 129.1, 127.9, 126.7, 123.2, 107.7, 107.5, 100.6, 100.3, 77.5, 77.1, 76.8, 64.4 ($CH_2$), 14.5 ($CH_3$). $^{19}$F NMR (376 MHz, $CDCl_3$, δ) -110.46-(-110.53) (m, 1F).

**3-(2-fluoro-5-methylphenyl) quinoline (5h)**

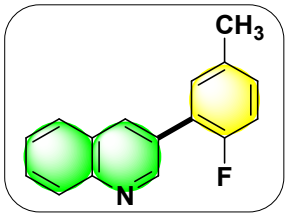


Purified by column chromatography (12% ethyl acetate in hexane), Yellow solid. $^{1}$H NMR (400 MHz, $CDCl_3$, δ) 9.09 (s, 1H, Ar H), 8.29 (s, 1H, Ar H), 8.13 (d, *J* = 8.4 Hz, 1H, Ar H), 7.84 (d, *J* = 8.0 Hz, 1H, Ar H), 7.74-7.69 (m, 1H, Ar H), 7.58-7.53 (m, 1H, Ar H), 7.32 (d, *J* = 7.2 Hz, 1H, Ar H), 7.18-7.06 (m, 2H, Ar H), 2.39 (s, 3H; $CH_3$). $^{13}$C NMR (100 MHz, $CDCl_3$, δ) 159.5, 157.1, 150.8, 147.2, 135.6, 134.3, 131.1, 130.5, 130.4, 129.7, 129.2, 128.1, 127.8, 127, 125.3, 125.2, 20.80 ($CH_3$). $^{19}$F NMR (376 MHz, $CDCl_3$, δ) -122.94-(-123) (m, 1F).

**3-(2-chlorothiophen-3-yl) quinoline (5i)**

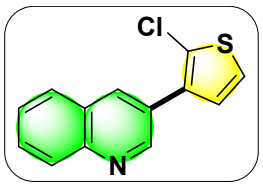


Purified by column chromatography (16% ethyl acetate in hexane), Yellow solid. $^{1}$H NMR (400 MHz, $CDCl_3$, δ) 9.11 (d, *J* = 1.6 Hz, 1H, Ar H), 8.37 (d, *J* = 1.6 Hz, 1H, Ar H), 8.15 (d, *J* = 8.4 Hz, 1H, Ar H), 7.87 (d, *J* = 8.4 Hz, 1H, Ar H), 7.76-7.72 (m, 1H, Ar H), 7.60-7.56 (m, 1H, Ar H), 7.26-7.24 (m, 1H, Ar H), 7.18 (d, *J* = 5.6 Hz, 1H, Ar H). $^{13}$C NMR (100 MHz, $CDCl_3$, δ) 150.2, 135.3, 134.9, 129.9, 129, 128.1, 128, 127.2, 123.6.

**3-(6-methoxypyridin-3-yl) quinoline (5j)**

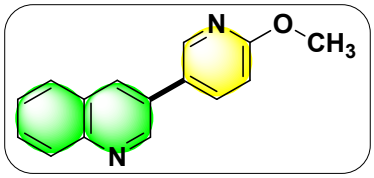


Purified by column chromatography (22% ethyl acetate in hexane), Pale orange solid. $^{1}$H NMR (400 MHz, $CDCl_3$, δ) 9.03 (d, *J* = 2.0 Hz, 1H, Ar H), 8.43 (dd, *J* = 2.6, 0.6 Hz, 1H, Ar H), 8.12 (d, *J* = 2.4 Hz, 1H, Ar H), 8.06 (d, *J* = 8.8 Hz, 1H, Ar H), 7.81-7.75 (m, 2H, Ar H), 7.65-7.61 (m, 1H, Ar H), 7.50-7.46 (m, 1H, Ar H), 6.80 (dd, *J* = 8.6, 0.6 Hz, 1H, Ar H), 3.93 (s, 3H; $CH_3$). $^{13}$C NMR (100 MHz, $CDCl_3$, δ) 164.1, 149.2, 147.2, 145.4, 137.4, 132.6, 130.7, 129.5, 129.2, 127.9, 127.2, 126.8, 111.3, 53.7 ($CH_3$).

**4.3. 7-chloro-4-phenylquinolines** [19]

**7-chloro-4-phenylquinoline (7a)**

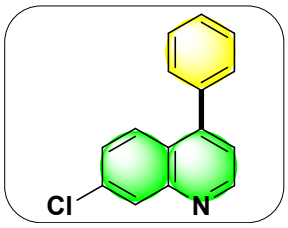


Purified by column chromatography (11% ethyl acetate in hexane), Brown gel. $^{1}$H NMR (400 MHz, $CDCl_3$, δ) 8.93 (d, *J* = 4.8 Hz, 1H, Ar H), 8.21 (d, *J* = 2.0 Hz, 1H, Ar H), 7.54-7.44 (m, 6H, Ar H), 7.35 (d, *J* = 4.8 Hz, 1H, Ar H). $^{13}$C NMR (100 MHz, $CDCl_3$, δ) 151, 150.4, 137.3, 129.5, 129.2, 128.9, 128.8, 128.7, 128.2, 127.5, 125.7, 121.5.

**7-chloro-4-(p-tolyl) quinoline (7b)**

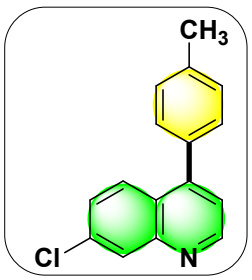


Purified by column chromatography (9% ethyl acetate in hexane), Pale orange gel. $^{1}$H NMR (400 MHz, $CDCl_3$, δ) 8.90 (d, *J* = 4.4 Hz, 1H, Ar H), 8.17 (d, *J* = 2.0 Hz, 1H, Ar H), 7.88 (d, *J* = 8.8 Hz, 1H, Ar H), 7.38-7.32 (m, 4H, Ar H), 7.01 (d, *J* = 8.4 Hz, 1H, Ar H), 6.75 (d, *J* = 8.0 Hz, 1H, Ar H), 2.45 (s, 3H; $CH_3$). $^{13}$C NMR (100 MHz, $CDCl_3$, δ) 153.9, 150.8, 149.1, 148.9, 138.8, 135.5, 134.5, 130.1, 129.5, 129.4, 128.4, 127.7, 127.5, 125.4, 121.5, 115.2, 21.3 ($CH_3$).

**7-chloro-4-(4-methoxyphenyl) quinoline (7c)**

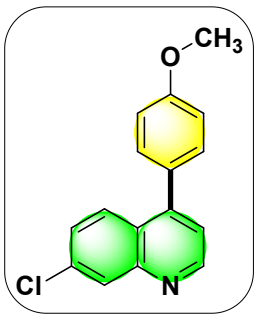


Purified by column chromatography (12% ethyl acetate in hexane), Pale orange gel. $^{1}$H NMR (400 MHz, $CDCl_3$, δ) 8.89 (d, *J* = 4.4 Hz, 1H, Ar H), 8.15 (d, *J* = 2.0 Hz, 1H, Ar H), 7.89 (d, *J* = 9.2 Hz, 1H, Ar H), 7.45-7.40 (m, 3H, Ar H), 7.30 (d, *J* = 4.4 Hz, 1H, Ar H), 7.05 (dd, *J* = 6.6, 2.5 Hz, 1H, Ar H), 6.78 (d, *J* = 3.0 Hz, 1H, Ar H), 3.89 (s, 3H; $CH_3$). $^{13}$C NMR (100 MHz, $CDCl_3$, δ) 160.2, 150.8, 149, 148.6, 135.4, 130.8, 129.7, 128.5, 127.6, 127.5, 125.5, 121.5, 116.2, 114.9, 114.3, 55.5 ($CH_3$).

**7-chloro-4-(4-chlorophenyl) quinoline (7d)**

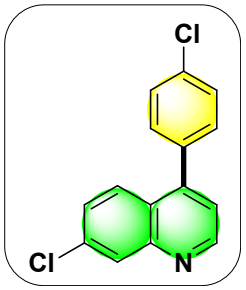


Purified by column chromatography (12% ethyl acetate in hexane), Orange gel. $^{1}$H NMR (400 MHz, $CDCl_3$, δ) 8.92 (d, *J* = 4.4 Hz, 1H, Ar H), 8.18 (d, *J* = 2.4 Hz, 1H, Ar H), 7.78 (q, *J* = 9.0 Hz, 1H, Ar H), 7.52-7.40 (m, 4H, Ar H), 7.17-7.15 (m, 1H, Ar H), 6.79-6.75 (m, 1H, Ar H). $^{13}$C NMR (100 MHz, $CDCl_3$, δ) 154.7, 150.8, 135.8, 135.7, 135.1, 130.8, 129.5, 129.1, 128.6, 128, 127, 121.5, 116.8.

**4-(7-chloroquinolin-4-yl) benzoic acid (7e)**

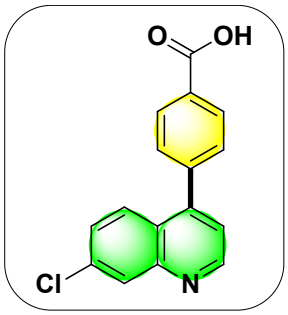


Purified by column chromatography (53% ethyl acetate in hexane), Pink gel. $^{1}$H NMR (400 MHz, $CDCl_3$, δ) 8.92 (d, *J* = 4.4 Hz, 1H; OH), 8.16 (d, *J* = 2.0 Hz, 1H, Ar H), 7.85 (d, *J* = 9.2 Hz, 1H, Ar H), 7.53-7.45 (m, 6H, Ar H), 7.34-7.32 (m, 1H, Ar H). $^{13}$C NMR (100 MHz, $CDCl_3$, δ) 151 (O-C=O), 149.1, 148.7, 137.5, 135.4, 129.5, 129.1, 128.8, 128.7, 127.7, 127.4, 121.5, 115.5.

**7-chloro-4-(4-chloronaphthalen-1-yl) quinoline (7f)**

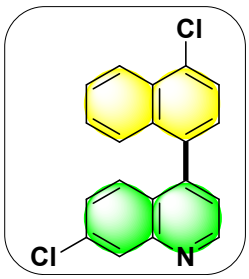


Purified by column chromatography (8% ethyl acetate in hexane), Orange gel. $^{1}$H NMR (400 MHz, DMSO-$d_6$, δ) 8.42 (dd, *J* = 7.6, 1.6 Hz, 3H, Ar H), 8.17 (dd, *J* = 8.4, 1.2 Hz, 1H, Ar H), 7.68-7.56 (m, 7H, Ar H). $^{13}$C NMR (100 MHz, DMSO-$d_6$, δ) 137.3, 132.5, 132.3, 130.1, 129.8, 127.4, 127.1, 126, 124.2.

**4,7-bis(6-methoxypyridin-3-yl) quinoline (7g)**

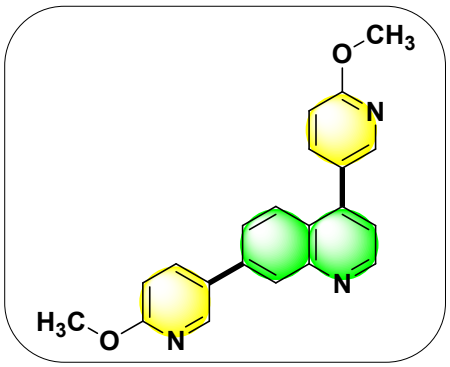


Purified by column chromatography (72% ethyl acetate in hexane), Yellow gel. $^{1}$H NMR (400 MHz, $CDCl_3$, δ) 8.90 (d, *J* = 4.4 Hz, 1H, Ar H), 8.28 (dd, *J* = 3.0, 1.0 Hz, 1H, Ar H), 8.16 (d, *J* = 2.0 Hz, 1H, Ar H), 7.82 (d, *J* = 8.8 Hz, 1H, Ar H), 7.77 (dd, *J* = 4.0, 0.4 Hz, 1H, Ar H), 7.70 (dd, *J* = 8.4, 2.4 Hz, 1H, Ar H), 7.47 (dd, *J* = 9.0, 2.2 Hz, 1H, Ar H), 7.32 (d, *J* = 4.4 Hz, 1H, Ar H), 7.20 (dd, *J* = 9.0, 3.0 Hz, 1H, Ar H), 6.91 (dd, *J* = 8.4, 0.6 Hz, 1H, Ar H), 6.62 (dd, *J* = 8.8, 0.4 Hz, 1H, Ar H), 4.01 (s, 3H; $CH_3$), 3.83 (s, 3H; $CH_3$). $^{13}$C NMR (100 MHz, $CDCl_3$, δ) 171.5, 164.5, 158.3, 150.6, 148.3, 147.1, 145.8, 139.7, 136.1, 132.7, 128.3, 128.2, 128, 126.9, 126.2, 125.4, 121.7, 111, 53.9 ($CH_3$), 53.7 ($CH_3$).

## 5. Notes and references


1. L. Boubakri, A. S. Al-Ayed, L. Mansour, N. Abutaha, A. H. Harrath, I. Özdemir, S. Yasar and N. Hamdi, J. Coord. Chem., 2019, 72, 2688-2704.
2. H. Veisi, N. H. Nasrabadi and P. Mohammadi, Appl. Organomet. Chem., 2016, 30, 890-896.
3. F. R. Fortea-Pérez, I. Schlegel, M. Julve, D. Armentano, G. De Munno and S.-E. Stiriba, J. Organomet. Chem., 2013, 743, 102-108.
4. M. Ghiaci, M. Zarghani, F. Moeinpour and A. Khojastehnezhad, Appl. Organomet. Chem., 2014, 28, 589-594.
5. A. Ghorbani-Choghamarani, B. Tahmasbi and P. Moradi, Appl. Organomet. Chem., 2016, 30, 422-430.
6. R. Hosseini, R. Ranjbar-Karimi and K. Mohammadiannejad, J. Iran. Chem. Soc., 2022, 19, 1143-1158.
7. C. Wolf and K. Ekoue-Kovi, 2006, https://doi.org/https://doi.org/10.1002/ejoc.200500843.
8. R. Sharma, P. S. Sagara, D. Sharma and A. Chaudhary, J. Organomet. Chem., 2024, 1018, 123294.
9. S. Gnanasekar, J. Murugaraj, B. Dhivyabharathi, V. Krishnamoorthy, P. K. Jha, P. Seetharaman, R. Vilwanathan and S. Sivaperumal, J. Appl. Biomed., 2018, 16, 59-65.
10. F. Gulbagca, A. Aygün, M. Gülcan, S. Ozdemir, S. Gonca and F. Şen, Appl. Organomet. Chem., 2021, 35, e6272.
11. S. Mohana and S. Sumathi, J. Clust. Sci., 2020, 31, 391-400.
12. N. Prakashkumar, M. Vignesh, K. Brindhadevi, A. Pugazhendhi and N. Suganthy, Prog. Org. Coat., 2021, 151, 106098.
13. M. S. Al-Fakeh, S. O. M. Osman, M. Gassoumi, M. Rabhi and M. Omer, Nanomaterials, 2021, 11, 2666.
14. M. Shahriari, M. A. H. Sedigh, M. Shahriari, M. Stenzel, M. M. Zangeneh, A. Zangeneh, B. Mahdavi, M. Asadnia, J. Gholami and B. Karmakar, Inorg. Chem. Commun., 2022, 141, 109523.
15. H. Mehmood, M. A. Iqbal, M. N. Ashiq and R. Hua, Molecules, 2021, 26, 6599.
16. X. L. Luo, X. X. Liu, J. H. Pu, W. F. Tian, X. Q. Zhou, D. D. Wei and G. S. Huang, ChemistrySelect, 2017, 2, 8658-8660.
17. R. Yan, X. Liu, C. Pan, X. Zhou, X. Li, X. Kang and G. Huang, Org. Lett., 2013, 15, 4876-4879.
18. V. K. Tiwari, G. G. Pawar, R. Das, A. Adhikary and M. Kapur, Org. Lett., 2013, 15, 3310-3313.
19. V. E. Murie, P. V. Nicolino, T. Dos Santos, G. Gambacorta, R. H. V. Nishimura, I. S. Perovani, L. C. Furtado, L. V. Costa-Lotufo, A. Moraes de Oliveira and R. Vessecchi, J. Org. Chem., 2021, 86, 13402-13419.

***Appendix I:*** **Spectral copies of GC-MS, $^{1}H$, $^{13}C$, and $^{19}F$ NMR of compounds obtained in this study**

## 3,5-diphenylpyridine (3a)

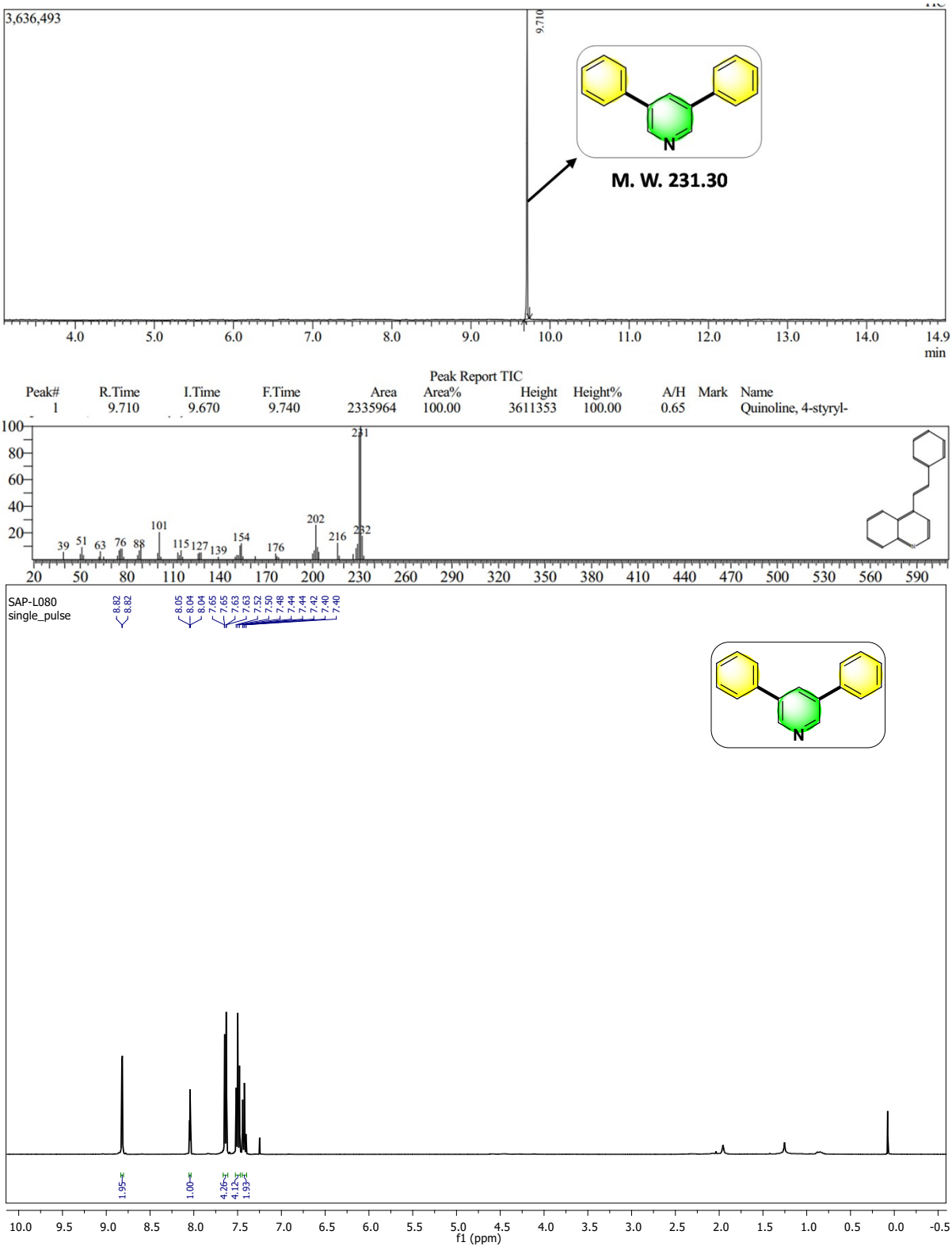

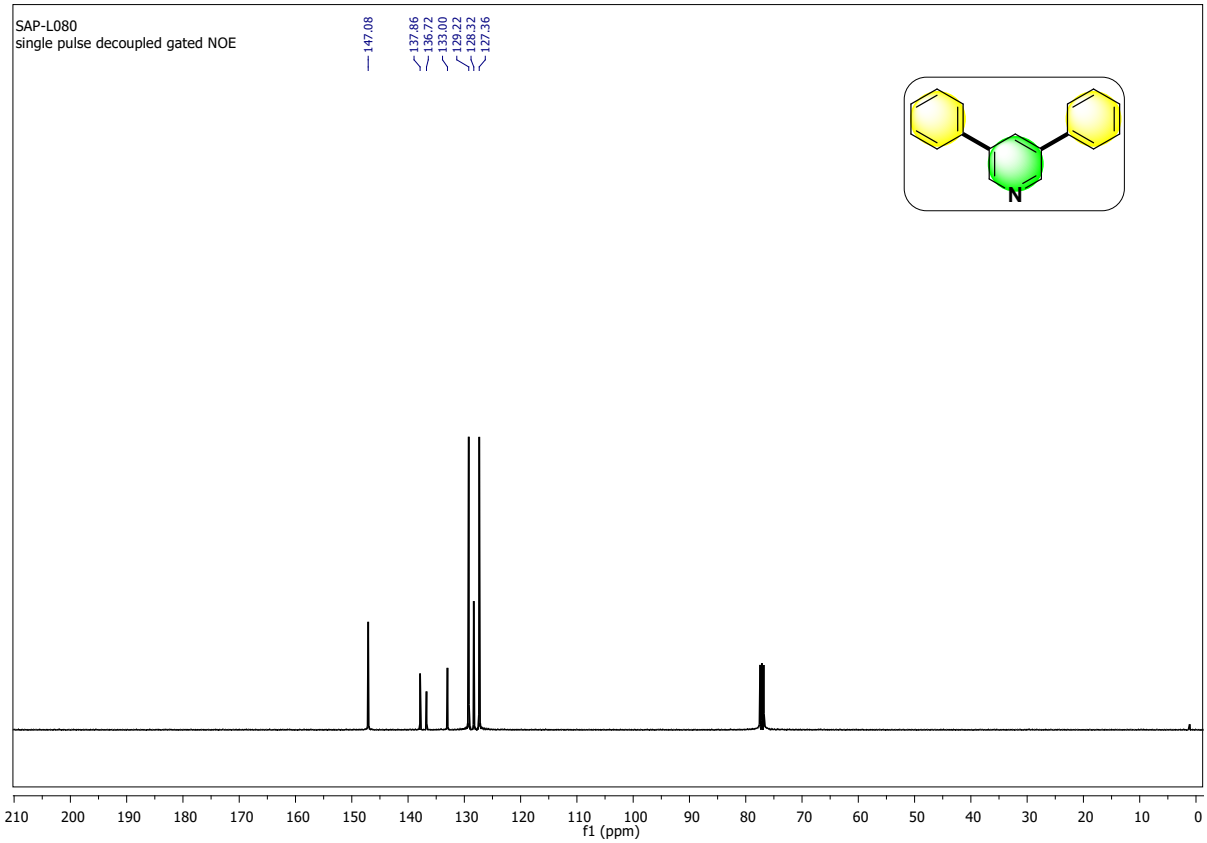


## 3,5-di-p-tolylpyridine (3b)

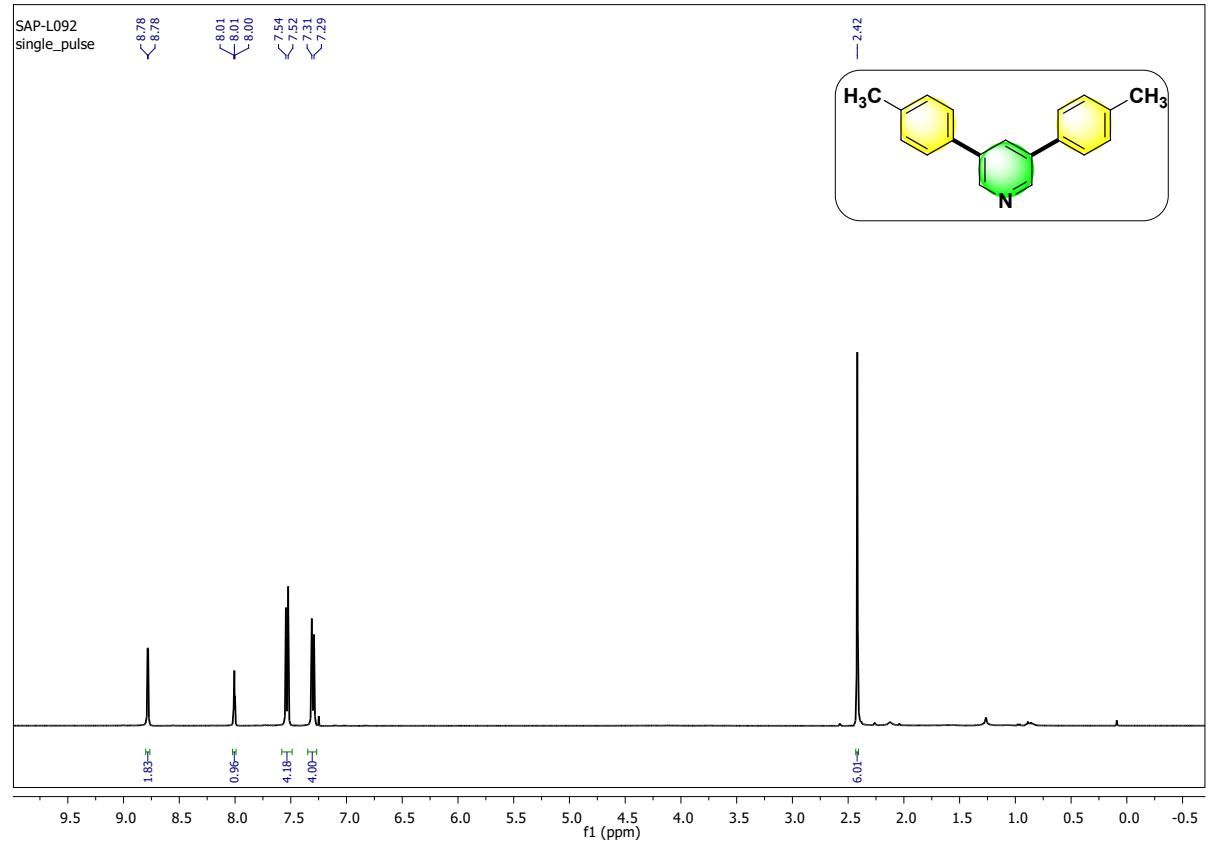

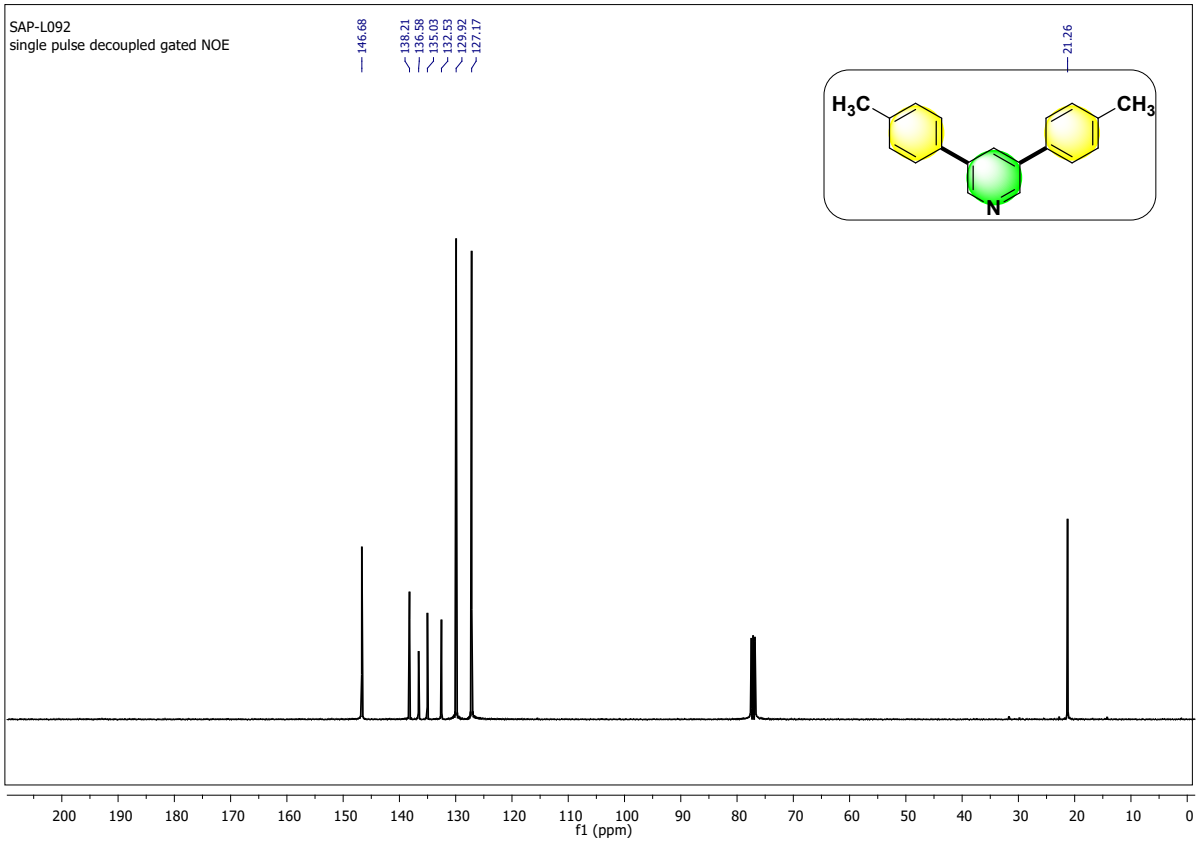


## 3,5-bis(4-methoxyphenyl) pyridine (3c)

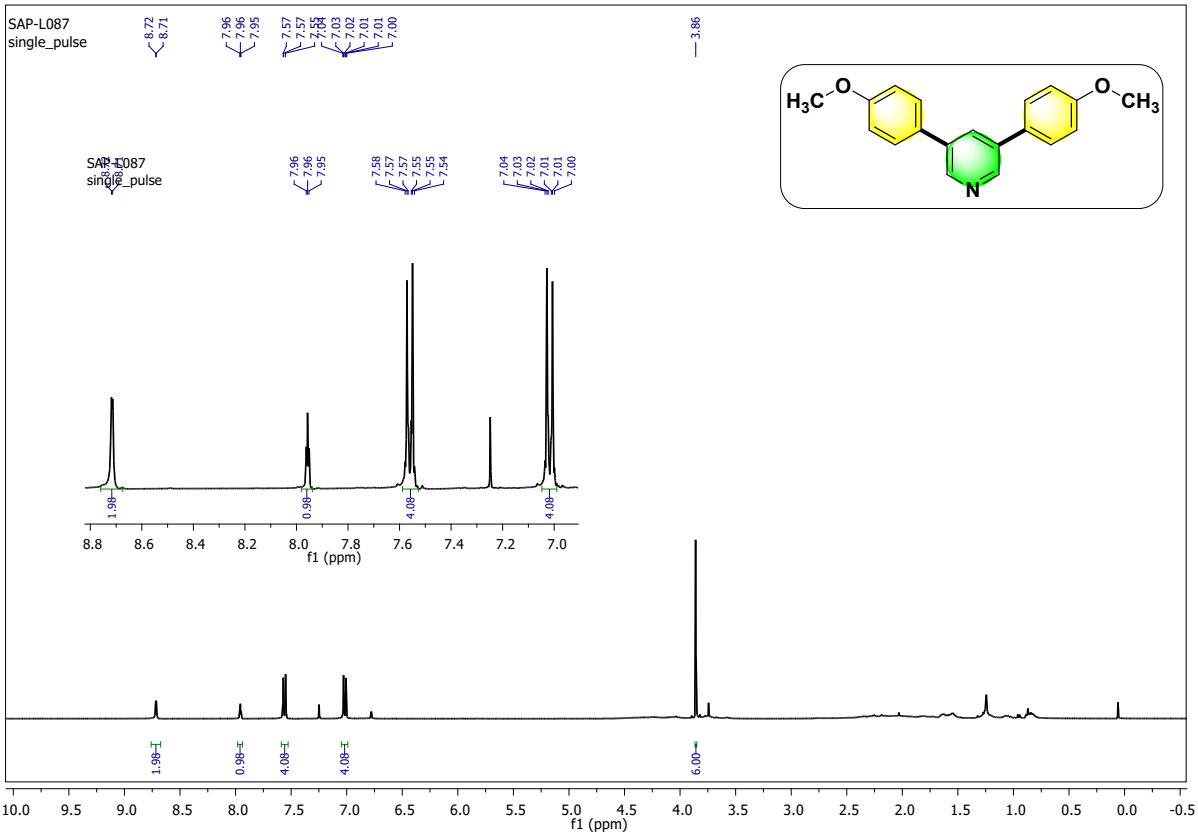

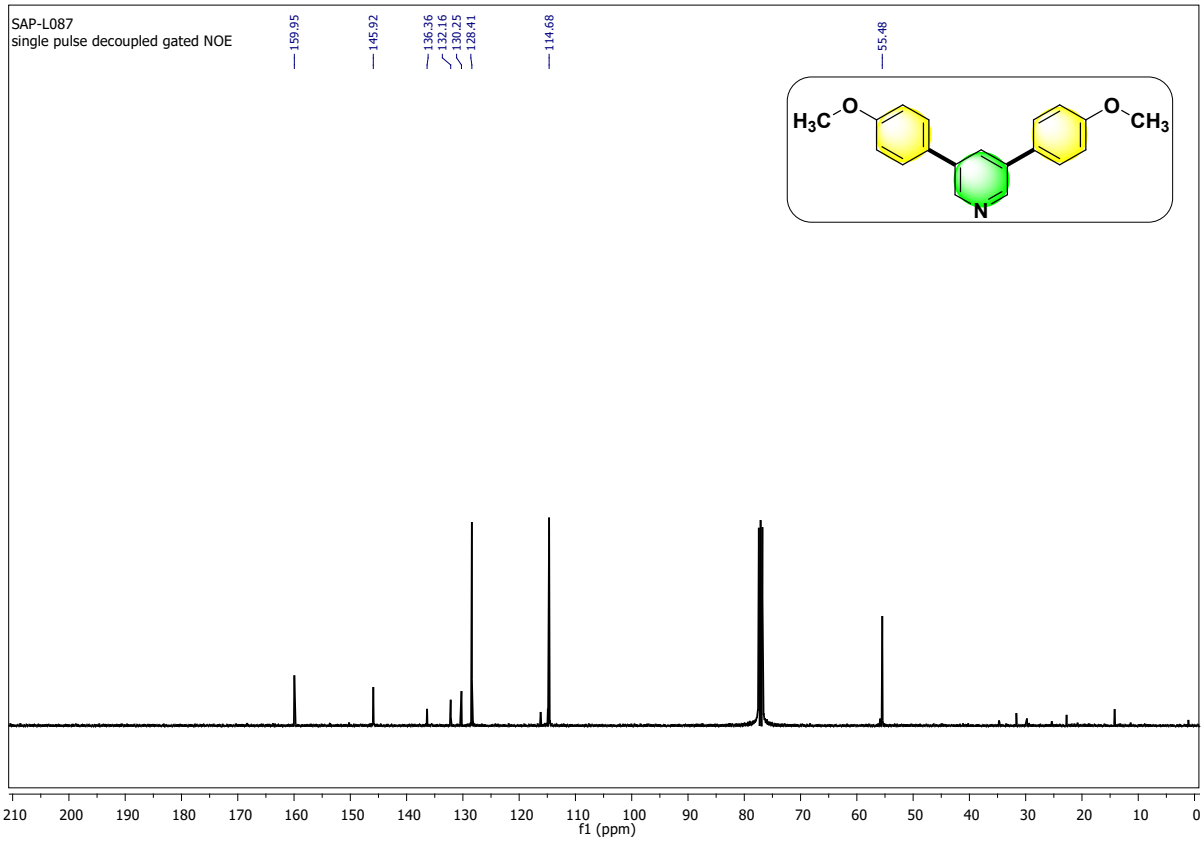


## 3,5-bis(4-chlorophenyl) pyridine (3d)

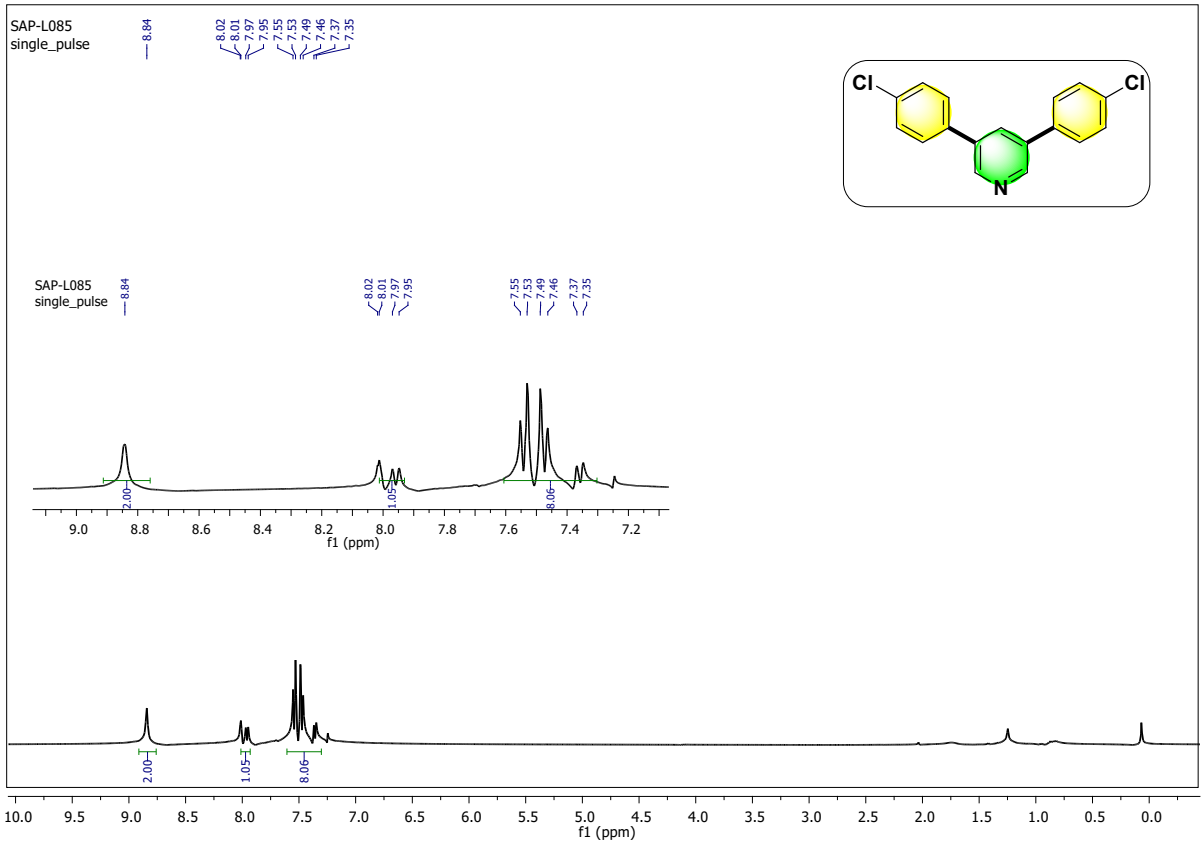

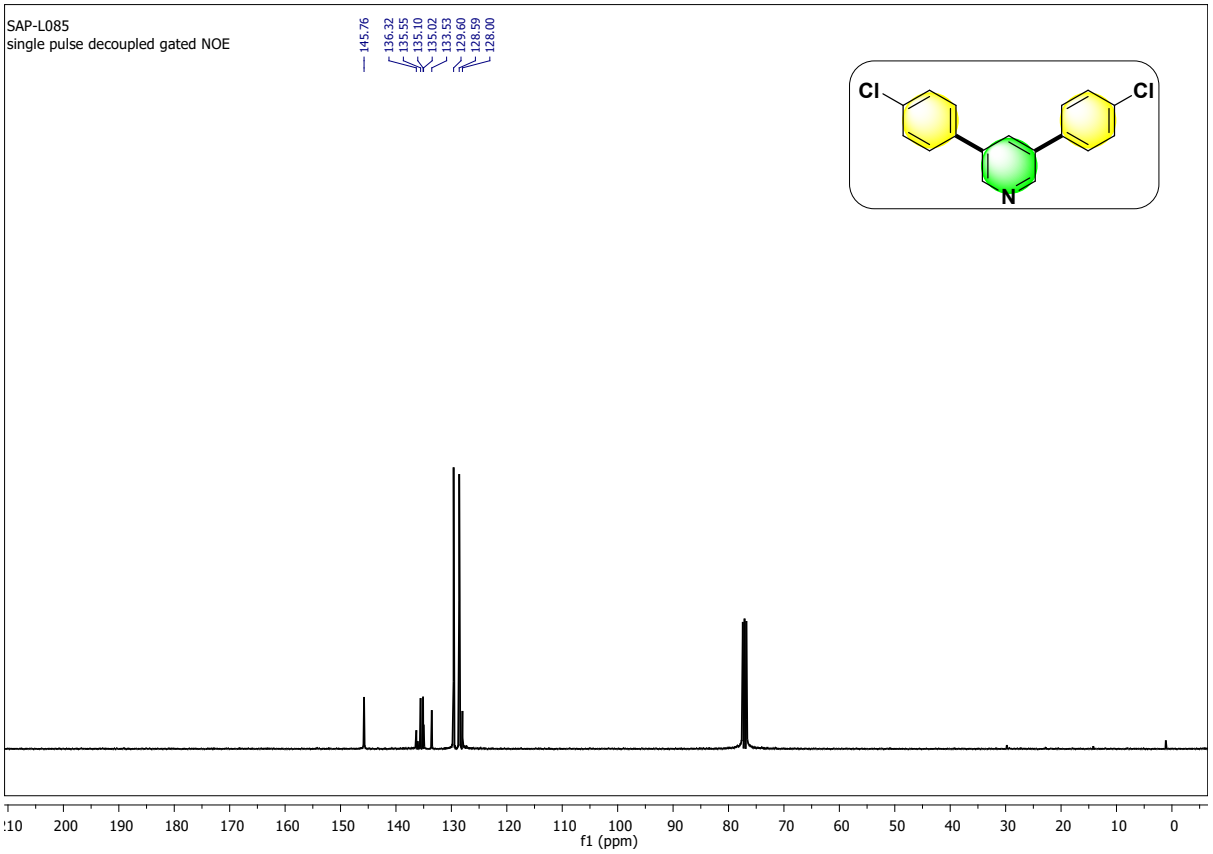


## 4,4'-(pyridine-3,5-diyl) diphenol (3e)

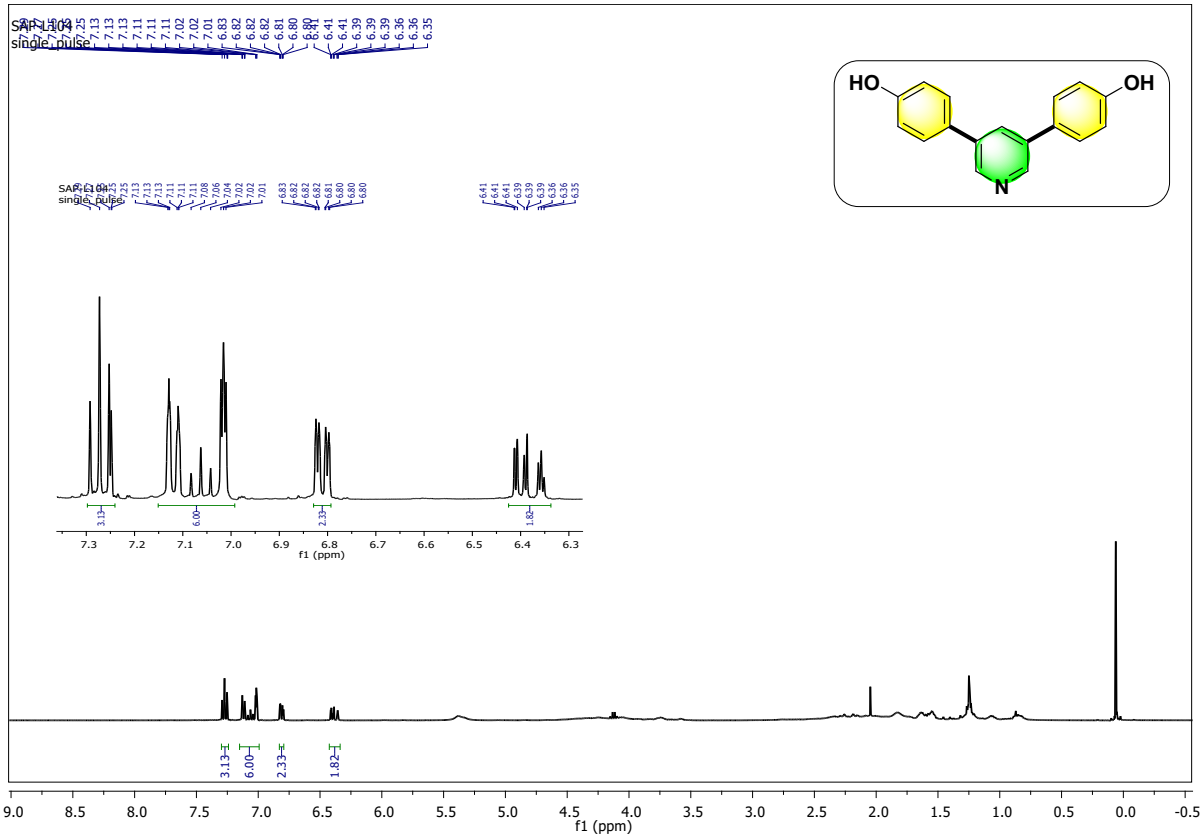

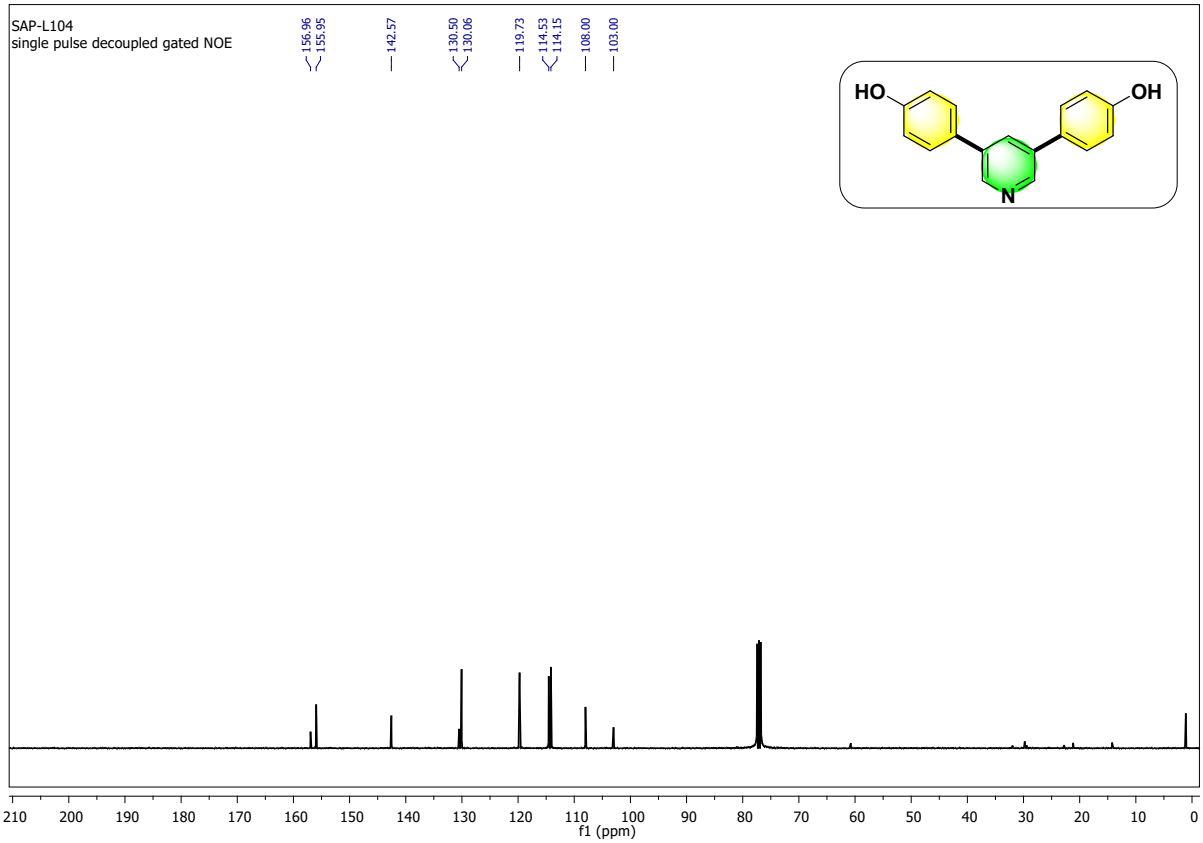


## 4,4'-(pyridine-3,5-diyl) di benzaldehyde (3f)

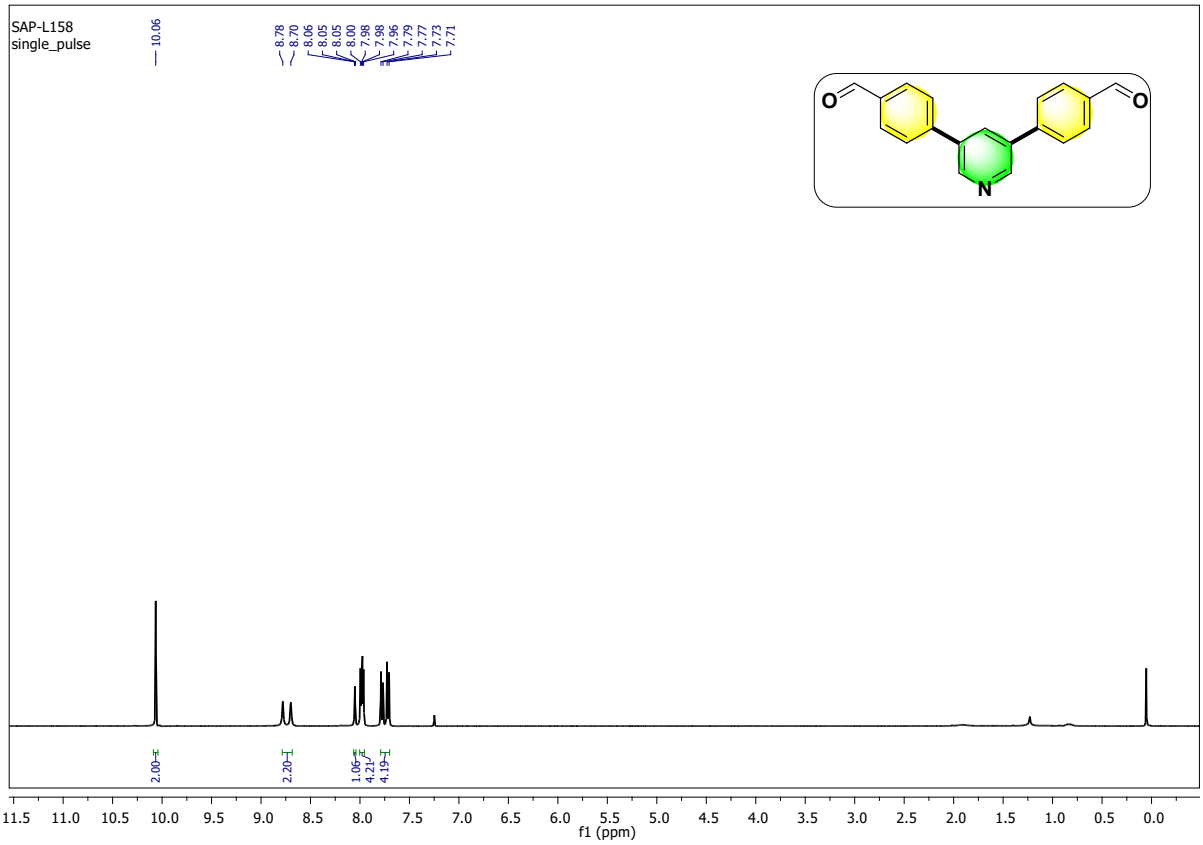

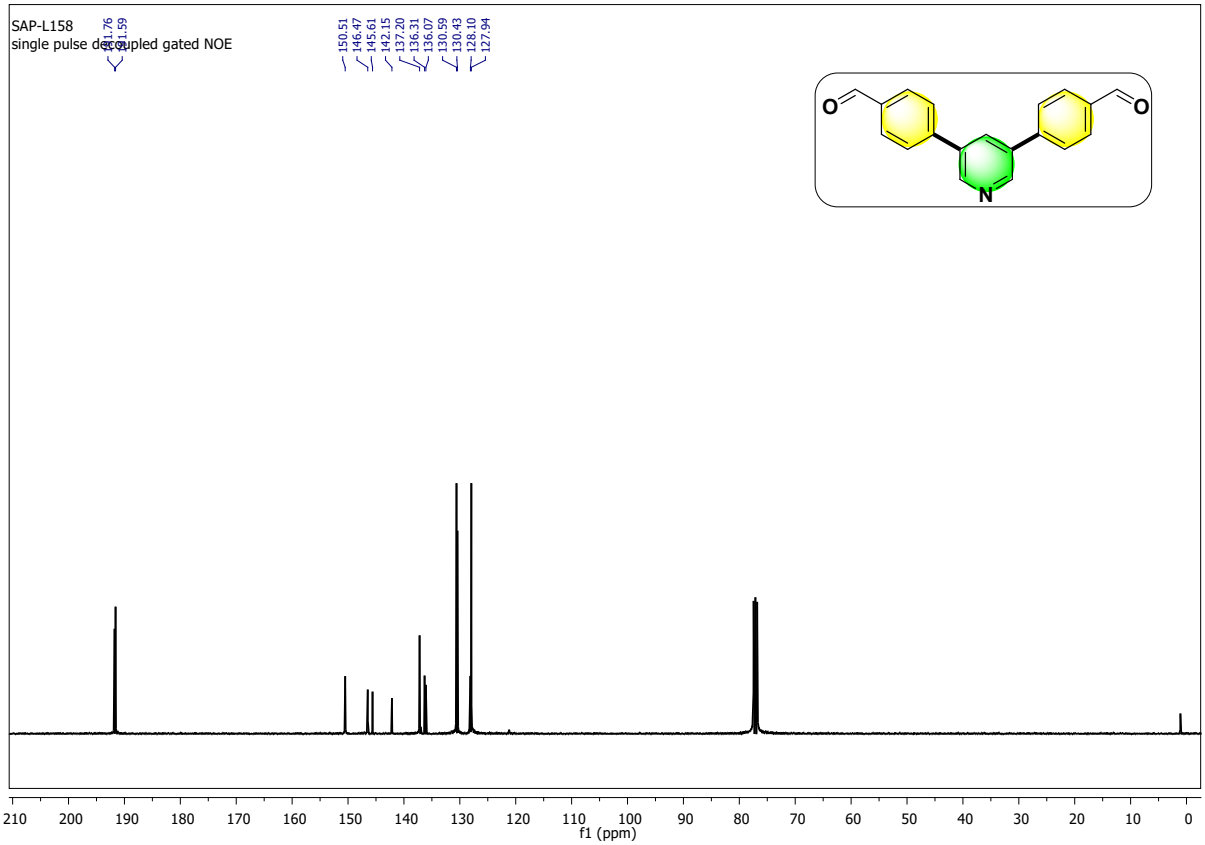


## 3,5-bis(4-chloronaphthalen-1-yl)pyridine (3 g)

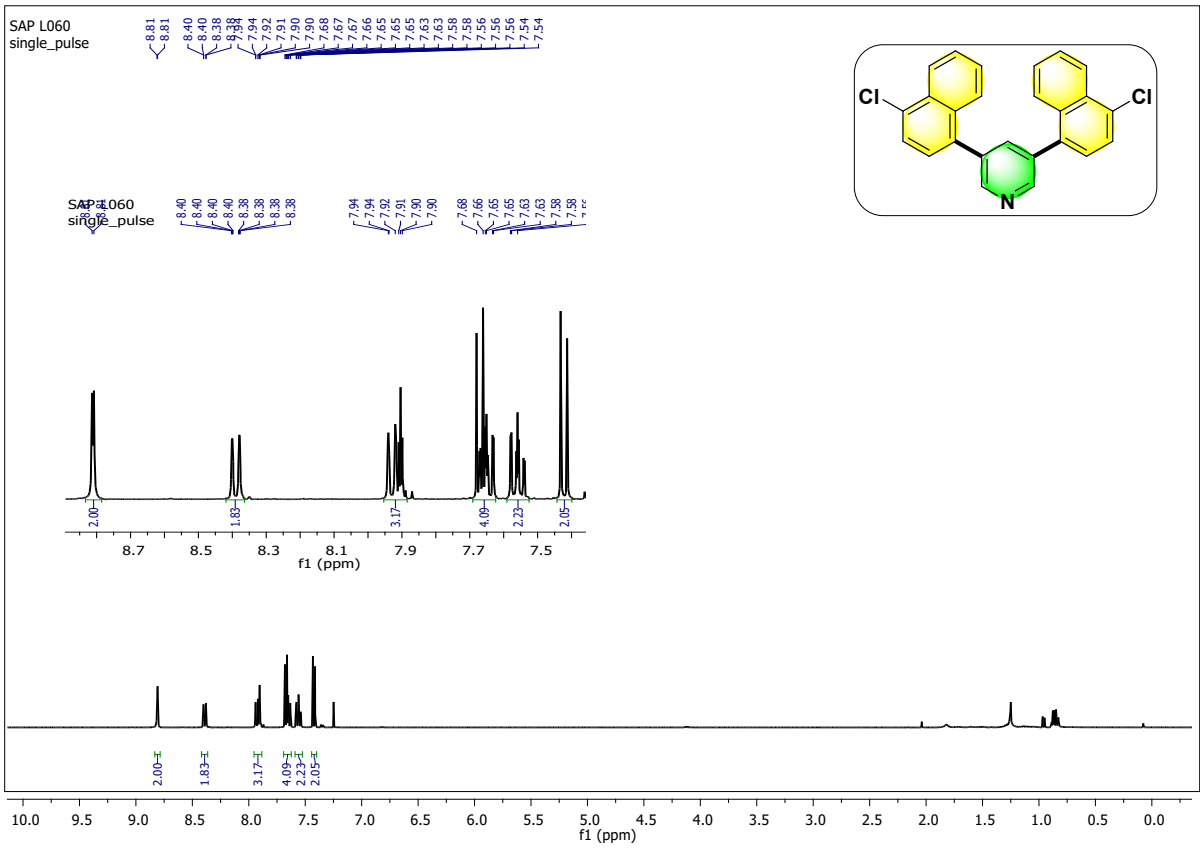

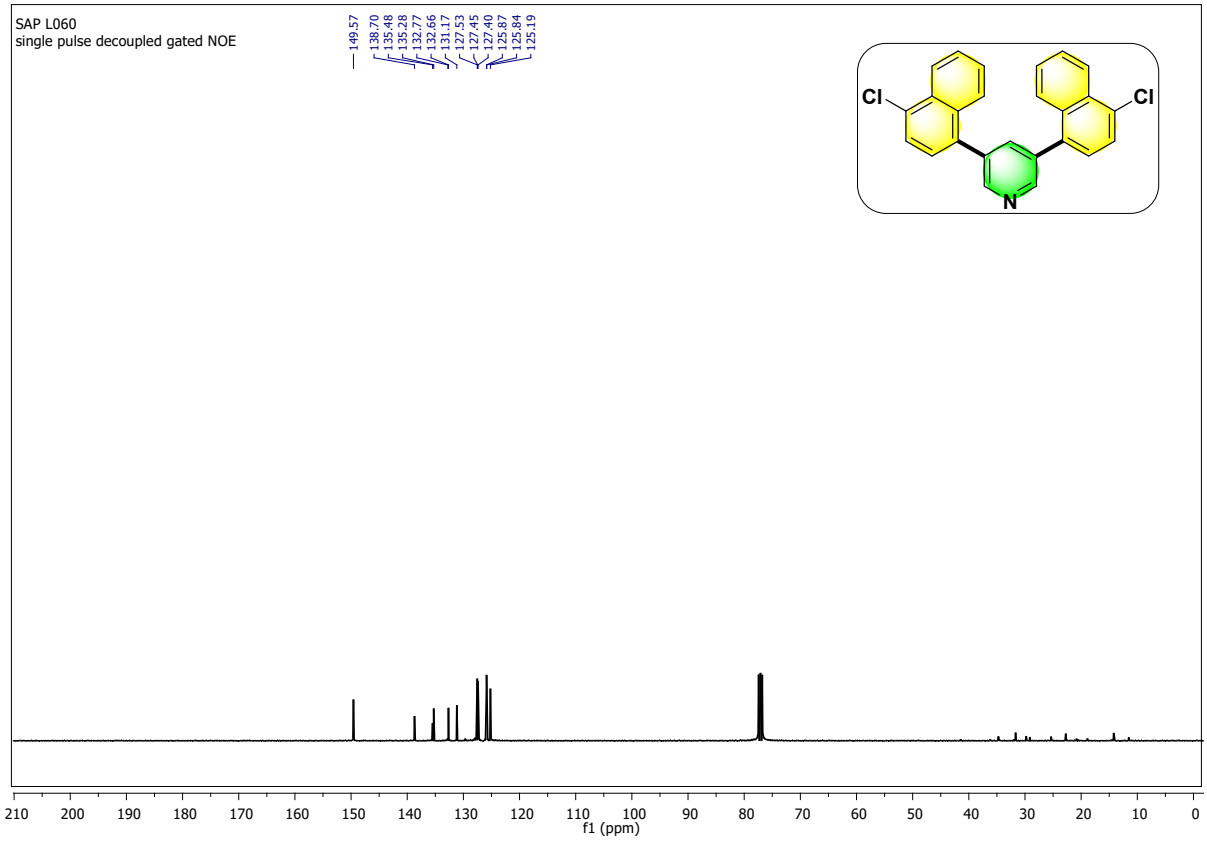


## 3,5-bis(2-ethoxy-4-fluorophenyl) pyridine (3h)

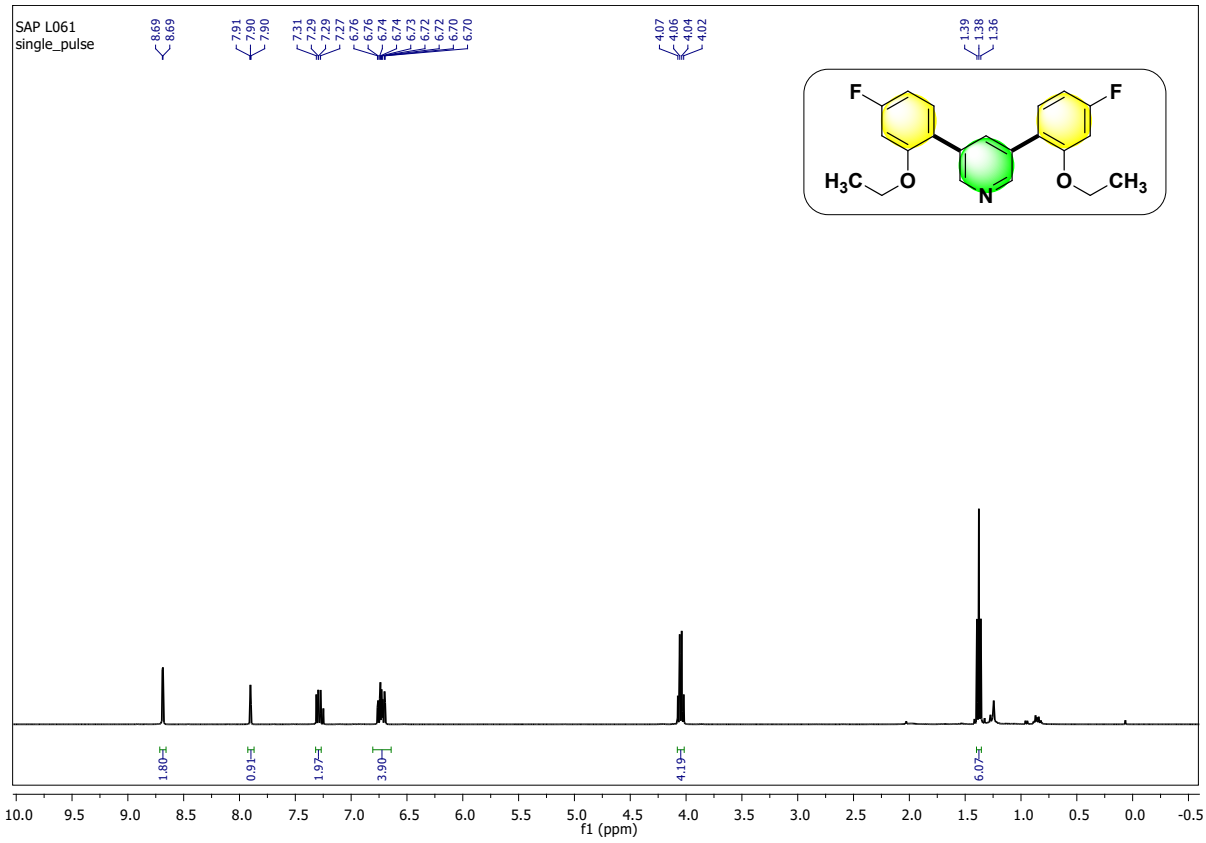

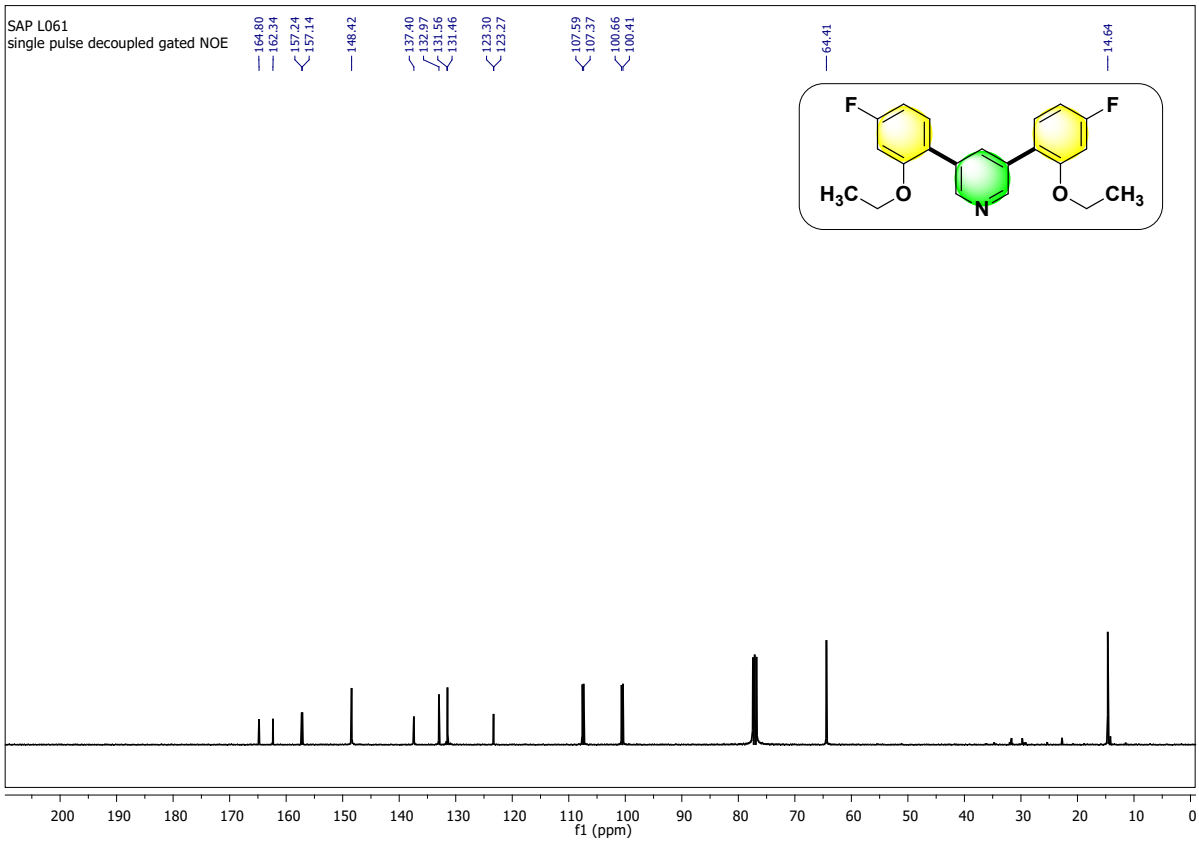
SAP L061
single pulse decoupled gated NOE
164.80
162.34
157.24
157.14
148.42
137.40
132.97
131.56
131.46
123.30
123.27
107.59
107.37
100.66
100.41
64.41
14.64
F
F
H3C
O
N
O
CH3
200 190 180 170 160 150 140 130 120 110 100 90 80 70 60 50 40 30 20 10 0
f1 (ppm)

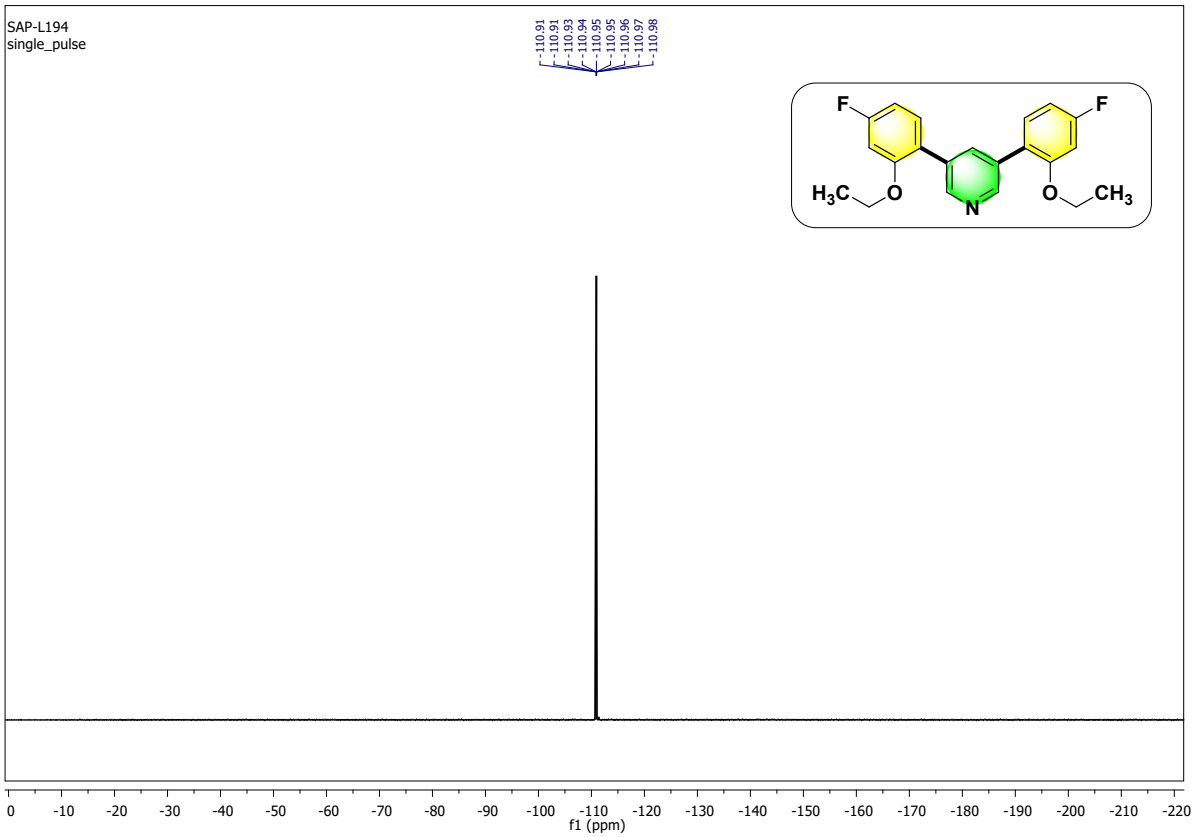
SAP-L194
single_pulse
-110.91
-110.91
-110.93
-110.94
-110.95
-110.95
-110.96
-110.97
-110.98
F
F
H3C
O
N
O
CH3
0 -10 -20 -30 -40 -50 -60 -70 -80 -90 -100 -110 -120 -130 -140 -150 -160 -170 -180 -190 -200 -210 -220
f1 (ppm)

## 3,5-bis(2-fluoro-5-methylphenyl) pyridine (3i)

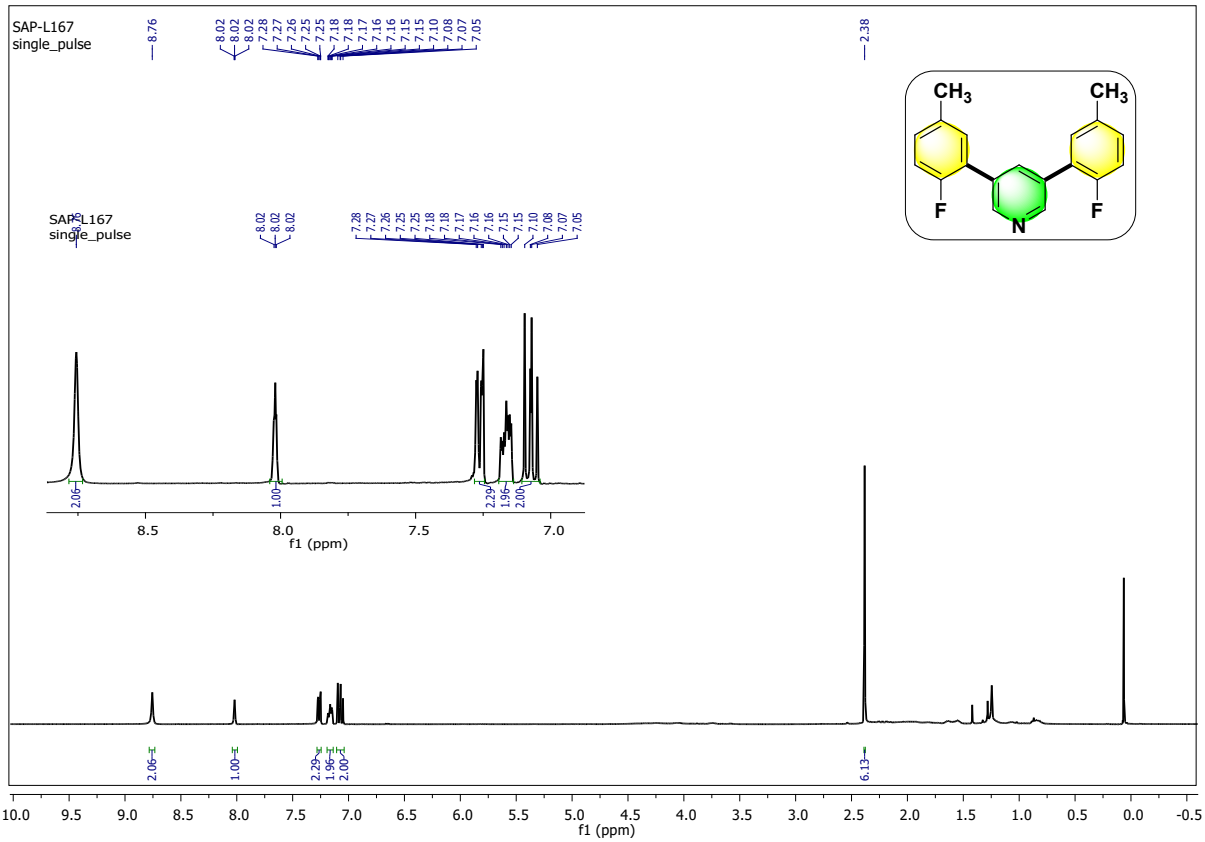


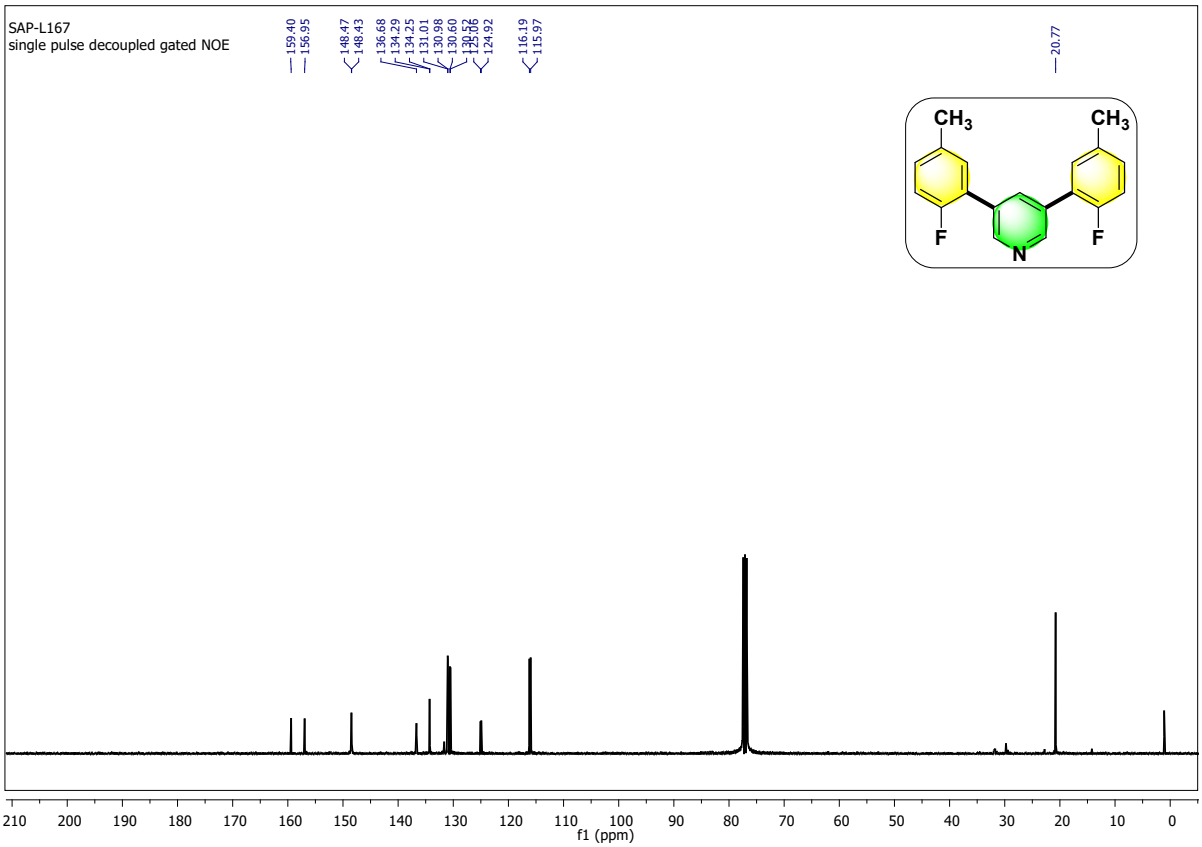

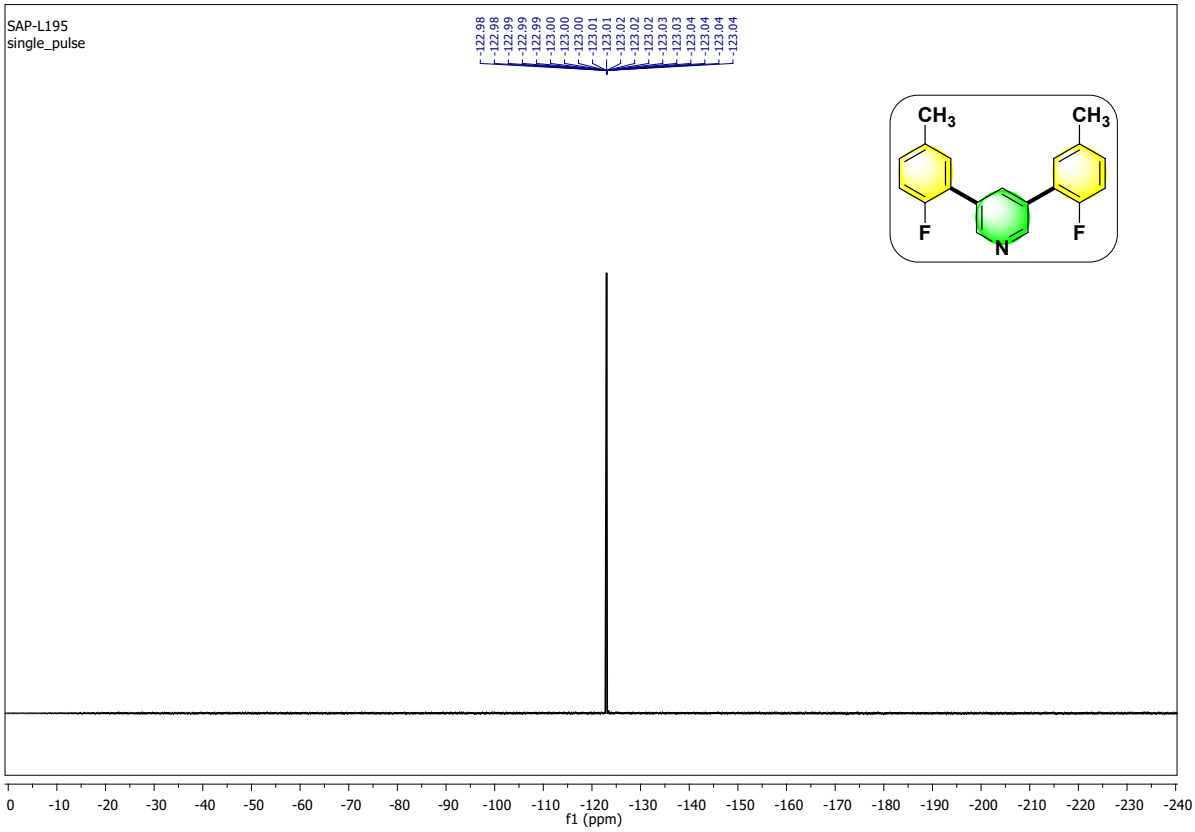


## 5-bromo-6'-methoxy-3,3'-bipyridine (3j)

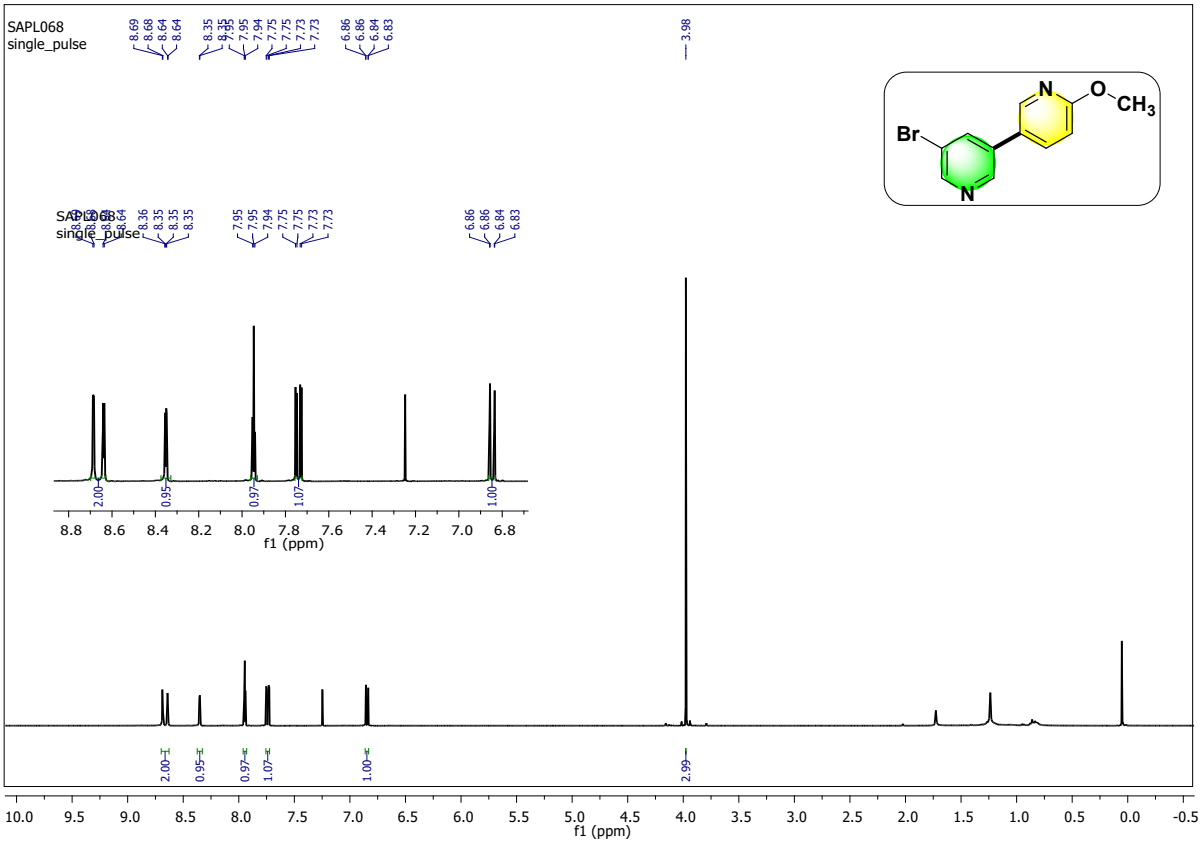

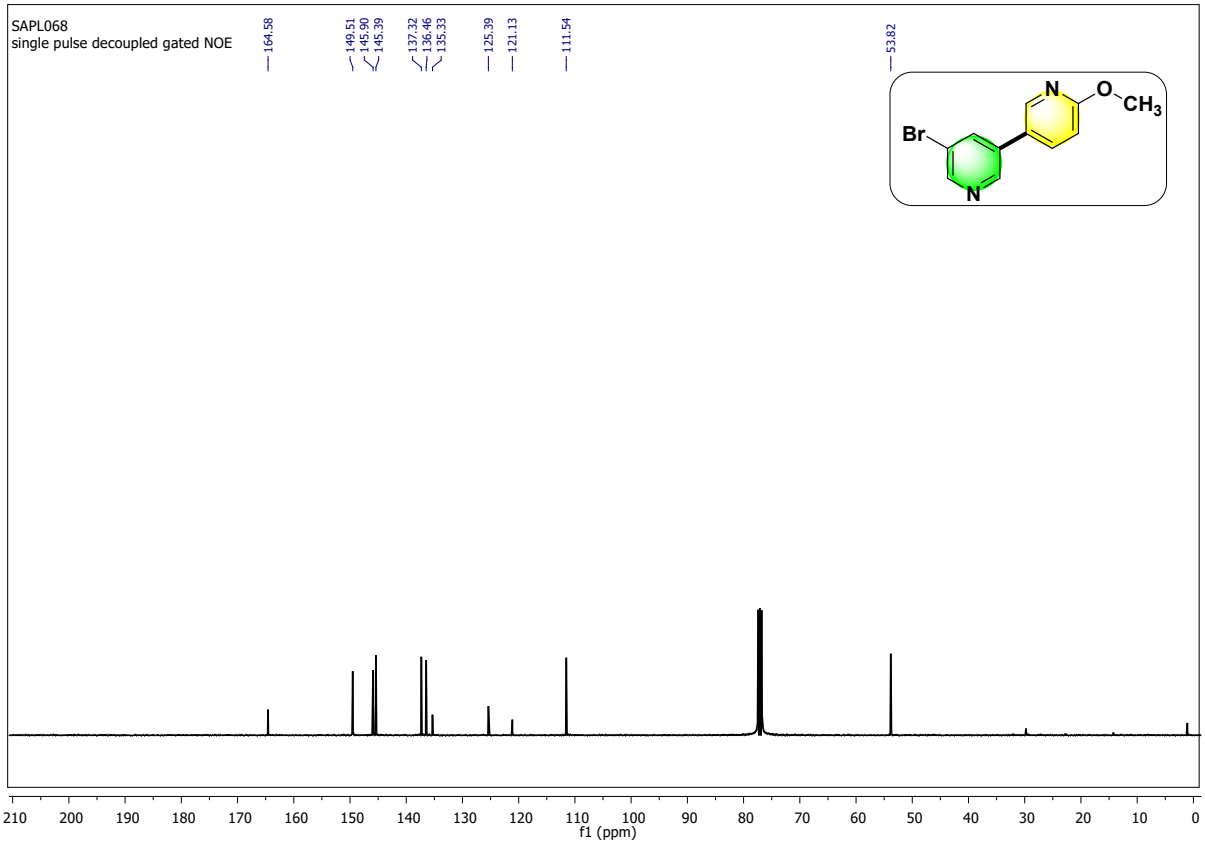


## 4-methyl-3,5-diphenylpyridine (3k)

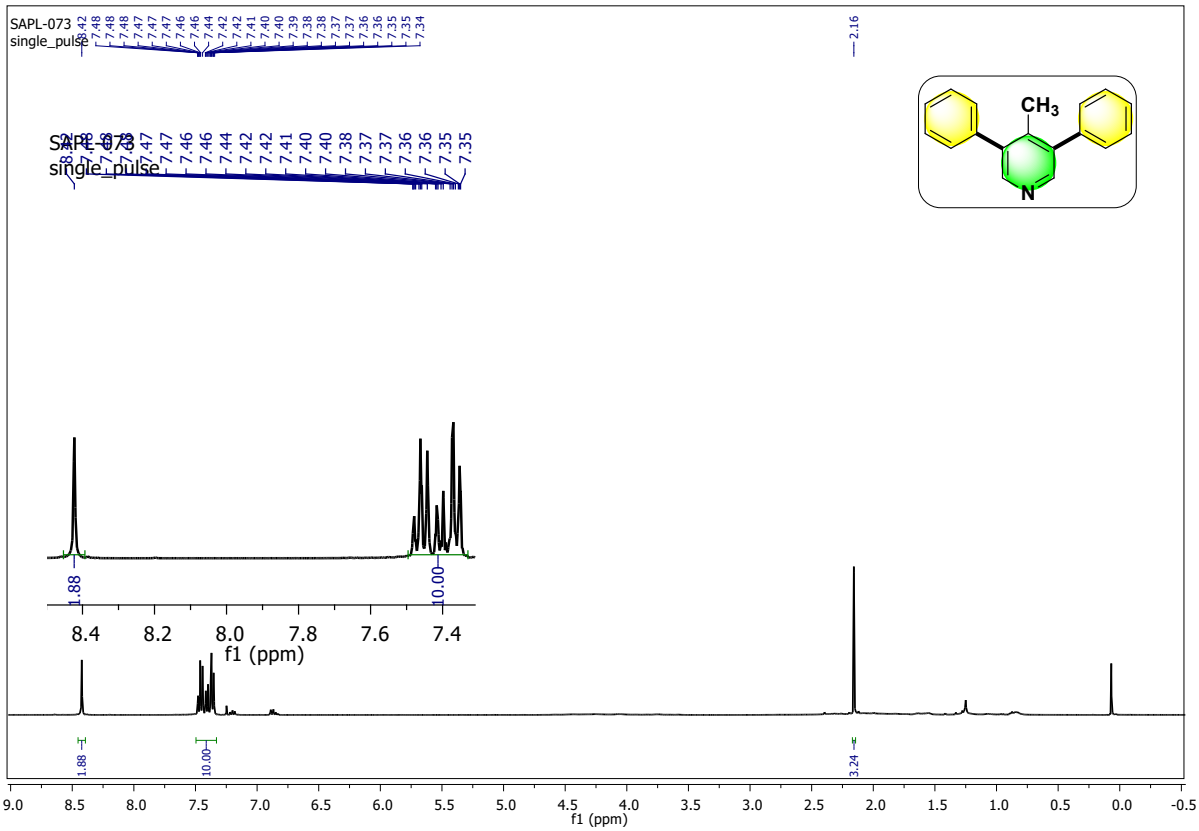

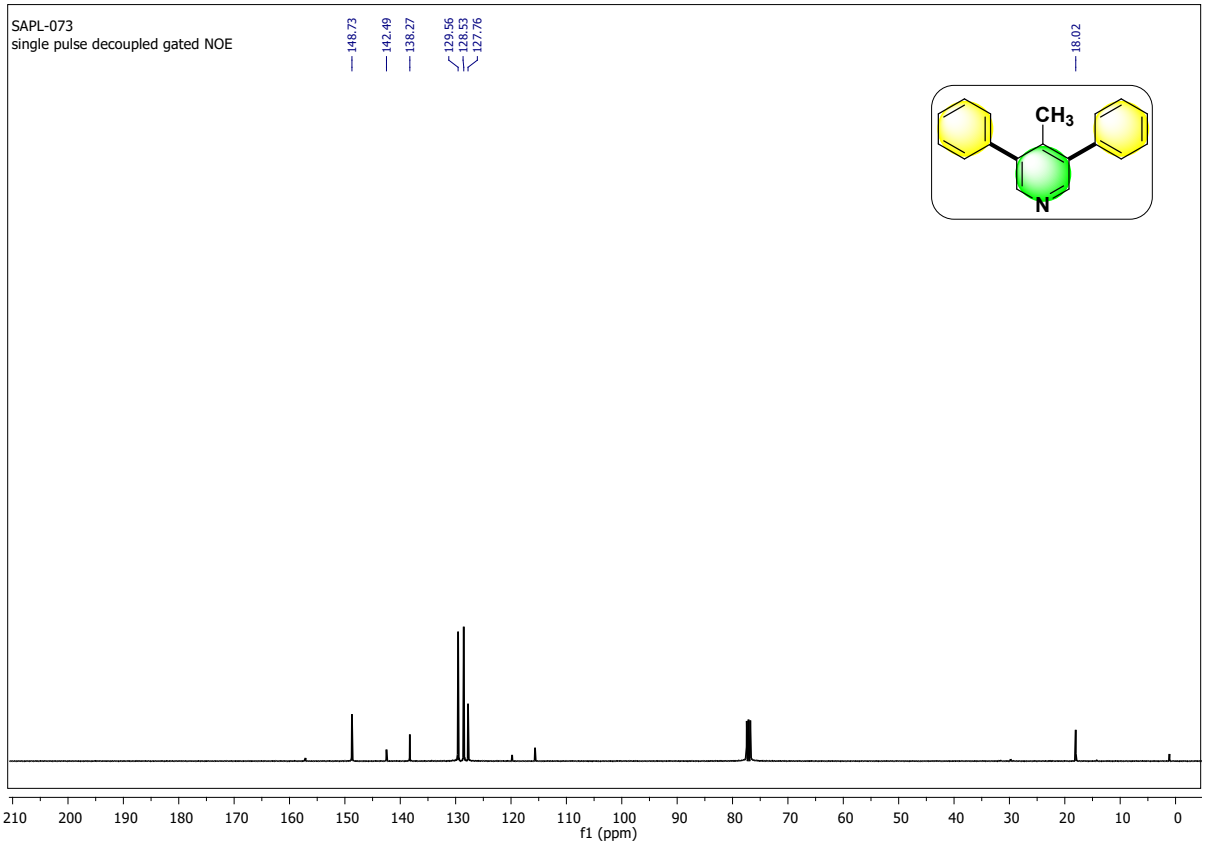


## 3-phenylquinoline (5a)

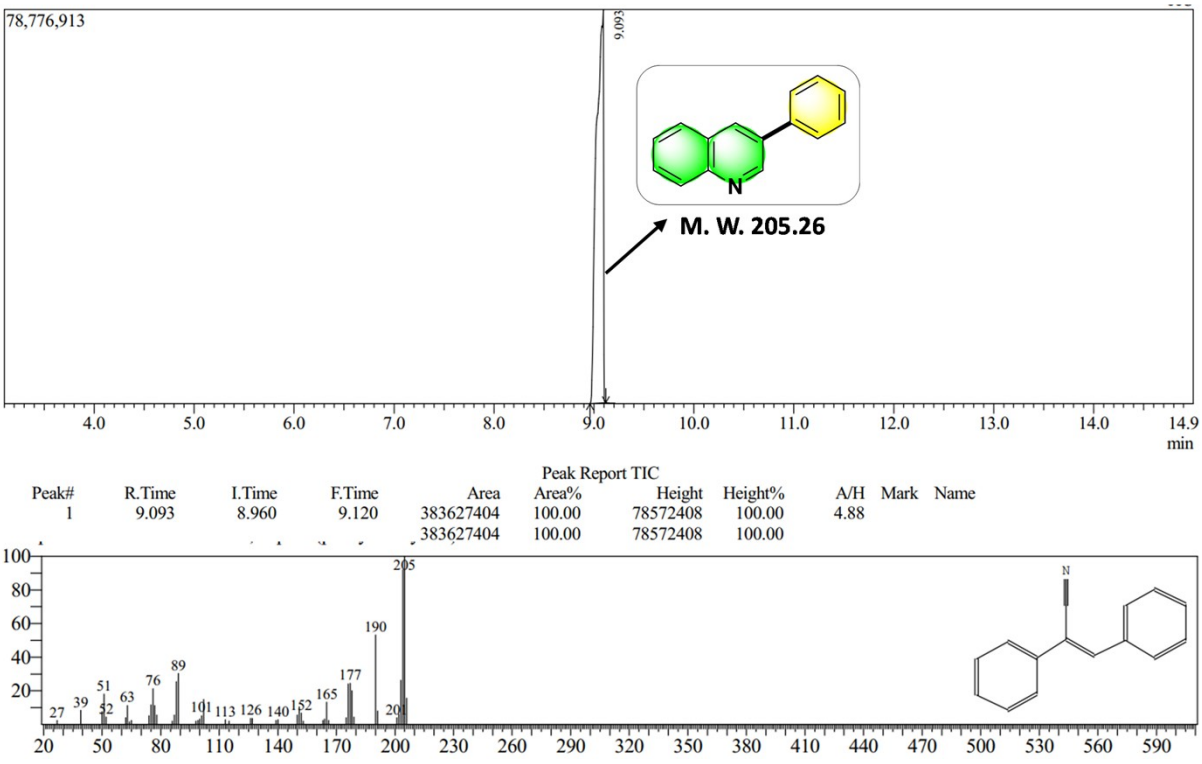


Peak Report TIC

| Peak# | R.Time | I.Time | F.Time | Area | Area% | Height | Height% | A/H | Mark | Name |
|---|---|---|---|---|---|---|---|---|---|---|
| 1 | 9.093 | 8.960 | 9.120 | 383627404 | 100.00 | 78572408 | 100.00 | 4.88 | | |
| | | | | 383627404 | 100.00 | 78572408 | 100.00 | | | |

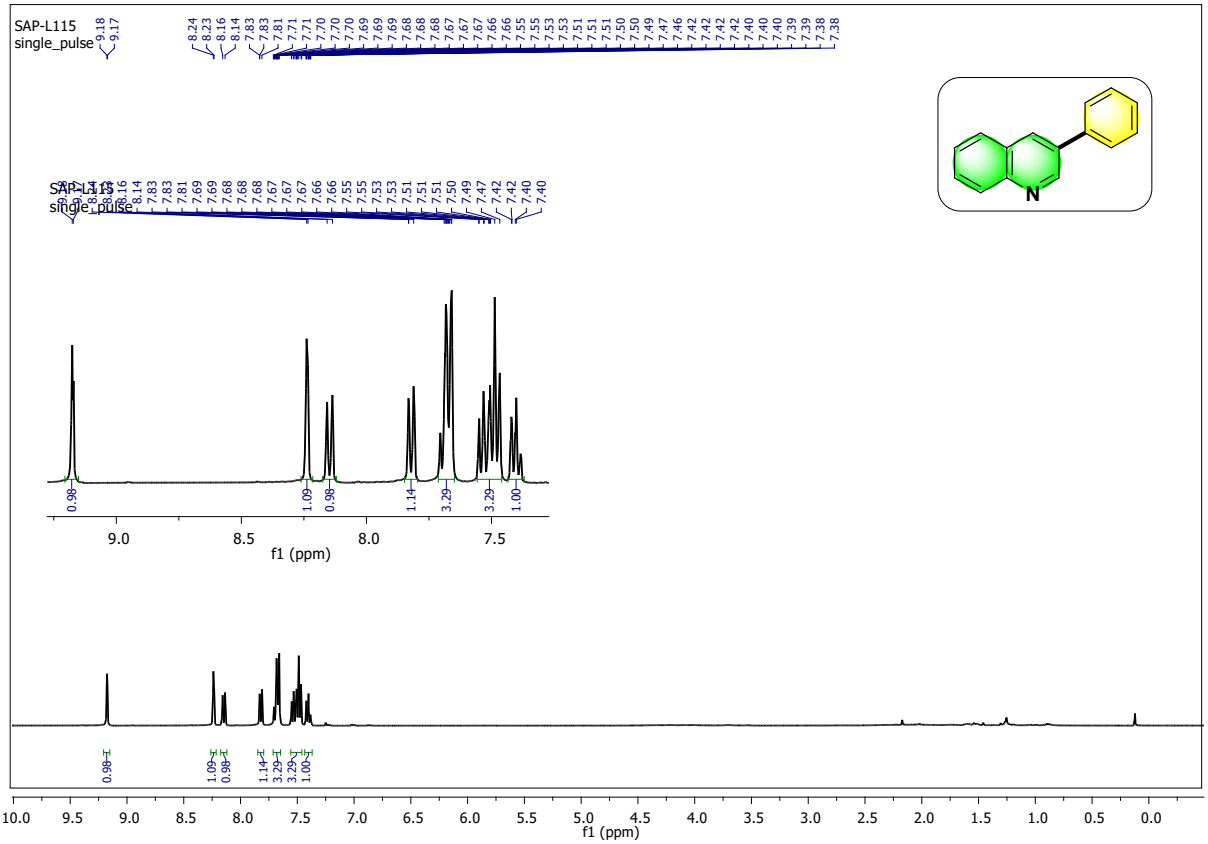
SAP-L115
single_pulse
N
f1 (ppm)

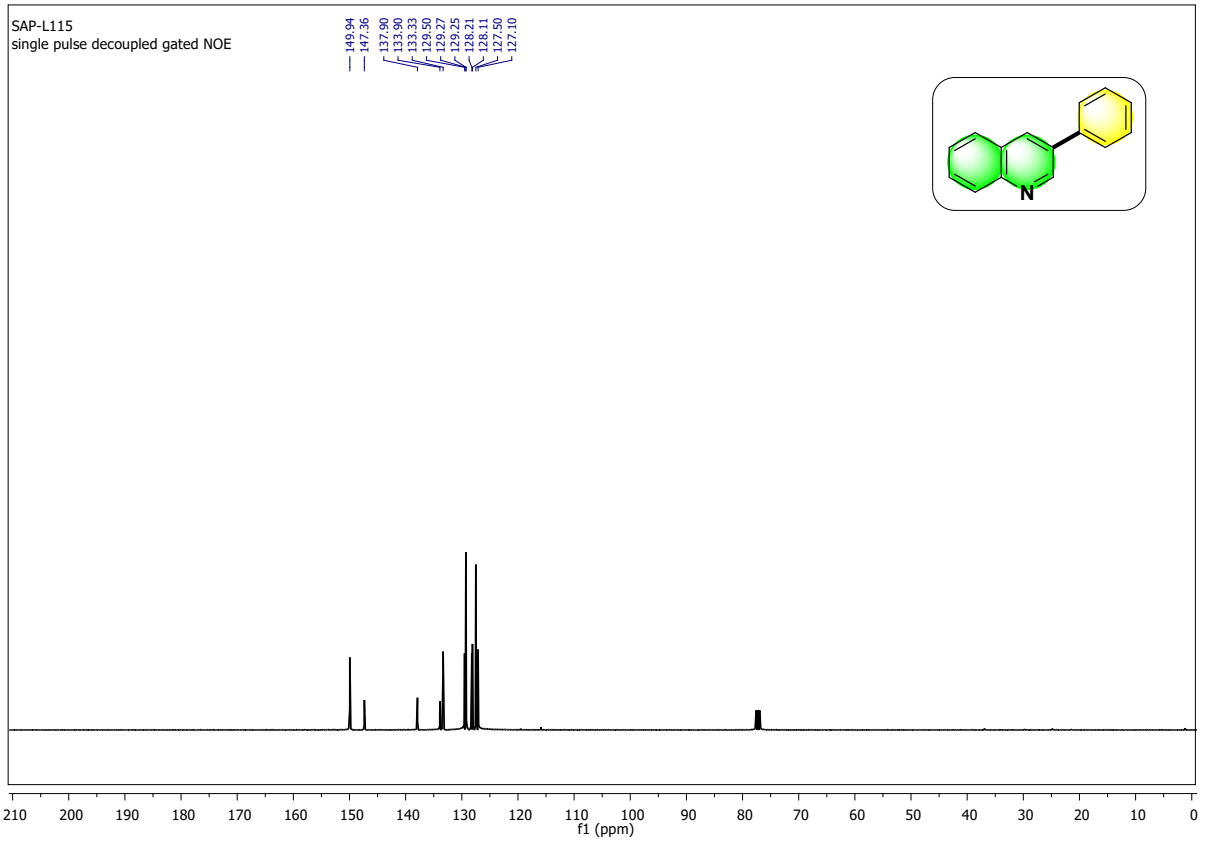
SAP-L115
single pulse decoupled gated NOE
N
f1 (ppm)

## 3-(p-tolyl) quinoline (5b)

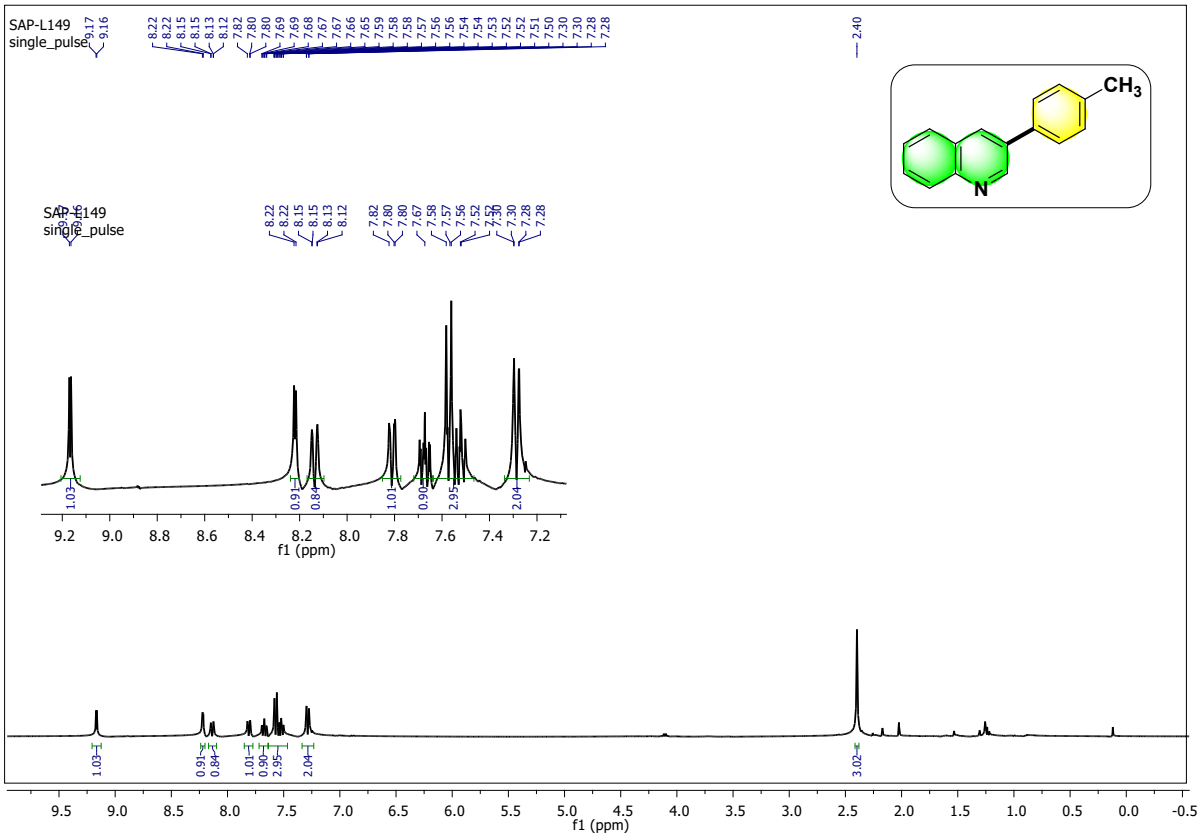


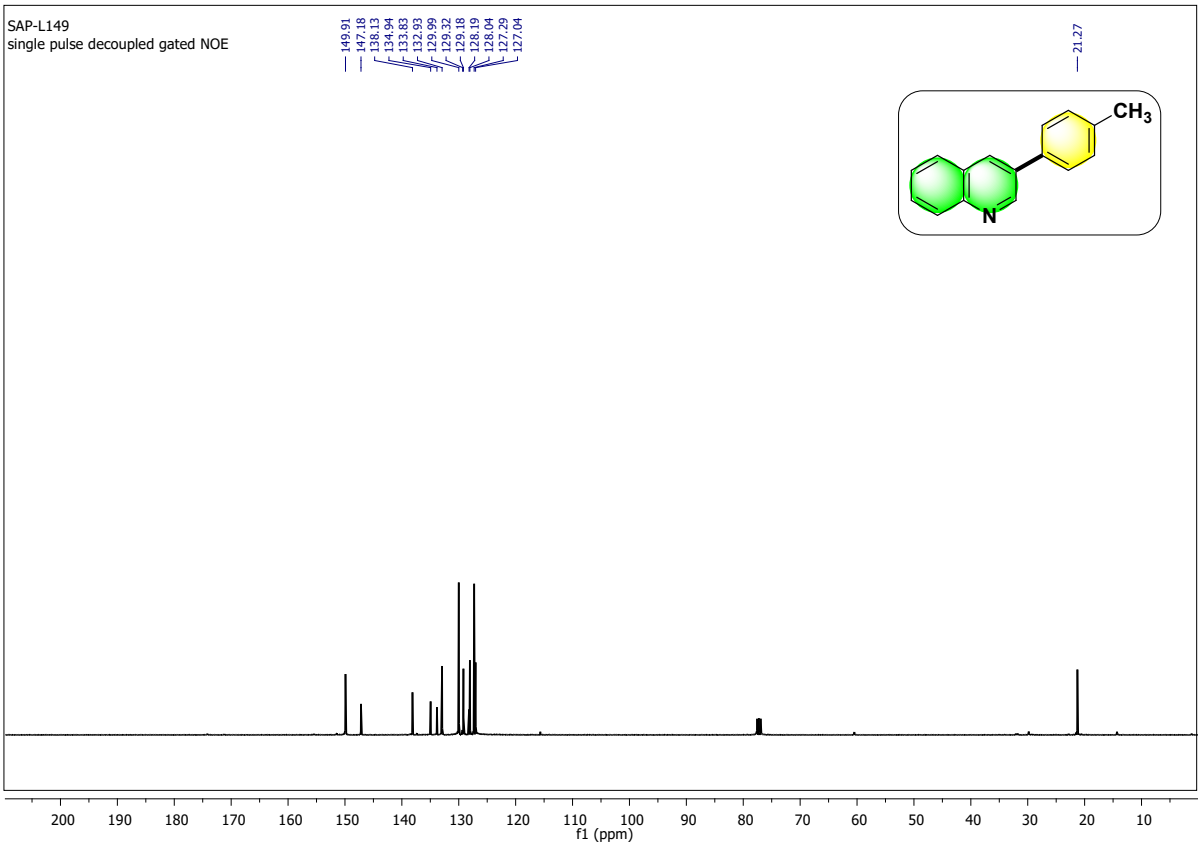

## 3-(4-methoxyphenyl) quinoline (5c)

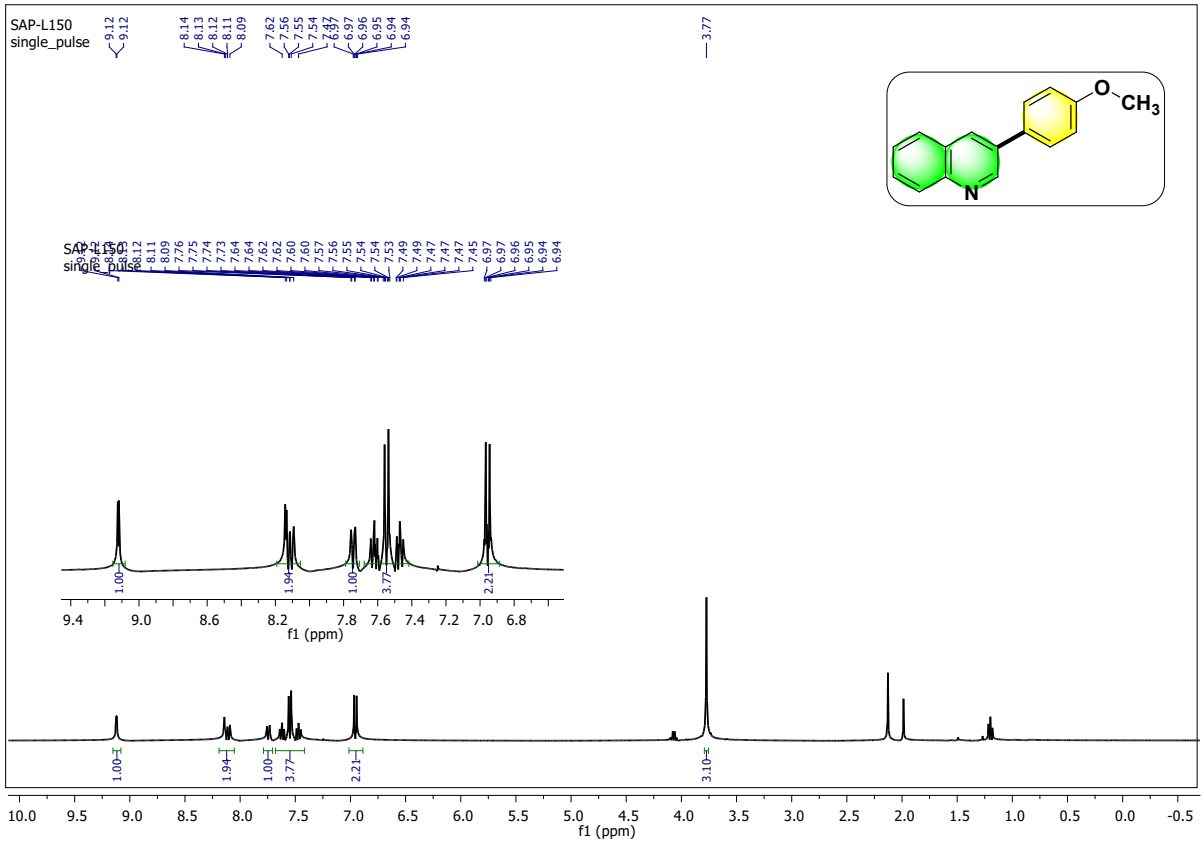


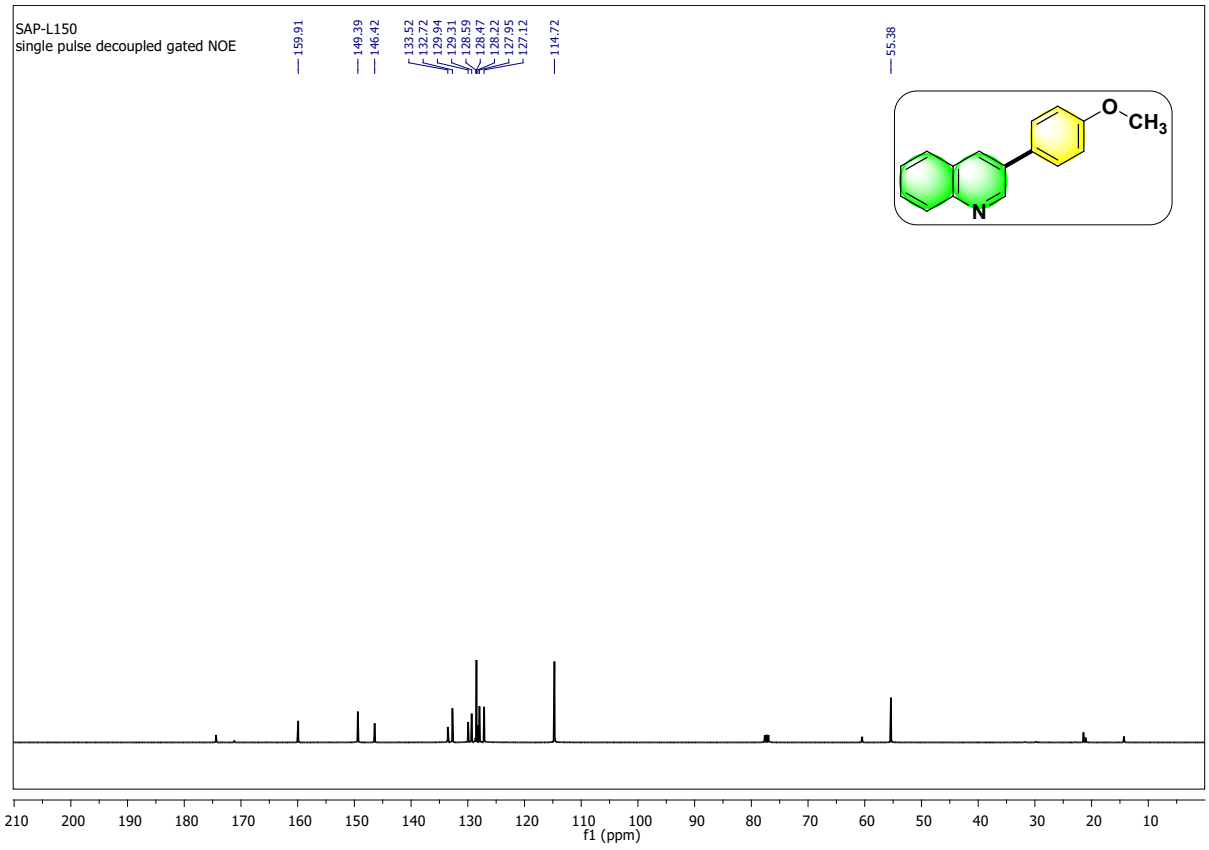

## 3-(4-chlorophenyl) quinoline (5d)

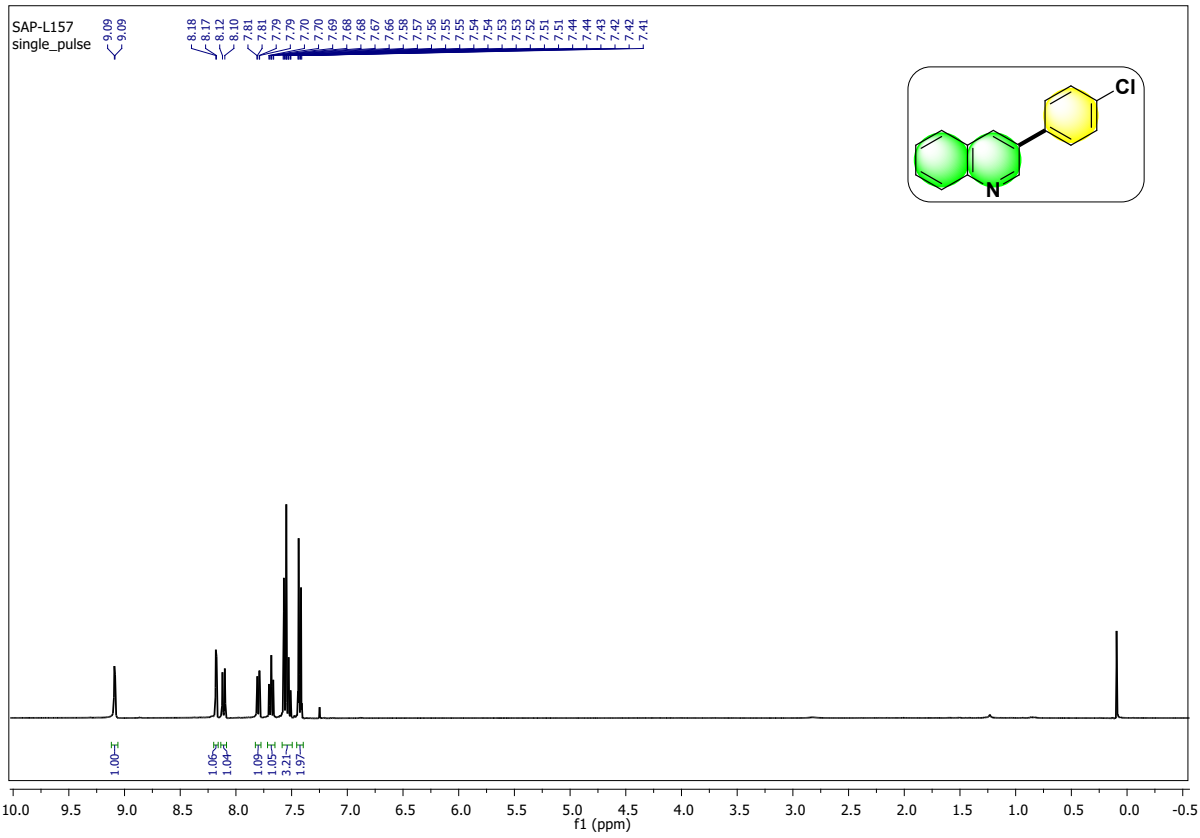


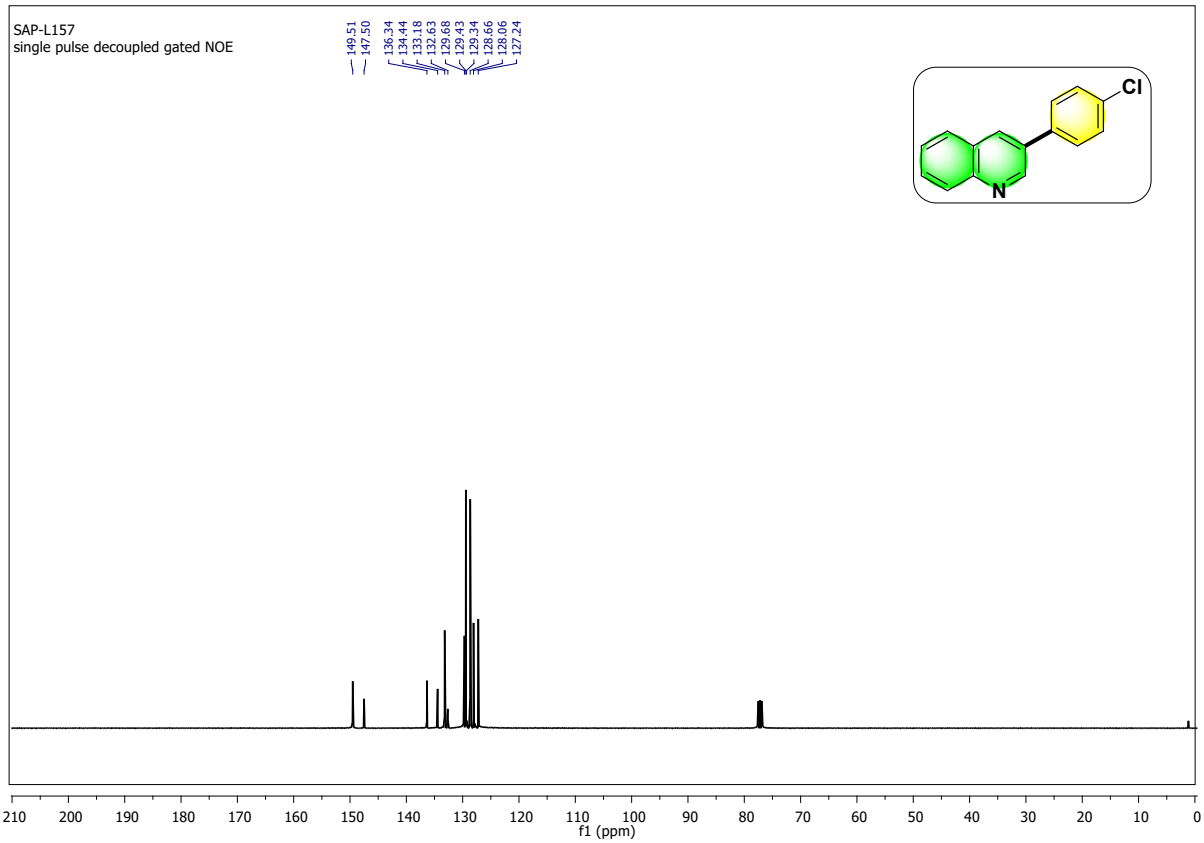

## 4-(quinolin-3-yl) benzaldehyde (5e)

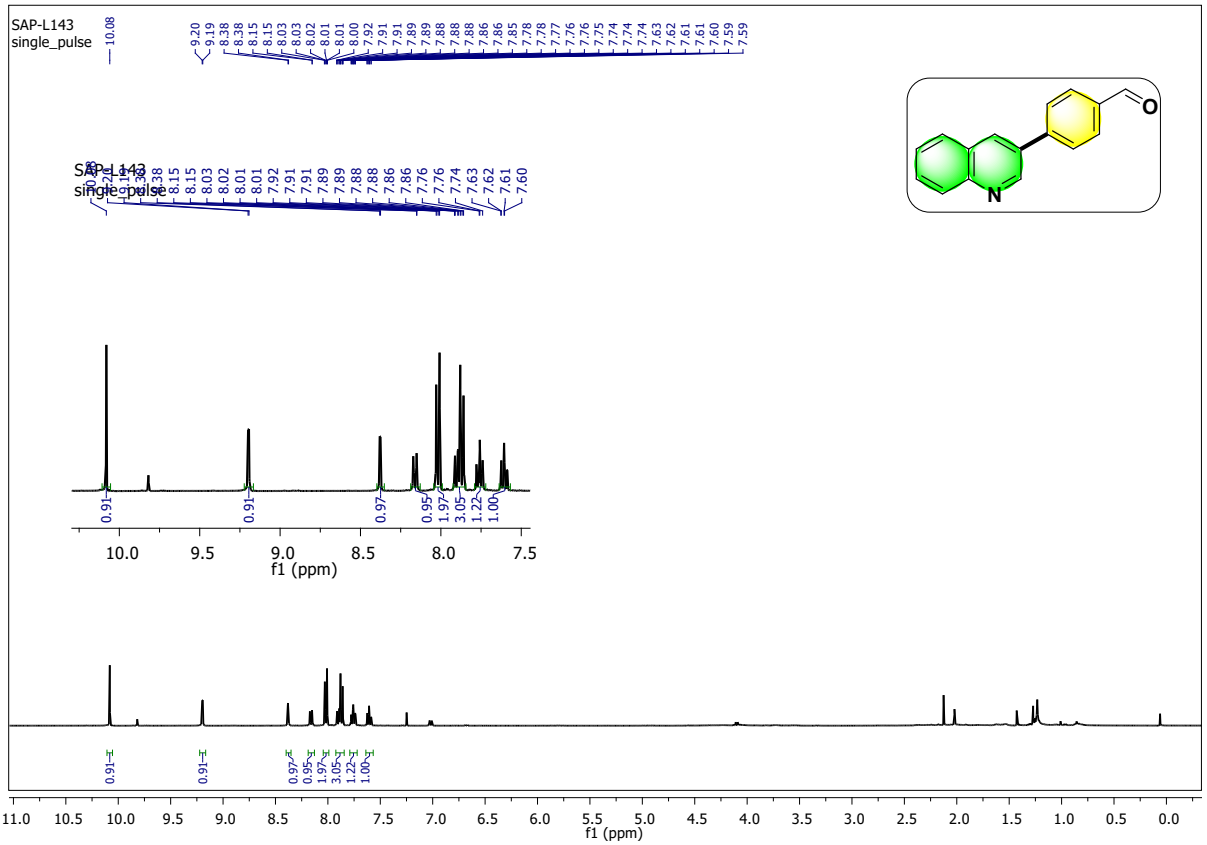


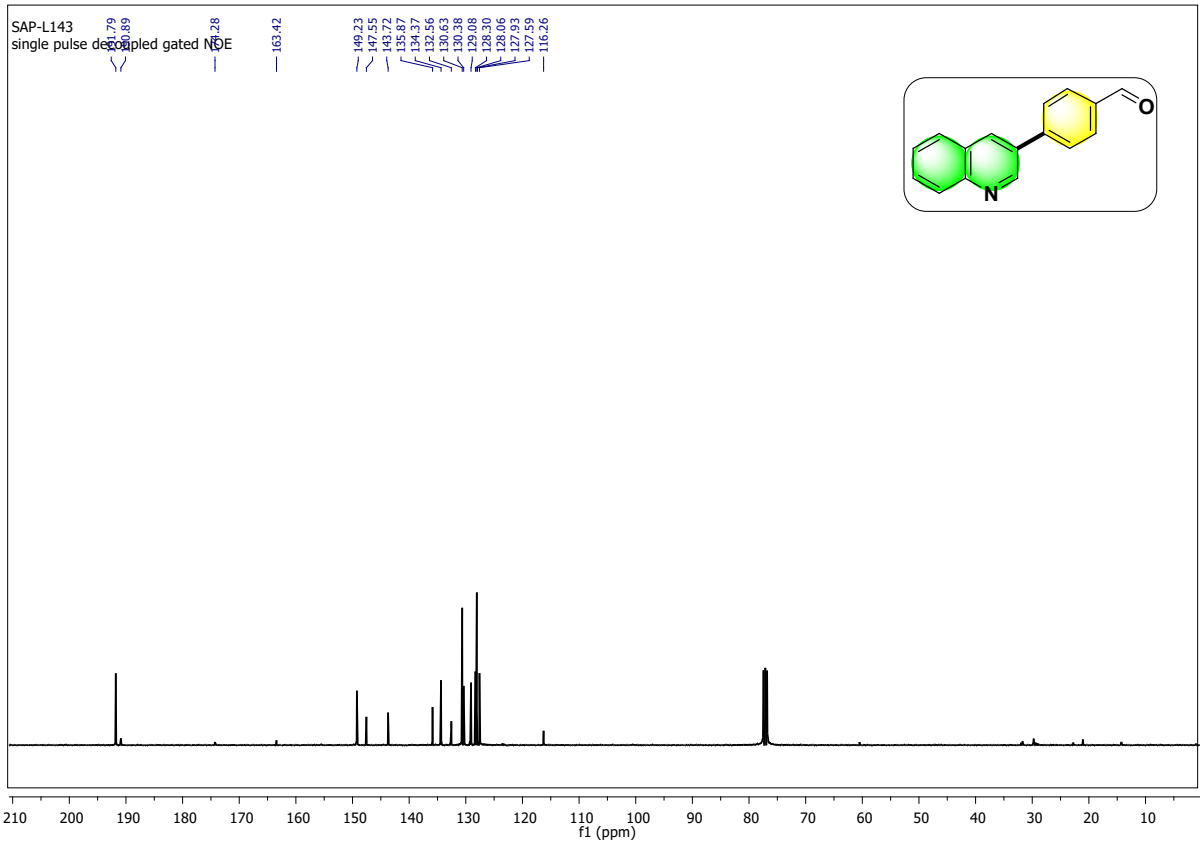

## 3-(4-chloronaphthalen-1-yl) quinoline (5f)

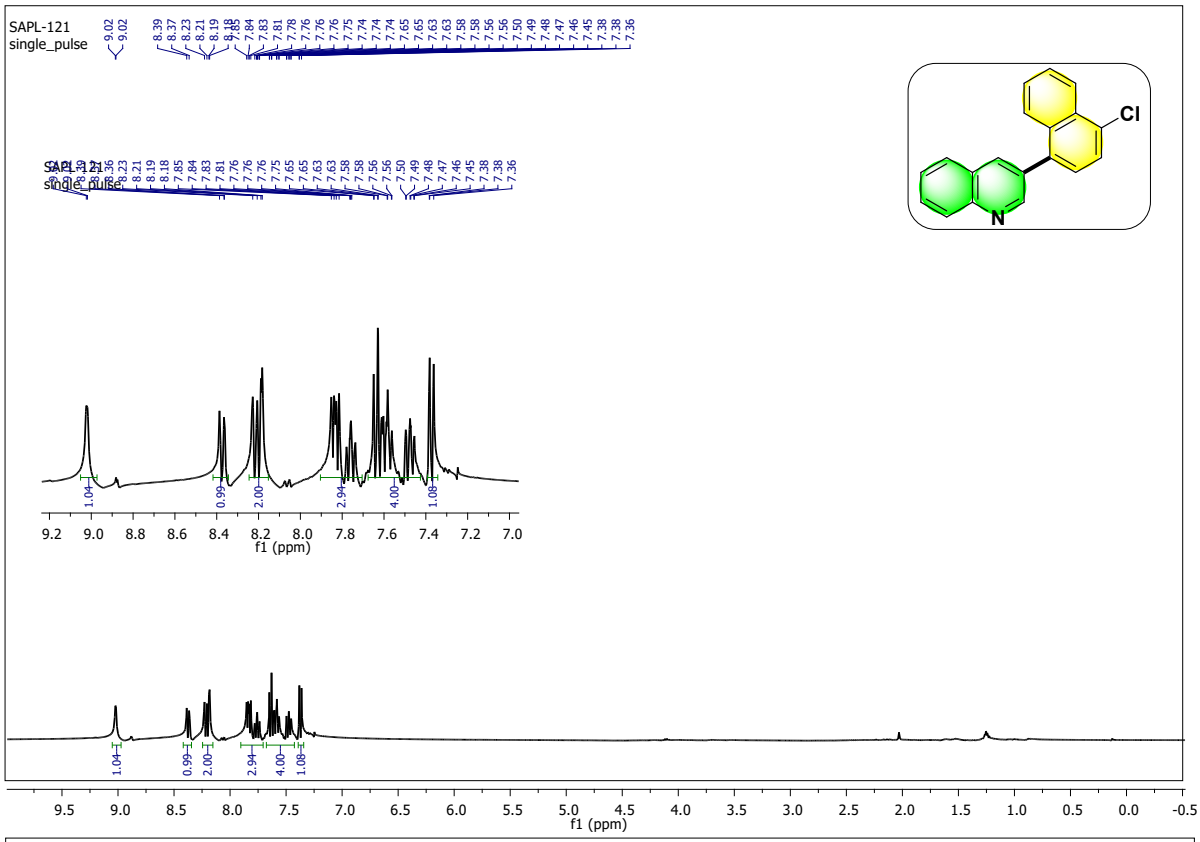


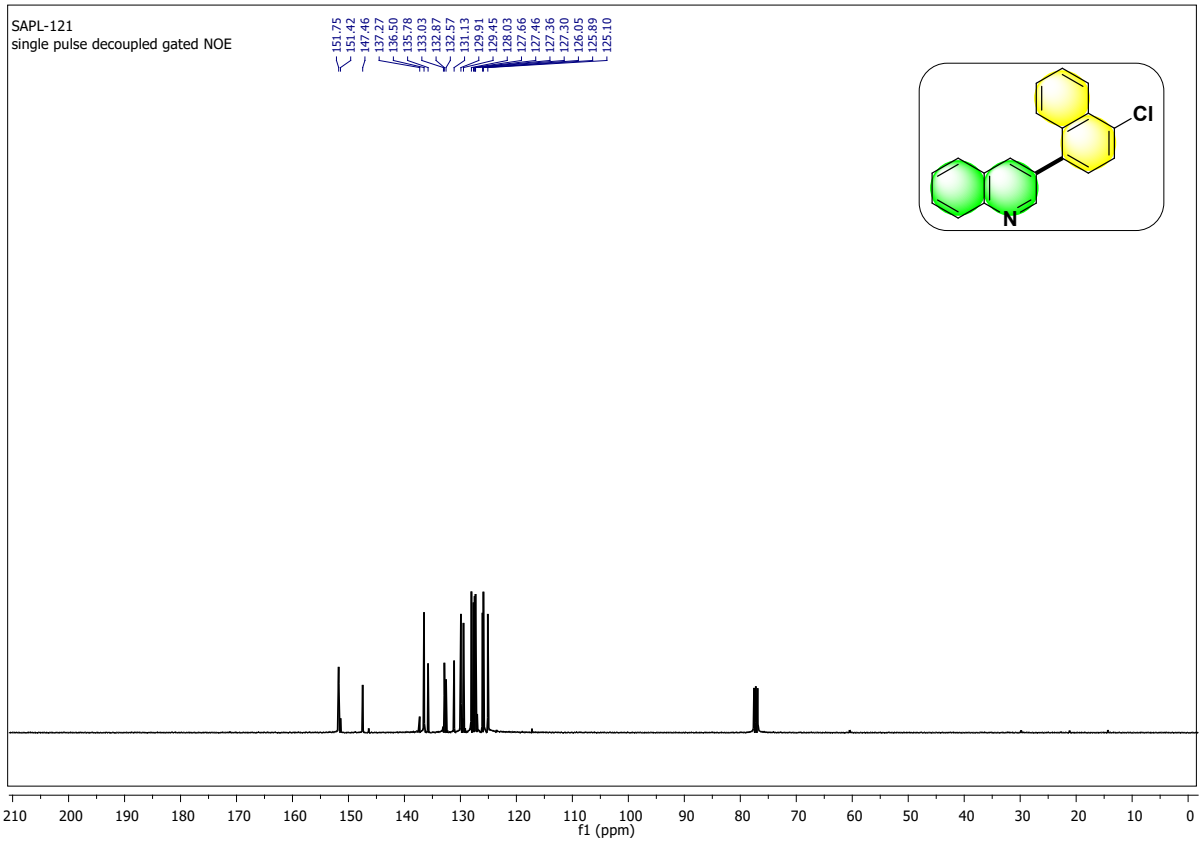

## 3-(2-ethoxy-4-fluorophenyl) quinoline (5g)

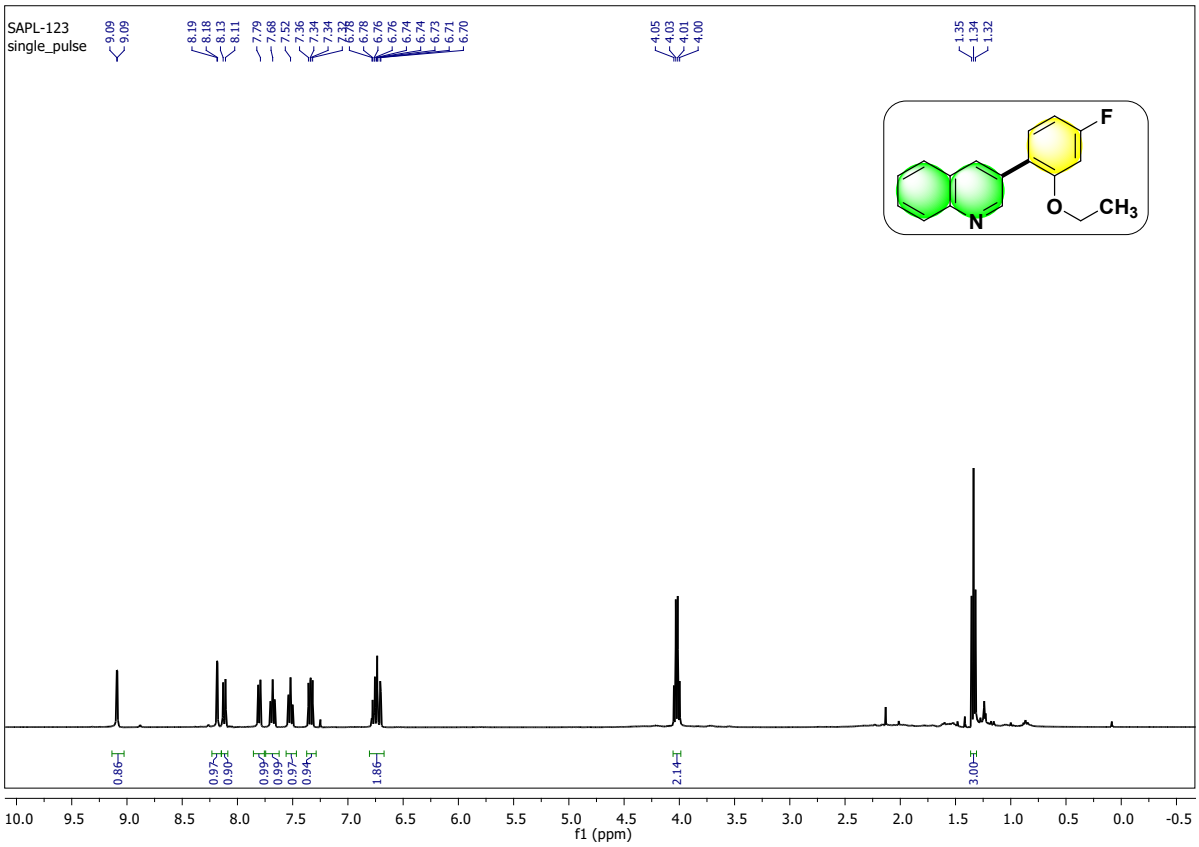


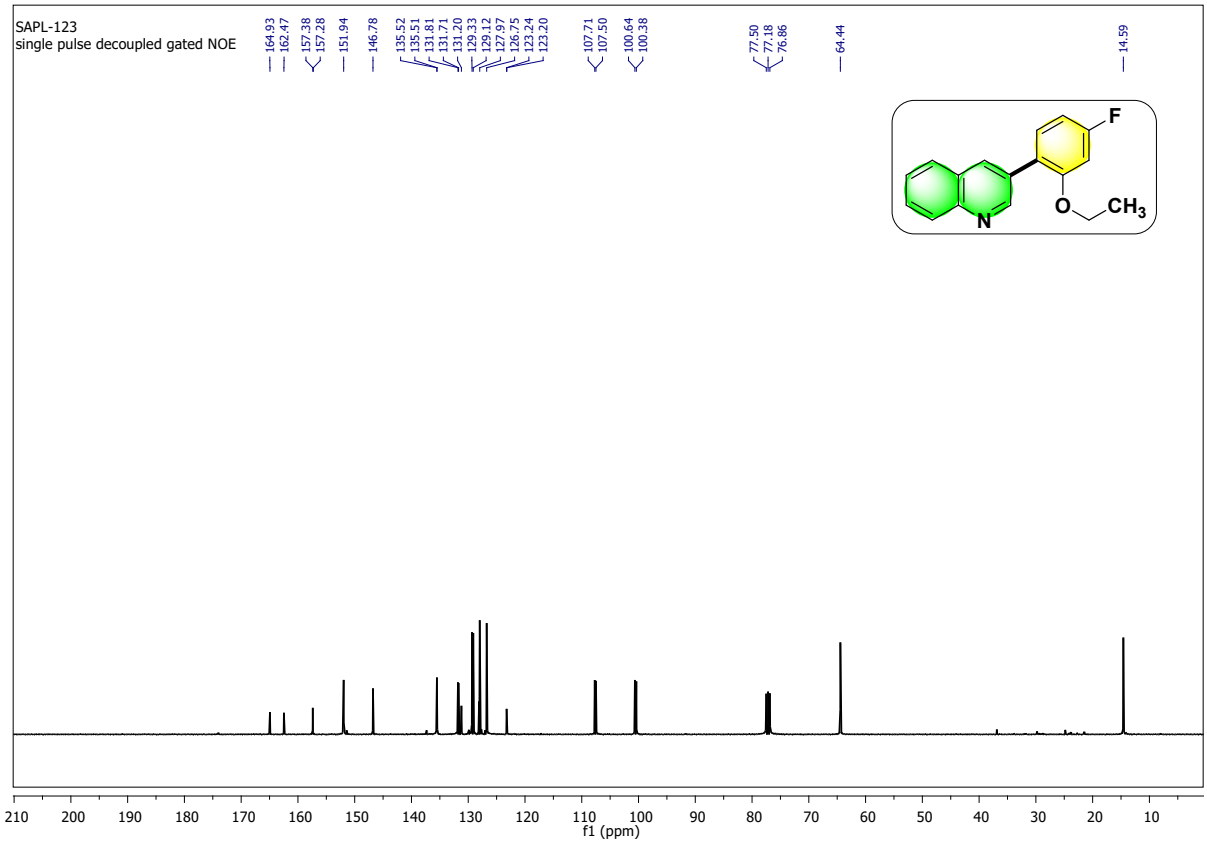

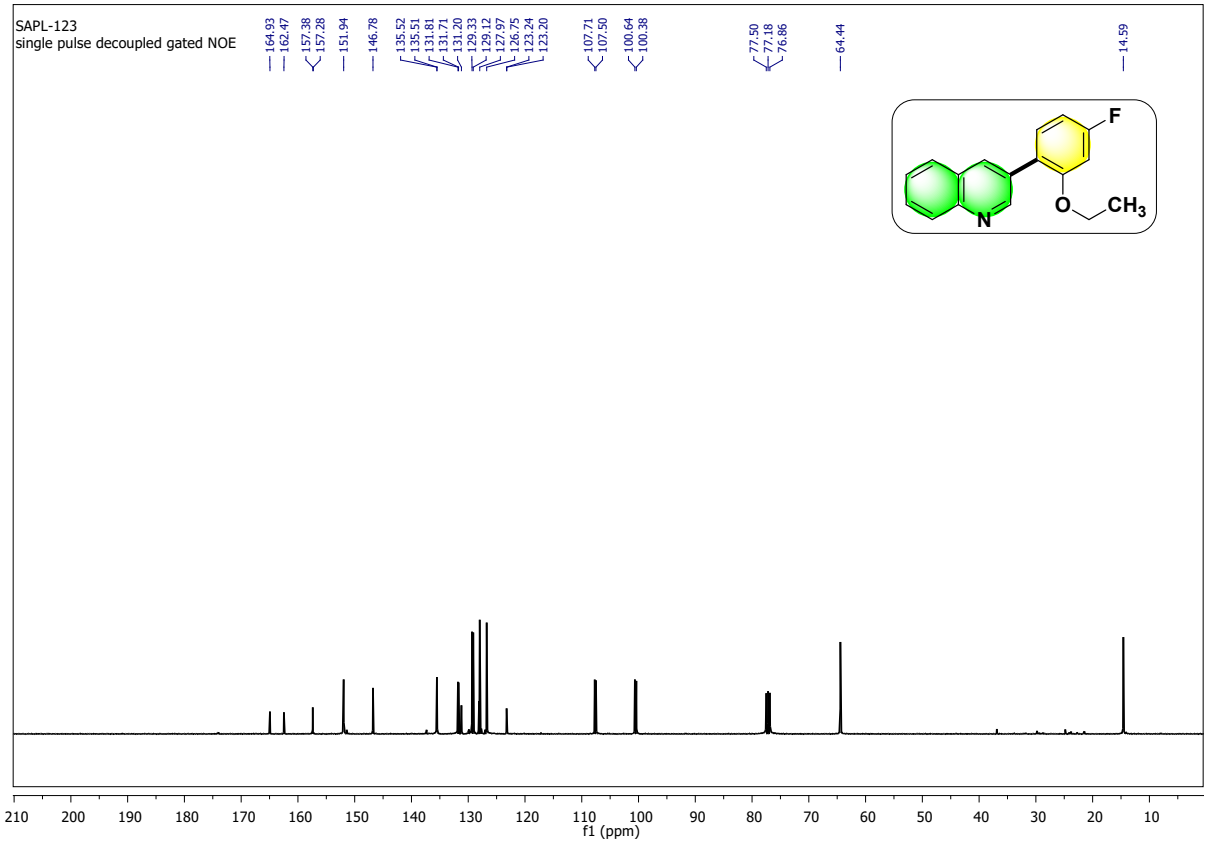


## 3-(2-fluoro-5-methylphenyl) quinoline (5h)

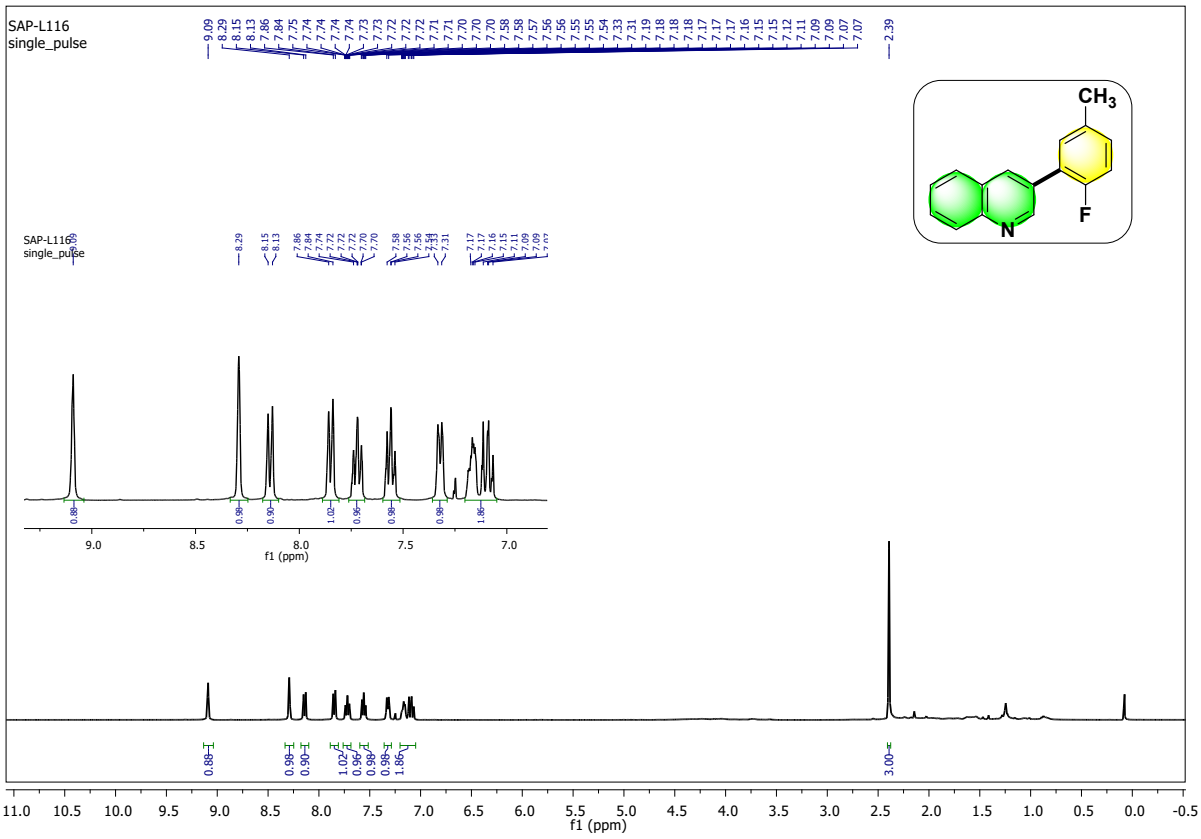

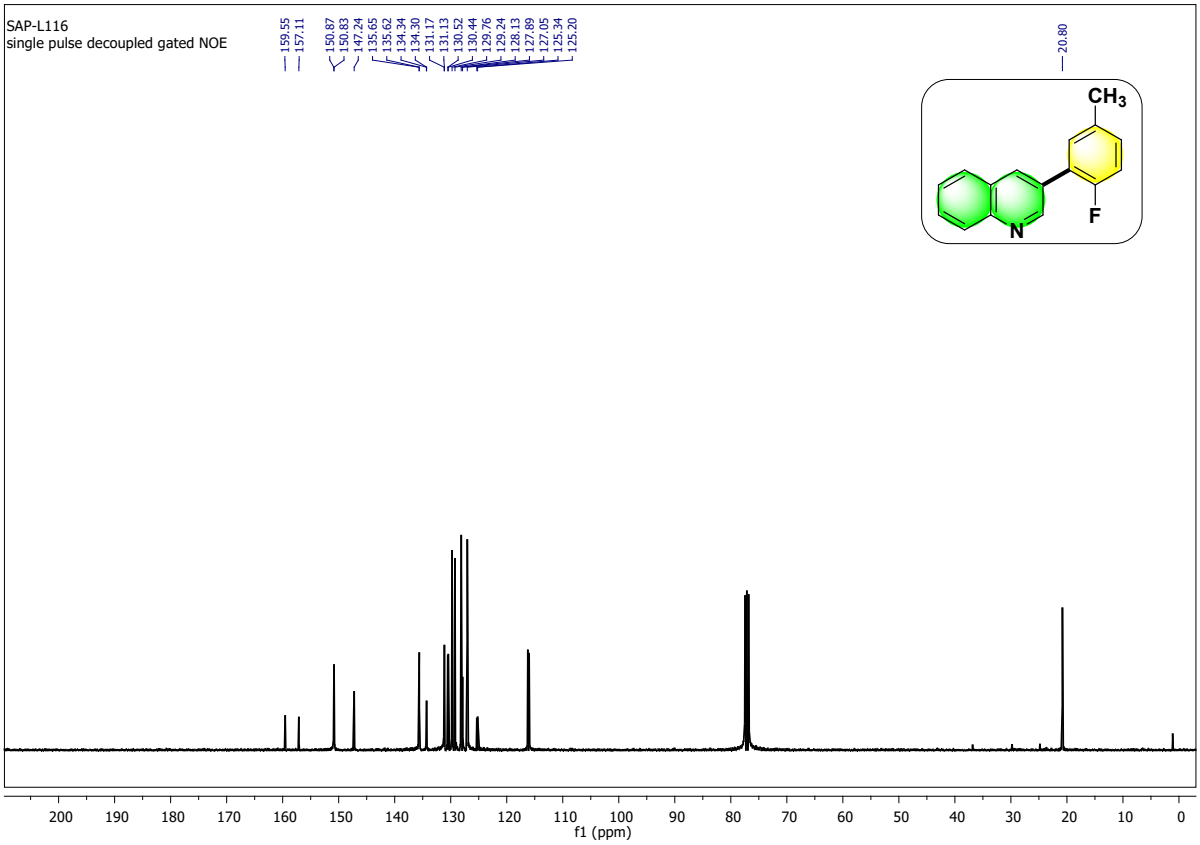
SAP-L116
single pulse decoupled gated NOE
159.55
157.11
150.87
150.83
147.24
135.65
135.62
134.34
134.30
131.17
131.13
130.52
130.44
129.76
129.24
128.13
127.89
127.05
125.34
125.20
20.80
CH3
F
N
200 190 180 170 160 150 140 130 120 110 100 90 80 70 60 50 40 30 20 10 0
f1 (ppm)

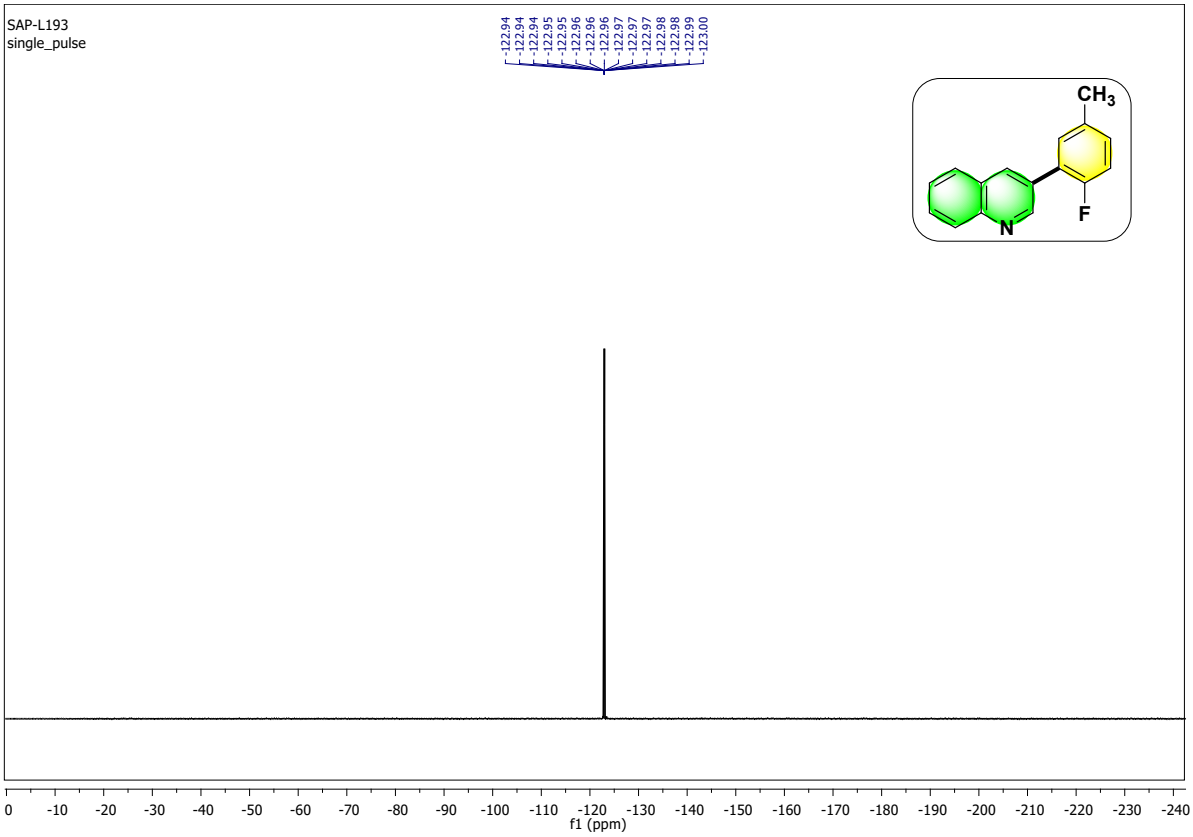
SAP-L193
single_pulse
-122.94
-122.94
-122.94
-122.95
-122.95
-122.96
-122.96
-122.96
-122.97
-122.97
-122.97
-122.98
-122.98
-122.98
-122.99
-123.00
CH3
F
N
0 -10 -20 -30 -40 -50 -60 -70 -80 -90 -100 -110 -120 -130 -140 -150 -160 -170 -180 -190 -200 -210 -220 -230 -240
f1 (ppm)

## 3-(2-chlorothiophen-3-yl) quinoline (5i)

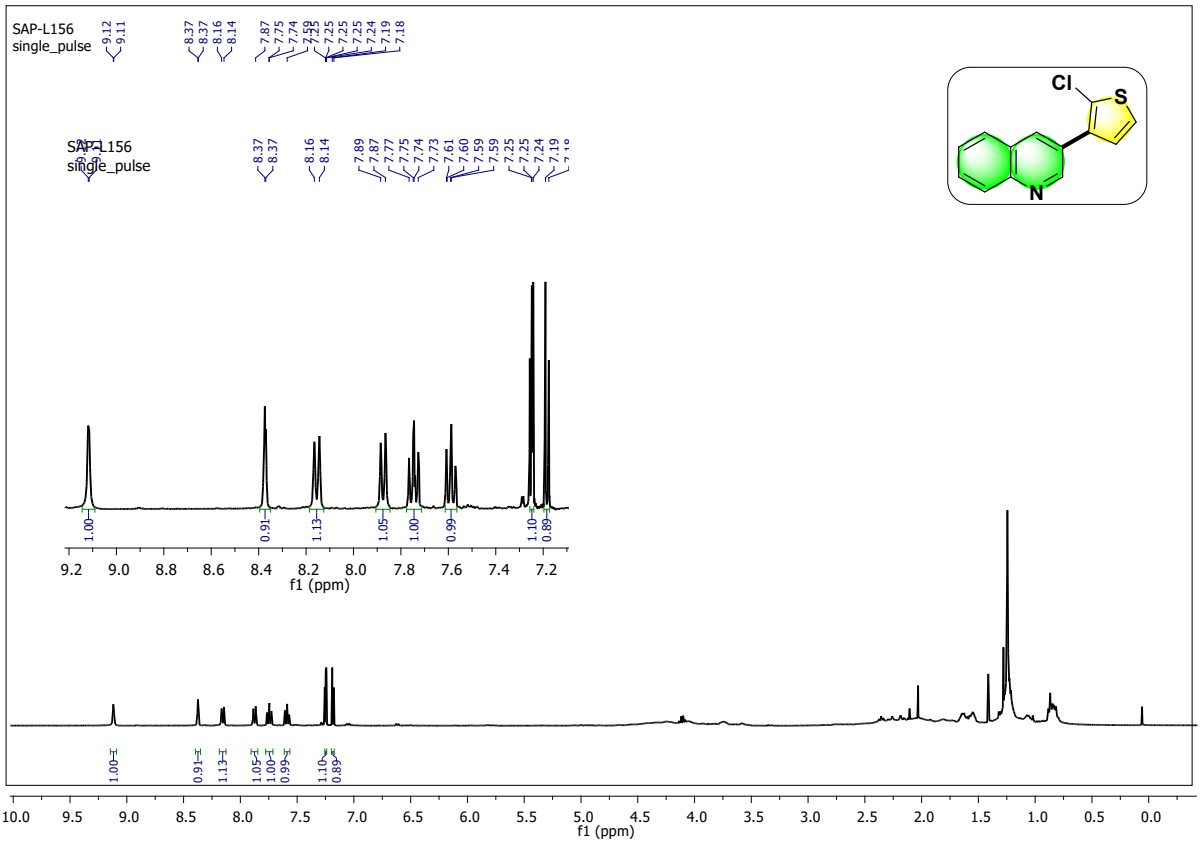


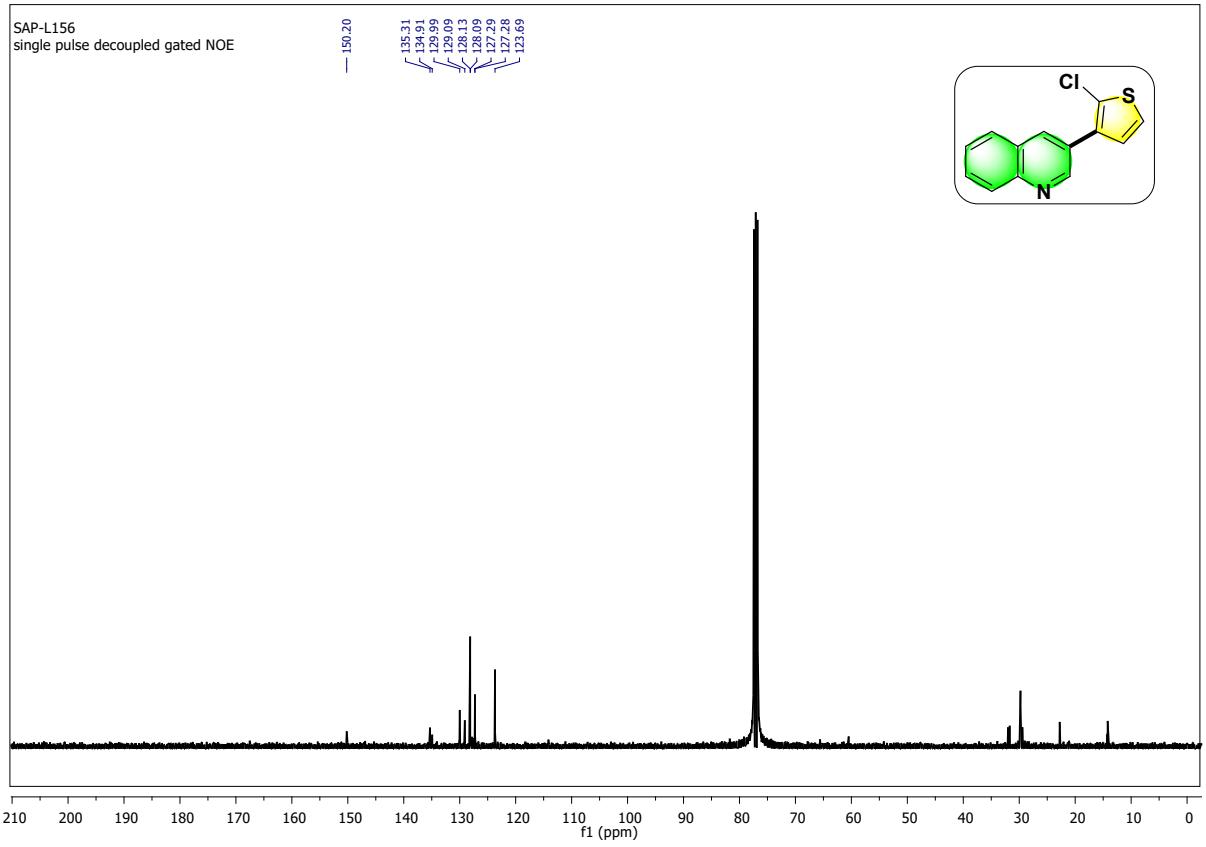

## 3-(6-methoxypyridin-3-yl) quinoline (5j)

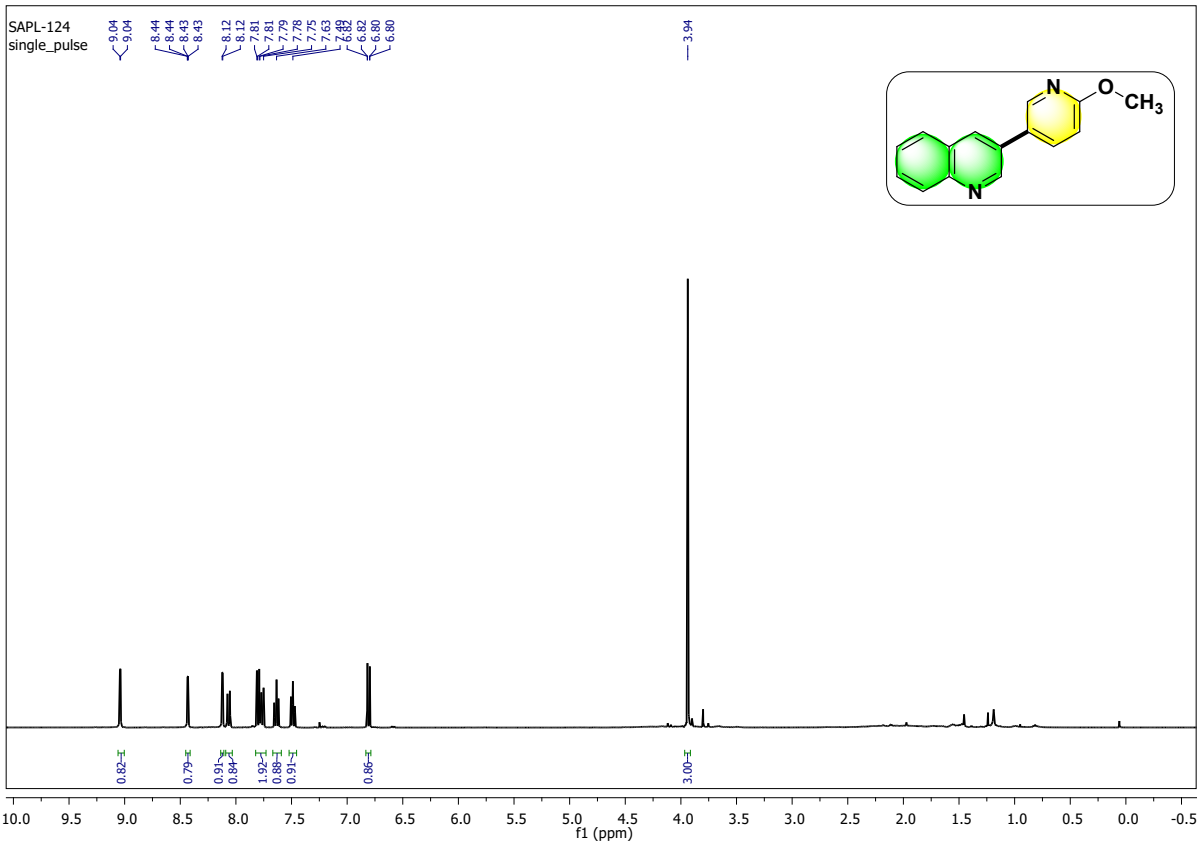


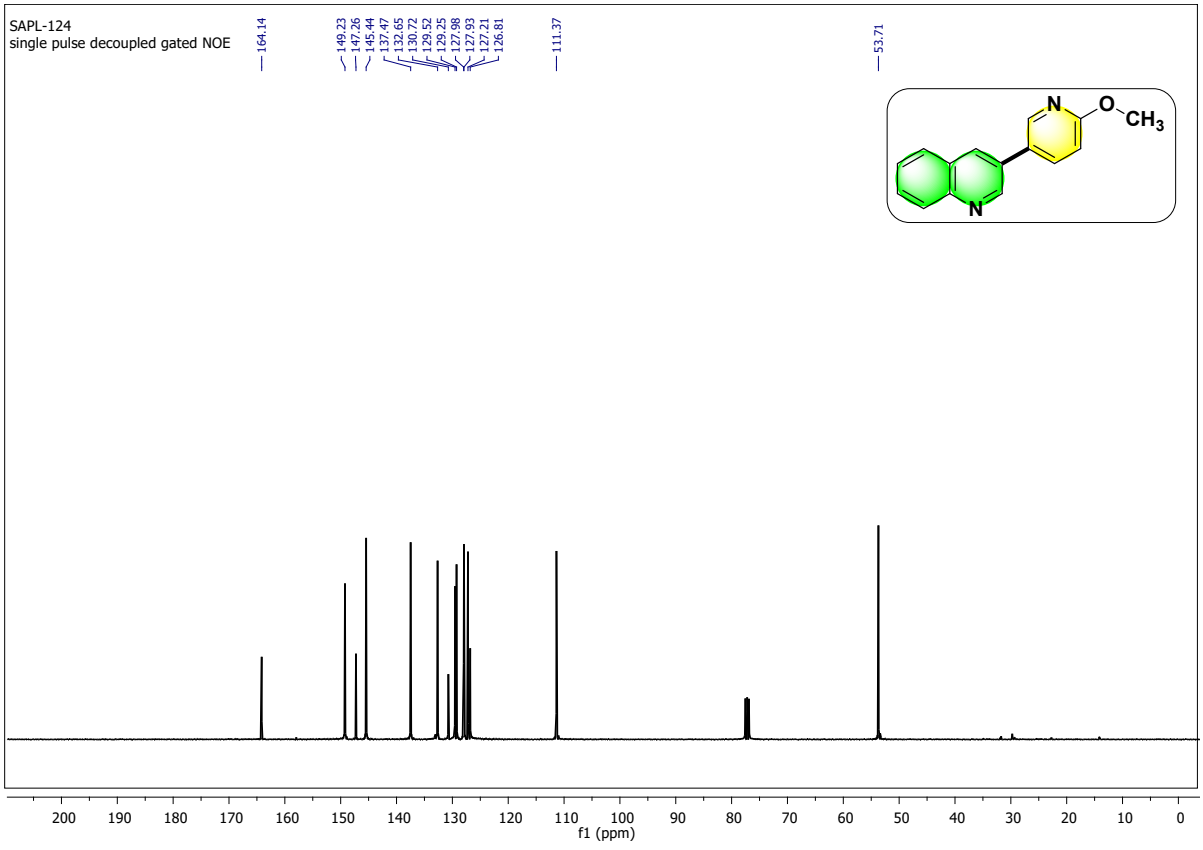

## 7-chloro-4-phenylquinoline (7a)

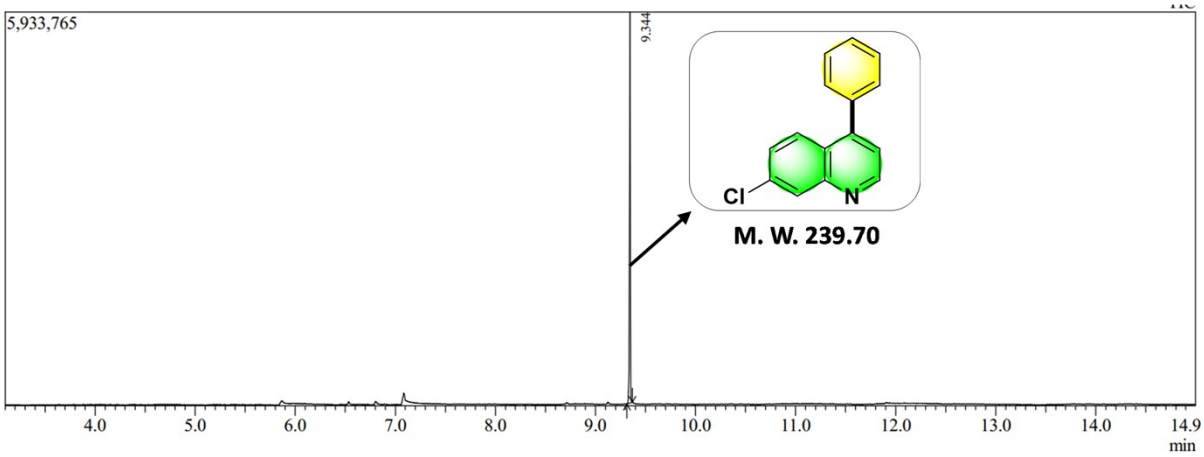


Peak Report TIC

| Peak# | R.Time | I.Time | F.Time | Area | Area% | Height | Height% | A/H | Mark | Name |
|---|---|---|---|---|---|---|---|---|---|---|
| 1 | 9.344 | 9.315 | 9.370 | 3521979 | 100.00 | 5893137 | 100.00 | 0.60 | | Benzene, 1-chloro-4-(2-cyano-2-phen |
| | | | | 3521979 | 100.00 | 5893137 | 100.00 | | | |

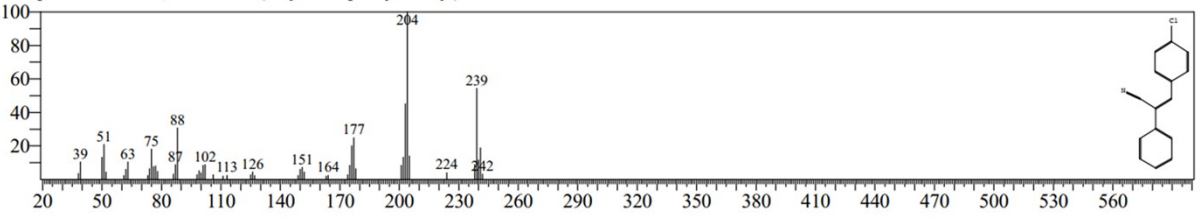


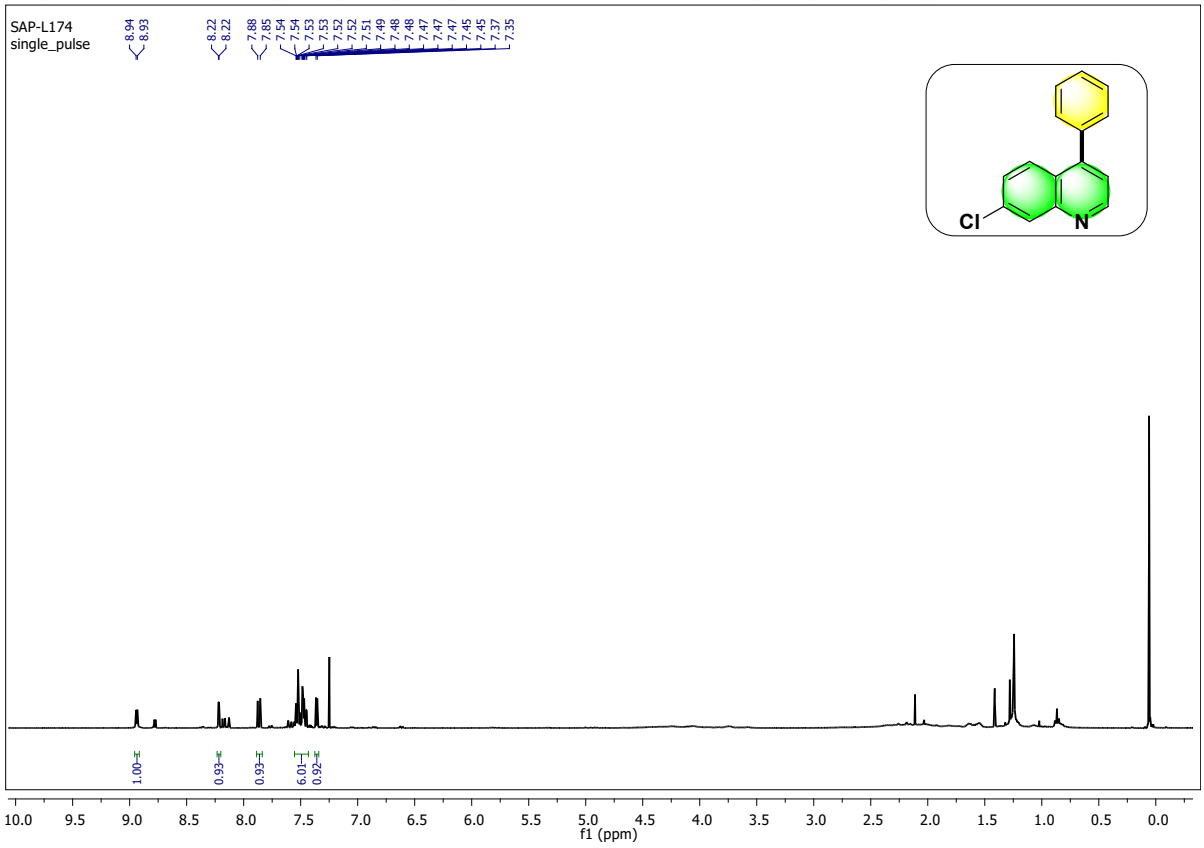

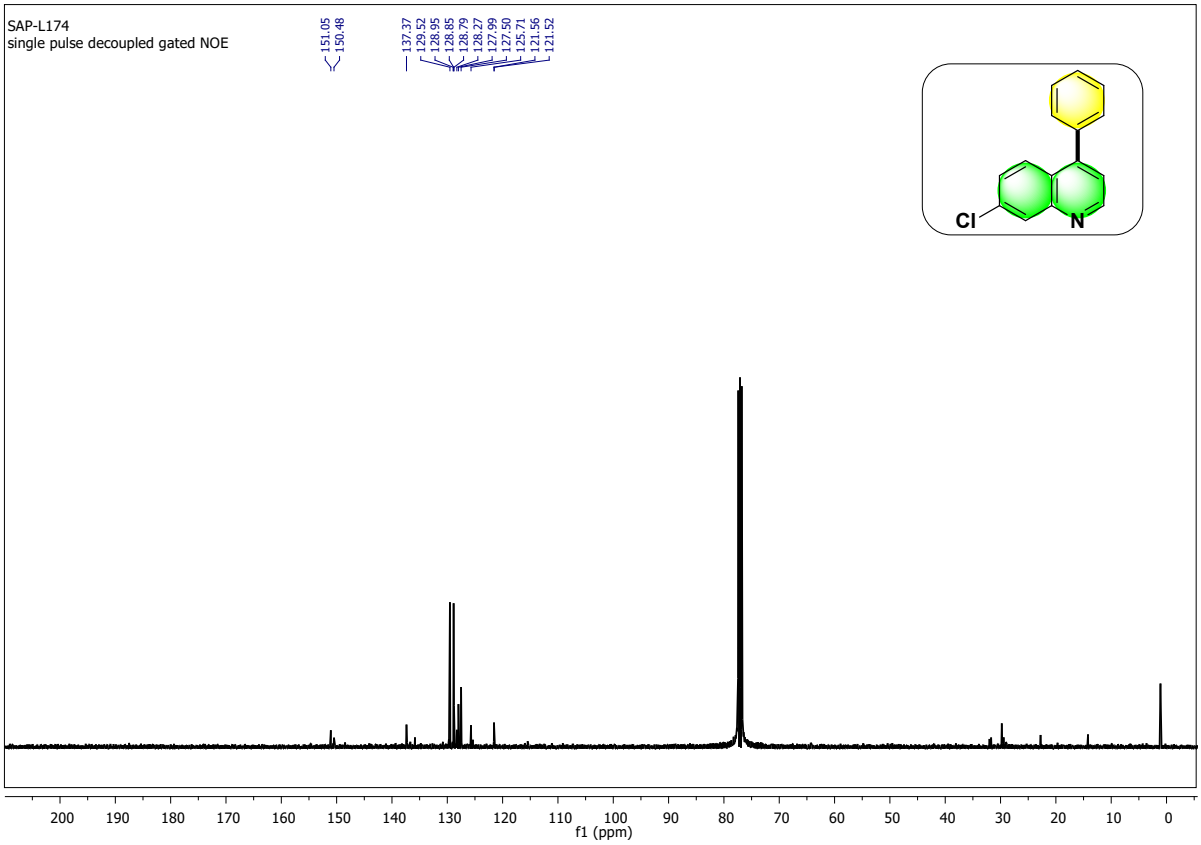


## 7-chloro-4-(p-tolyl) quinoline (7b)

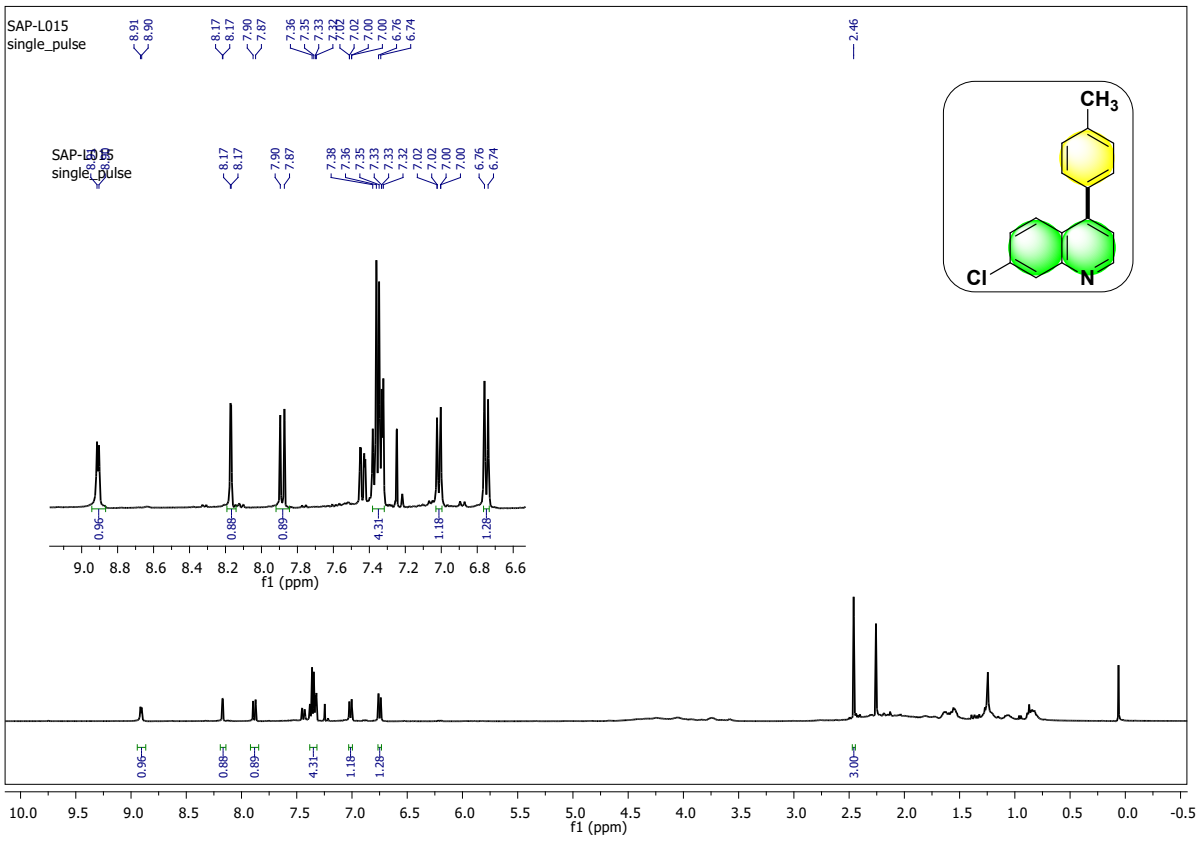

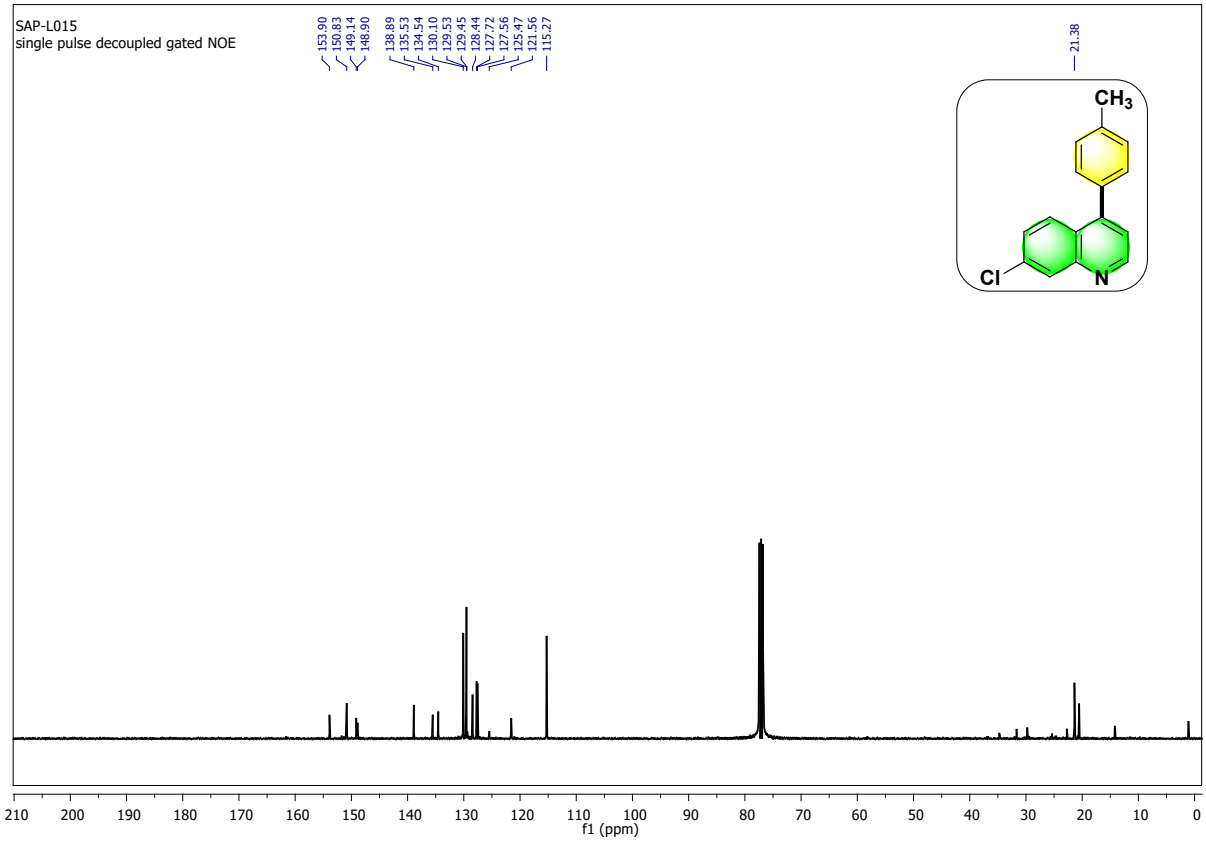


## 7-chloro-4-(4-methoxyphenyl) quinoline (7c)

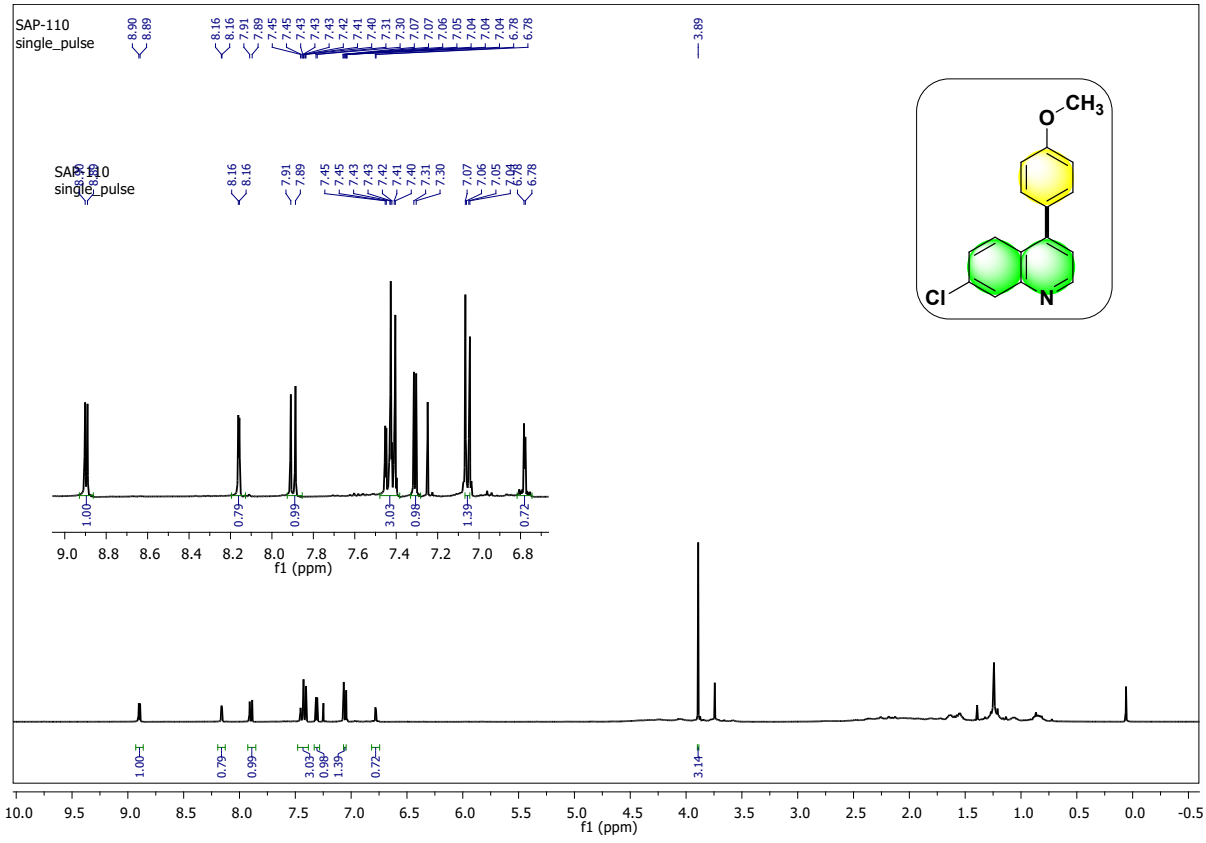

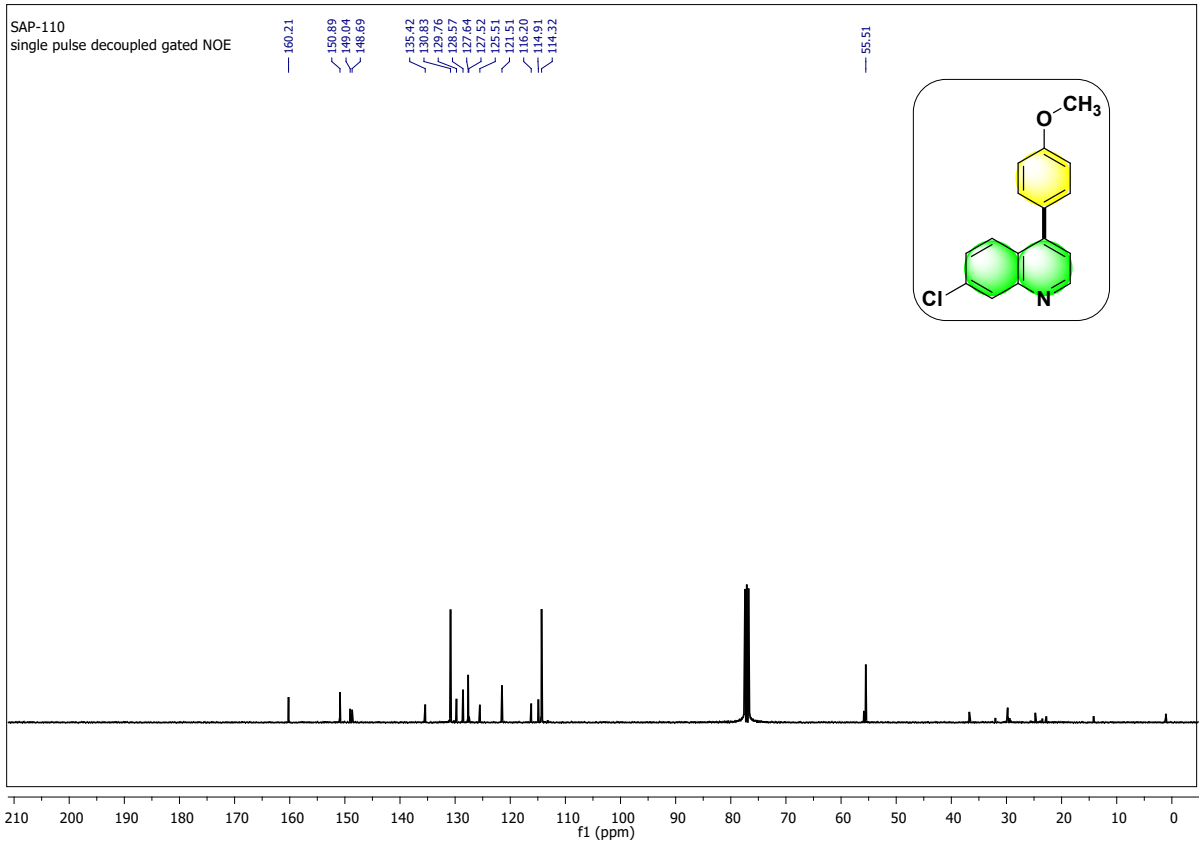


## 7-chloro-4-(4-chlorophenyl) quinoline (7d)

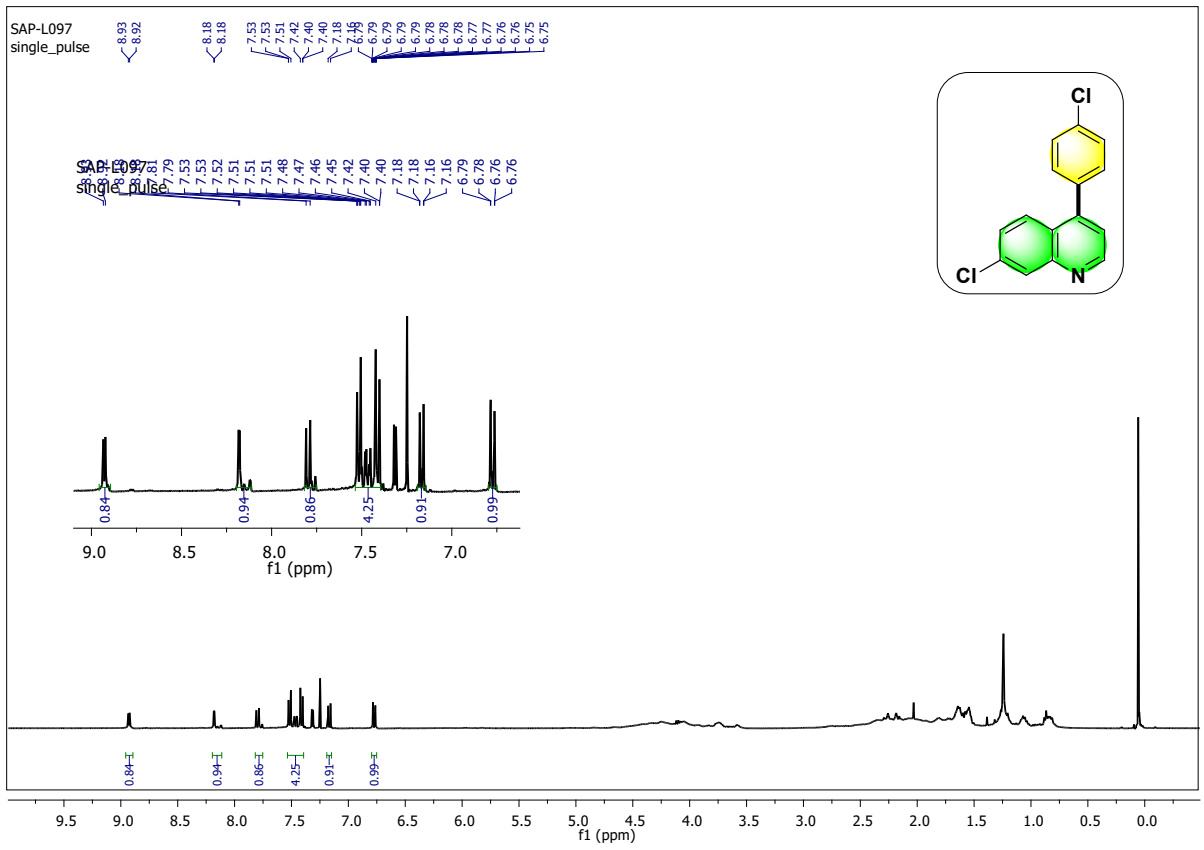

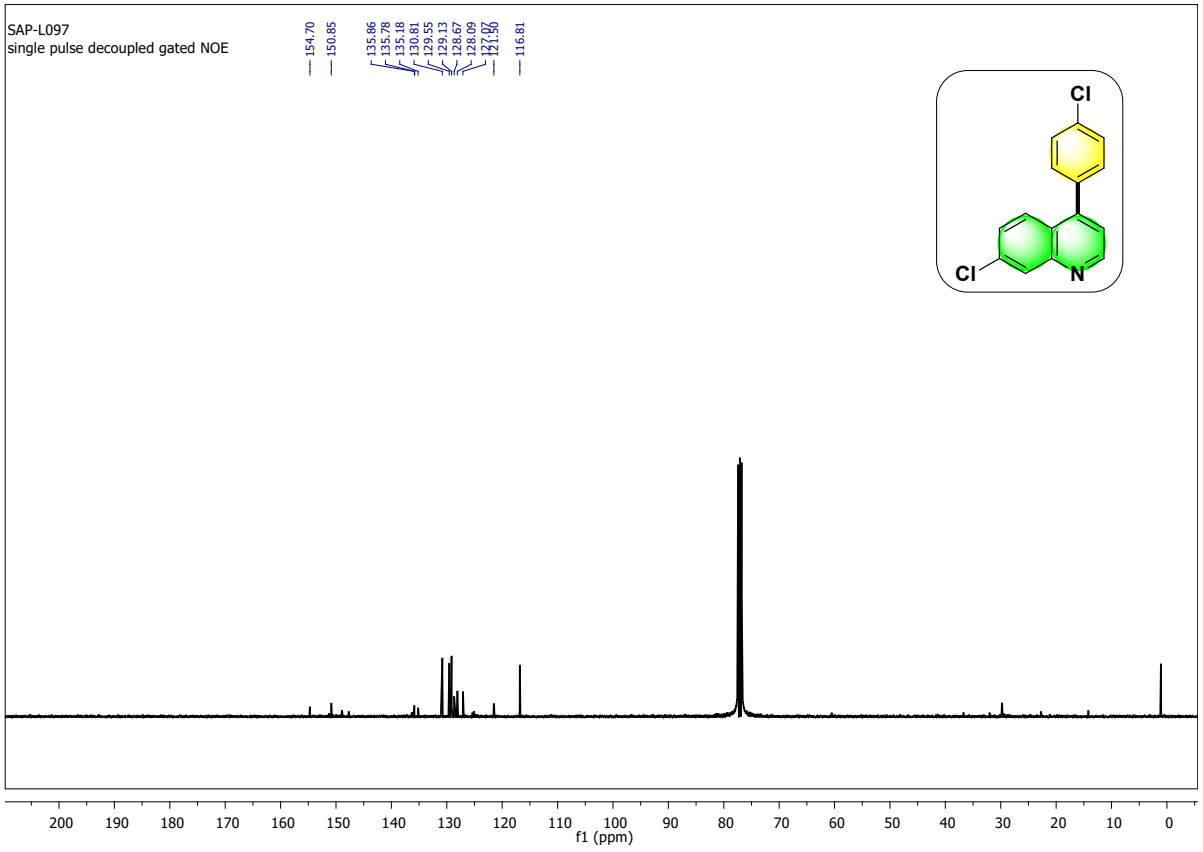


## 4-(7-chloroquinolin-4-yl) benzoic acid (7e)

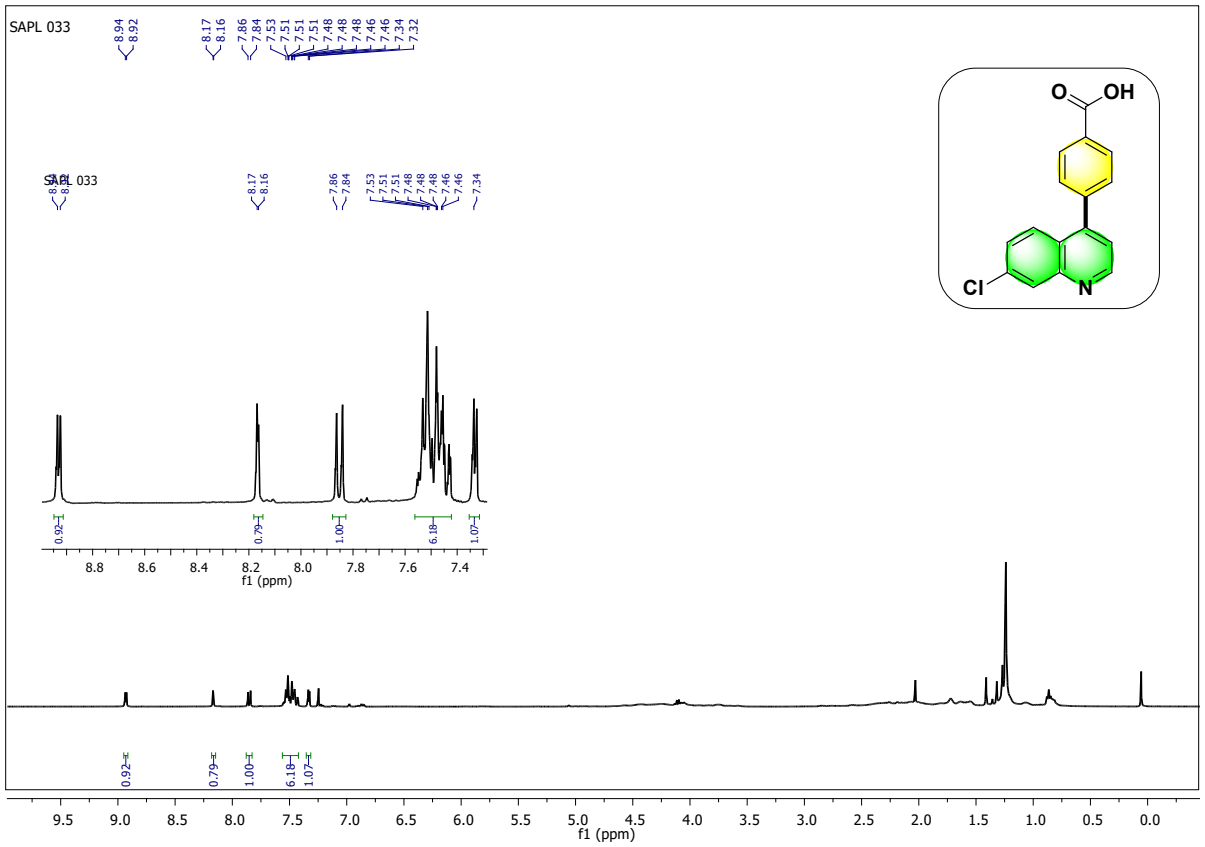

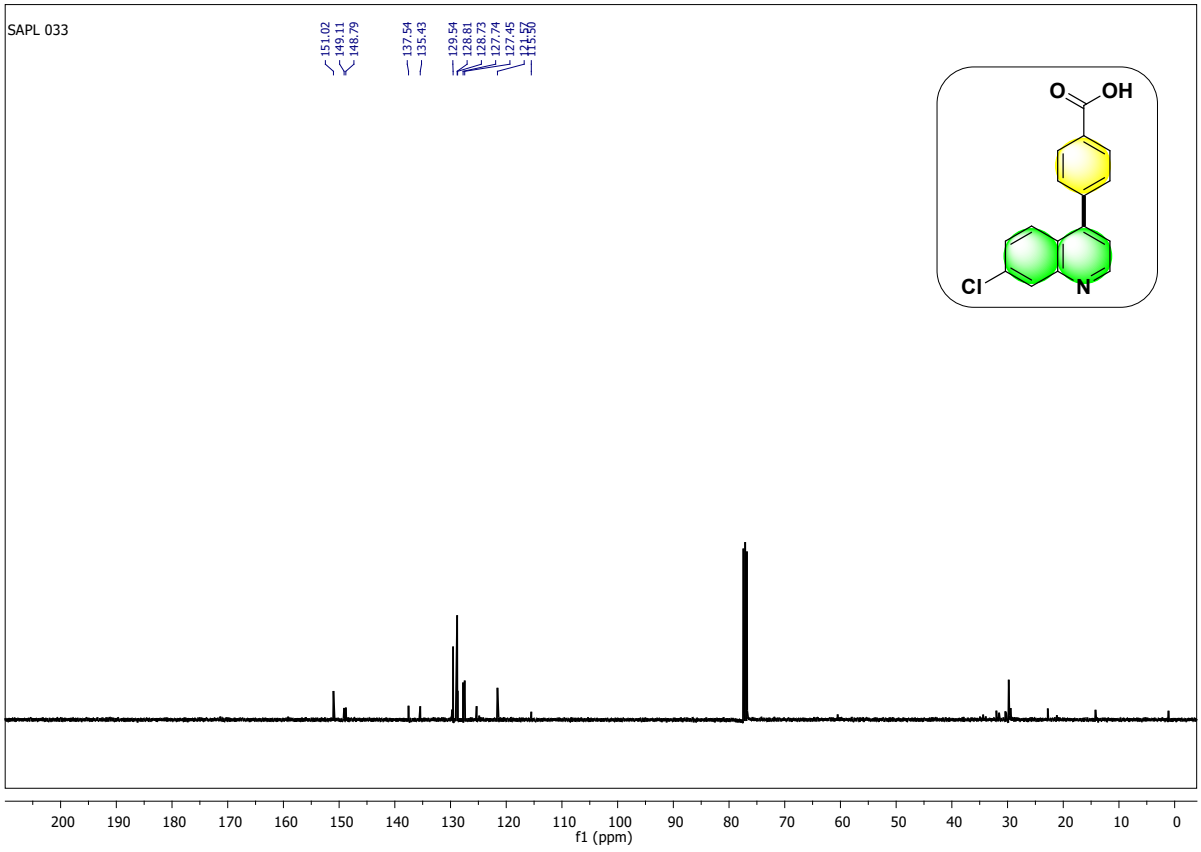


## 7-chloro-4-(4-chloronaphthalen-1-yl) quinoline (7f)

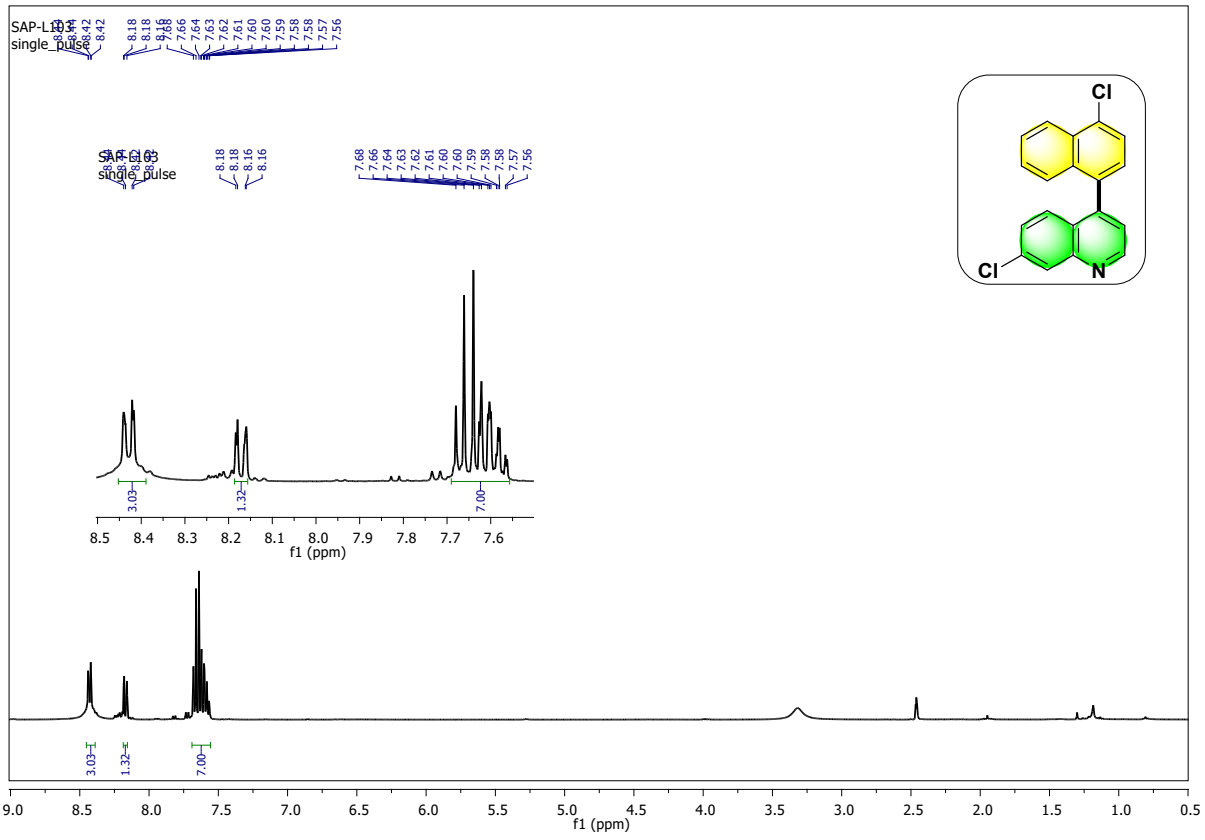

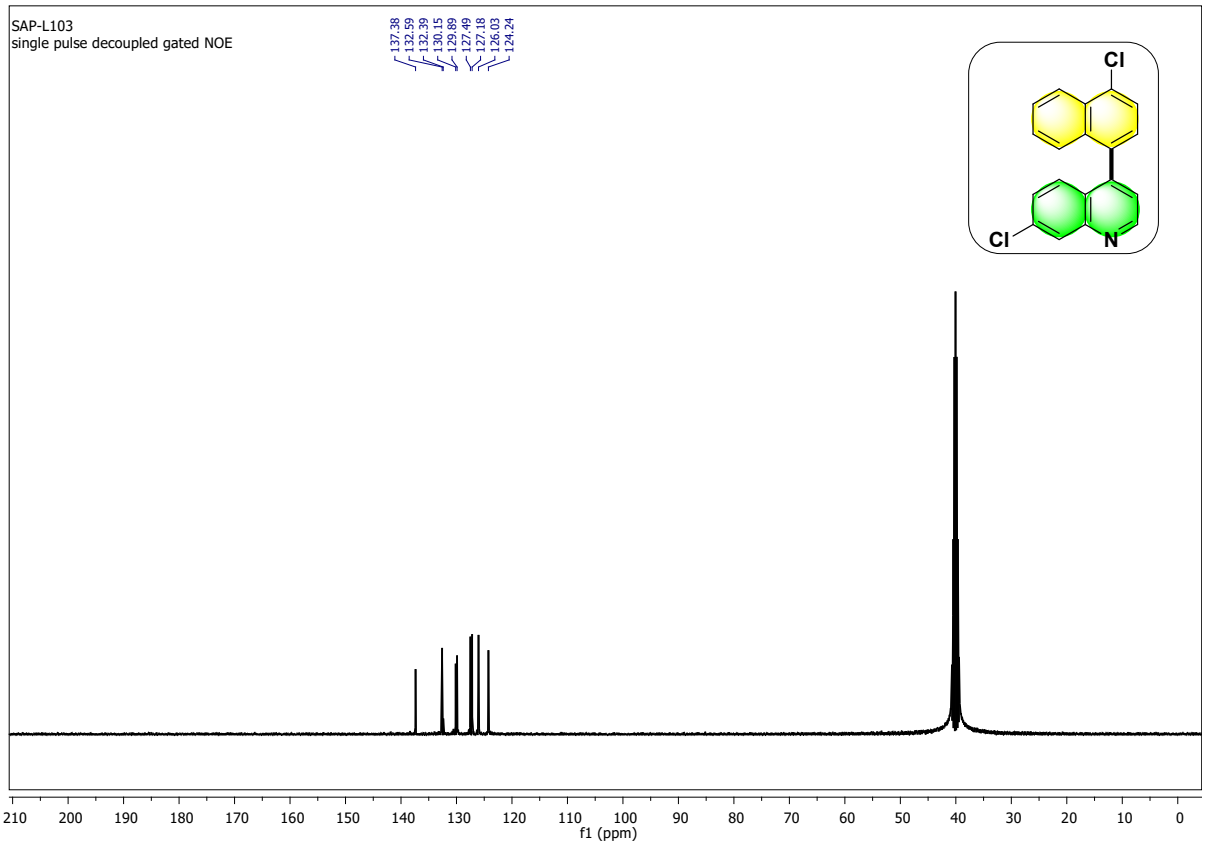


## 4,7-bis(6-methoxypyridin-3-yl)quinoline (7g)

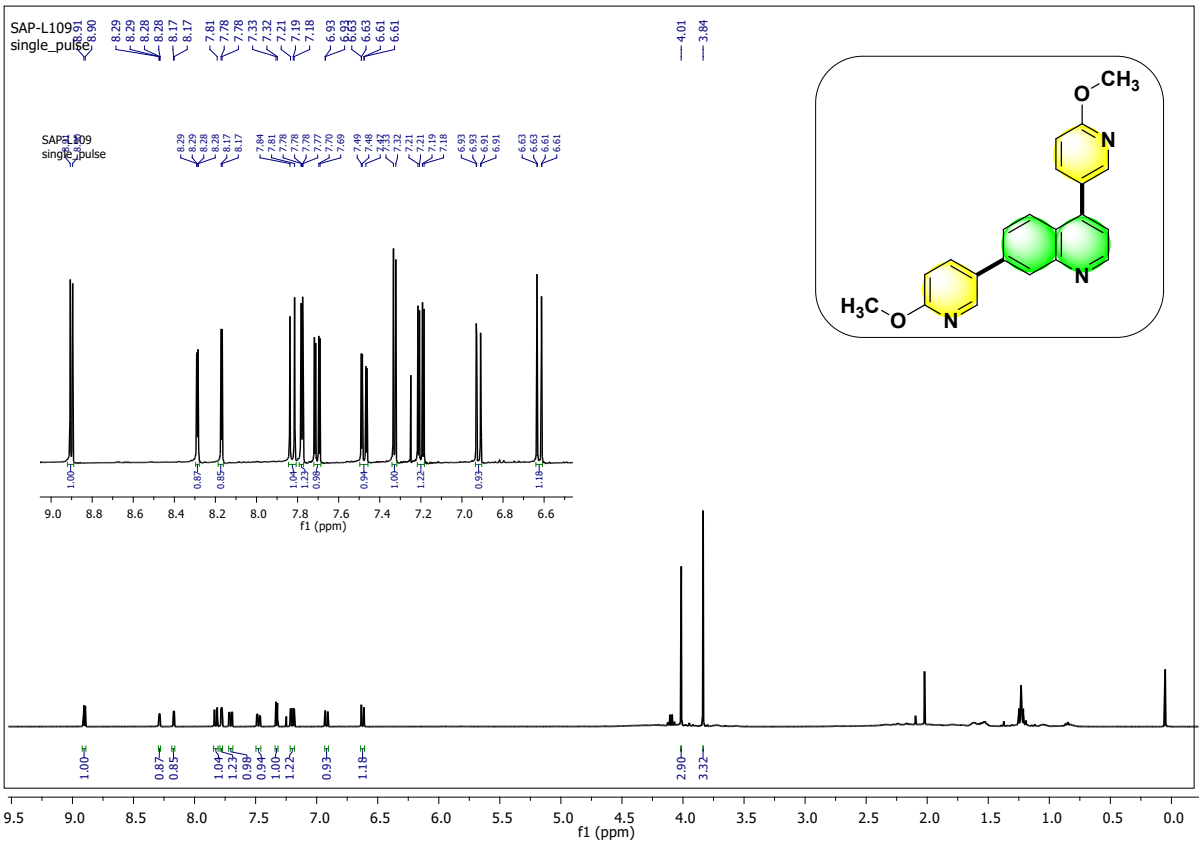

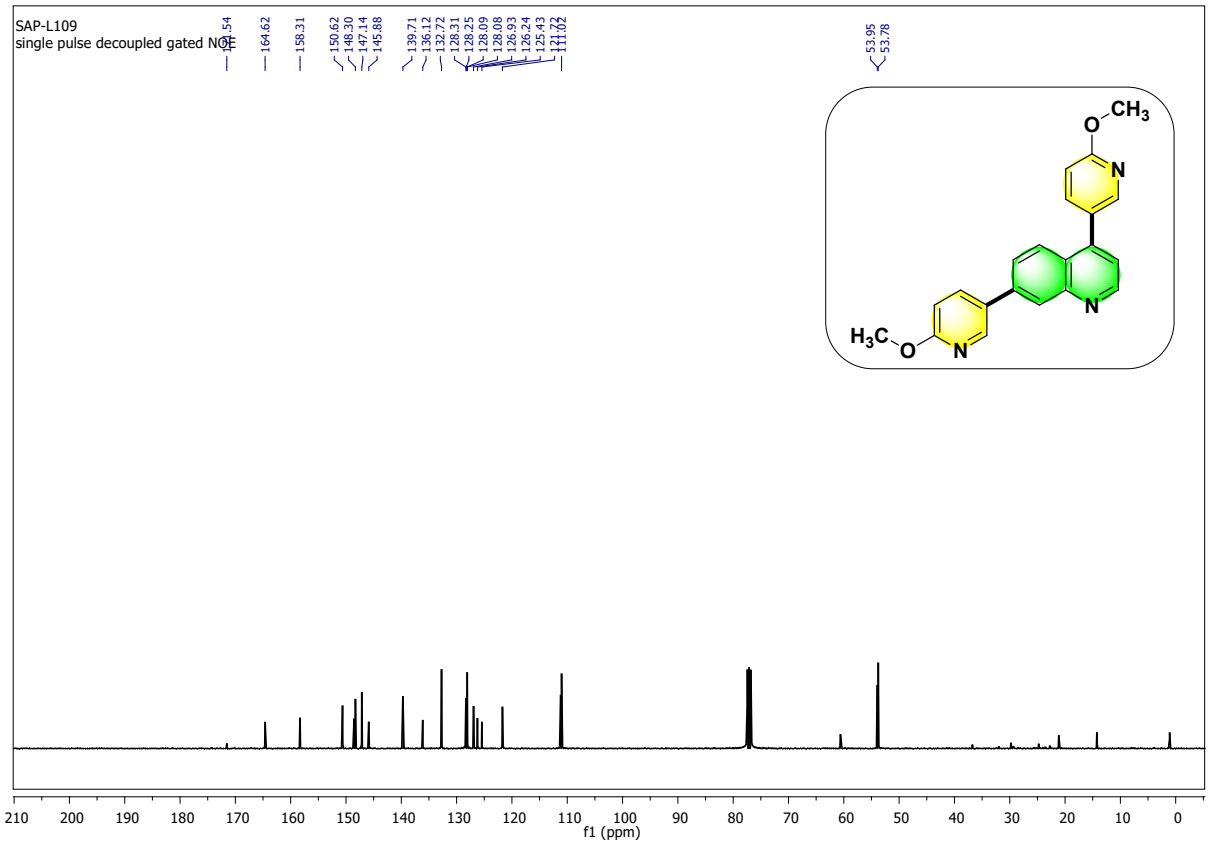
SAP-L109
single pulse decoupled gated NOE
168.54
164.62
158.31
150.62
148.30
147.14
145.88
139.71
136.12
132.72
128.31
128.25
128.09
128.08
126.93
126.24
125.43
111.72
111.02
53.95
53.78
O
CH3
N
N
H3C
O
N
210
200
190
180
170
160
150
140
130
120
110
100
90
80
70
60
50
40
30
20
10
0
f1 (ppm)